Transformations in TRIP-assisted Steels: Microstructure and Properties

A thesis submitted for the degree of

Doctor of Philosophy

Sourabh Chatterjee

Darwin College, University of Cambridge

November, 2006

. . . in memory of my father

Preface

This dissertation is submitted for the degree of Doctor of Philosophy at the University of Cambridge. The work reported herein was carried out under the supervision of Professor H. K. D. H. Bhadeshia in the Department of Materials Science and Metallurgy, University of Cambridge between January 2004 and October 2006.

To the best of my knowledge, this work is original, except where suitable references are made to previous work. Neither this, nor any substantially similar dissertation has been submitted for any degree, diploma or qualification at any other university or institution. This dissertation does not exceed 60,000 words in length.

The following publications have been made:

Chatterjee S. and Bhadeshia H. K. D. H., TRIP-assisted Steels: Cracking of High-carbon Martensite, *Materials Science and Technology* **22** (2006) 645

Chatterjee S., Wang H. S., Yang J. R. and Bhadeshia H. K. D. H., Mechanical Stabilisation of Austenite, *Materials Science and Technology* **22** (2006) 641

Maalekian M., Kozeschnik E., Chatterjee S. and Bhadeshia H. K. D. H., Mechanical Stabilisation of Eutectoid Steel, *Materials Science and Technology*, accepted

Sourabh Chatterjee

November, 2006

Acknowledgments

I am indebted to Prof. H. K. D. H. Bhadeshia for all his support, advice, inspiration and encouragement during the work and my stay here. I would also like to thank Prof. A. L. Greer for the facilities and the atmosphere in the department. I am sincerely grateful to the Management, Tata Steel, India for providing me with the opportunity to experience Cambridge.

Dr M. Murugananth, a past member of the PT-group, deserves especial thanks for the optimisation calculations used in my research work. I am also grateful to Dr D. Bhattacharjee and Dr N. Gope, Tata Steel for arranging the making of some alloys in the Research and Development laboratories.

I would like to thank every member of the department for being very kind to me. I wonder if this work would have been at all possible without Mr Kevin Roberts, Mr Michael Brand, Mr David Vowles, Mr Bryan Adams, Mr Andrew Rayment, Mr Frank Clarke and Mr Andrew Moss. I also wish to express my sincere thanks to Mr David Green, Engineering Department and his team for timely machining some test specimens used in my work.

I shall cherish for long the memory of being with the PT-group and I thank every member of the group for being so friendly with me. I would like to thank especially Dr Mohammed Y. Sherif and Mr Mathew J. Peet for being with me in every difficult situations. All the help from Dr Thomas Sourmail, Dr Richard Kemp, Mr Saurabh Kundu and other group members is also gratefully acknowledged.

The support from Darwin College, including the wonderful accommodation and the good food at the cafeteria, made my life a really enjoyable

one. The association with many friends in the College and the Department has been very beneficial. I would also like to thank Mrs Felicity Higginson and her family for allowing me to exploit the ambience of their home in the later days.

Finally, I wish to record my deep sense of appreciation for my mother and my two sisters and their families for relentlessly supporting me during the entire period, in spite of all their hardship.

Abstract

Despite the presence of high-carbon martensite, TRIP-assisted steels possess large uniform elongation. High-carbon martensite is normally brittle. In this thesis, it has been demonstrated that this apparent anomaly is due to the fine size of the martensite plates.

The mechanical properties of these steels are due to the transformation of retained austenite into martensite during deformation and hence appear to be dominated by the volume fraction and carbon content of retained austenite. These parameters have been related to the chemical composition and heat treatment of the steels with neural networks, using published data.

An optimum alloy was formulated by combining the neural network with a genetic algorithm, to minimise the silicon addition whilst maximising the retained austenite fraction. This resulted in the creation of a radically different microstructure, designated δ-TRIP.

Transformation of austenite into martensite during deformation ceases beyond a critical strain. A theory has been developed to predict this limit. Calculations using the theory indicate that the high-carbon austenite in these steels may transform into martensite due to stress, rather strain.

These materials are often tested for stretch-flangeability, a measure of formability. Neural network analysis of the published data revealed the ultimate tensile strength to be the most important tensile parameter influencing stretch-flangeability.

Contents

Chapter 1

Introduction

The worldwide demand for a reduction in greenhouse gas emissions, better fuel economy and safety in automobiles has led to the development of a variety of steels. In addition to the high strength, these materials can be formed into complex shapes. The steels rely on the transformation of austenite into martensite during deformation for achieving their mechanical properties and hence are known as transformation-induced plasticity (TRIP) steels.

There are two types of such steels. Those having a fully austenitic microstructure are called TRIP steels [Zackay *et al.*, 1967]. These steels tend to be rich in nickel and other expensive austenite stabilising elements. By contrast, austenite is only a minor phase in the overall microstructures of TRIP-assisted steels [Matsumura *et al.*, 1987a; Takechi *et al.*, 1987]. Allotriomorphic ferrite comprises about 50-60 vol.% of the microstructures of these materials, the remainder being a mixture of bainite and carbon-enriched retained austenite. TRIP-assisted steels are generally lean in solute content with only about 0.2 wt% carbon, 1.5 wt% manganese and some 1-2 wt% silicon. It is nevertheless possible to retain copious amounts of austenite in

the microstructure. This is due to the fact that silicon retards cementite precipitation from the untransformed austenite during bainite formation. The carbon that is partitioned into the untransformed austenite following the formation of bainite, stabilises it and allows it to be retained at ambient temperature.

1.1 Scope of the research

As will be evident from the next Chapter, there is a huge amount of published work on TRIP-assisted steels, hardly surprising given their technological implications. At the same time, much of this research is repetitive and has ignored some puzzling issues which are the subject of this thesis.

There is, for example, no theory to describe whether the transformation of the austenite during deformation is a consequence of stress, plastic strain or a combination of these. This is not a trivial issue because the effect of stress is purely thermodynamic whereas plastic strain has an ambivalent influence on martensitic transformation. Defects introduced by deformation may provide heterogeneous nucleation sites for martensite, thereby accelerating the decomposition of retained austenite. In contrast, martensitic transformations involve the displacement of glissile interfaces, which are hindered by dislocation debris created by plastic strain. Indeed, it has been known for a long time that excessive plastic strain can stop martensite from forming by a process of mechanical stabilisation. There is, however, no quantitative theory capable of predicting this phenomenon – to achieve such a description was one aim of the work.

There is much research on the roles of silicon in TRIP-assisted steels,

all of which aims to reduce its concentration to a minimum. This is in order to improve the all-important surface quality, a critical factor in automobile steels. However, attempts at doing this or to replace silicon with aluminium frequently fall foul of the need to retard the formation of cementite during the course of the bainite reaction. The concentrations of silicon-substitutes that can be added are limited by the fact that elements such as aluminium form γ-loops on phase diagrams. At a large enough concentration, it becomes impossible to fully austenitise the steel because of the stability of δ-ferrite.

It was felt at the outset that this fear of δ-ferrite is unjustified since TRIP-assisted steels contain a large amount of allotriomorphic ferrite. The latter could simply be substituted by δ-ferrite, to form a new class of steels, here designated δ-TRIP. This concept was another aim of the work.

A major puzzle which is neglected in published work, is why the formation of untempered, high-carbon strain-induced martensite does not embrittle the TRIP-assisted steels. The solution to this problem is an outcome of this thesis.

Finally, there are many measures of formability quoted in the literature, but development work seems to focus on an empirical product of the ultimate tensile strength and elongation. This makes it very difficult to define how good steel microstructures, which perform well during forming operations, can be developed. The justification for the formability criteria is another feature of the present work.

Chapter 2

TRIP-assisted steels

An overview of TRIP-assisted steels is presented in this chapter. Typical mechanical properties such as proof strength (YS), ultimate tensile strength (UTS), total elongation (TEL), strain-hardening exponent (n) and plastic anisotropy ($\bar{r}$) of various automobile steels are shown in Table 2.1. As can be seen, any increase in strength is in general associated with a loss of ductility. The exceptions are the TRIP-assisted steels, where considerable ductility is obtained in spite of the strength. These promising properties are thought to be due to transformation-induced plasticity.

Steel type	YS / MPa	UTS / MPa	TEL / %	n	$\bar{r}$
Mild 140/270	140	270	38-44	0.05-0.15	1.8
BH 210/340	210	340	34-39	0.23	1.8
BH 260/370	260	370	29-34	0.18	1.6
IF 260/410	260	410	34-38	0.13	1.7
DP 280/600	280	600	30-34	0.2	1.0
IF 300/420	300	420	29-36	0.21	1.6
DP 300/500	300	500	30-34	0.2	1.0
HSLA 350/450	350	450	23-27	0.16	1.0
DP 350/600	350	600	24-30	0.22	1.1
DP 400/700	400	700	19-25	0.14	1.0
TRIP 450/800	450	800	26-32	0.14	0.9
HSLA 490/600	490	600	21-26	0.24	1.0
DP 500/800	500	800	14-20	0.13	1.0
SF 570/640	570	640	20-24	0.14	1.0
CP 700/800	700	800	10-15	0.08	1.0
DP 700/1000	700	1000	12-17	0.13	0.9
Mart 950/1200	950	1200	5-7	0.09	0.9

Table 2.1: Typical mechanical properties of steels for automotive applications [ULSAB-AVC].

2.1 Martensite and TRIP steels

In steels, austenite can transform to ferrite either by a *reconstructive* or a *displacive* mechanism. In reconstructive transformation, all the atomic bonds are broken and the atoms are rearranged into the new form while minimising the overall strain energy. A displacive transformation occurs by a homogeneous deformation of the original crystal structure. Martensitic transformation is displacive and can occur at temperatures where diffusion is inconceivable within the time scale of the process. Transformation starts only after cooling to a particular temperature called *martensite-start temperature* or M_S. The fraction transformed increases with the undercooling

below M_S. A *martensite-finish temperature* or M_f is usually defined as the temperature where 95% of the austenite has decomposed. Unlike M_S, M_f has no fundamental significance.

Martensite can also be induced to form by stress or strain at temperatures above M_S [Scheil, 1932]. The work done by an external stress compensates for the shortfall in the driving force for transformation to occur above M_S [Patel and Cohen, 1953]. The higher the temperature above M_S, the greater is the magnitude of the stress required. However, the strength of the austenite is lower at high temperatures. When the stress required for transformation exceeds the strength of the austenite, plastic strain precedes transformation. This lowers the stress requirement for transformation, as illustrated in Figure 2.1. However, martensite can only form upto a certain maximum temperature limit termed as M_d temperature, above which austenite only deforms plastically.

In steels containing austenite in the temperature range M_S-M_d, the formation of martensite during plastic deformation helps to maintain strain-hardening. This delays the onset of necking, resulting a large uniform elongation. This is why TRIP steels are useful.

The first practical exploitation of TRIP came from Zackay and co-workers who developed steels with dramatically improved elongation, as a consequence of deformation-induced martensitic transformation [Zackay *et al.*, 1967]. However, these alloys contained large concentrations of expensive solutes which restricted their popularity (Table 2.2). The alloys were fully austenitic at ambient temperature.

The elongation obtained can vary with the tensile test temperature

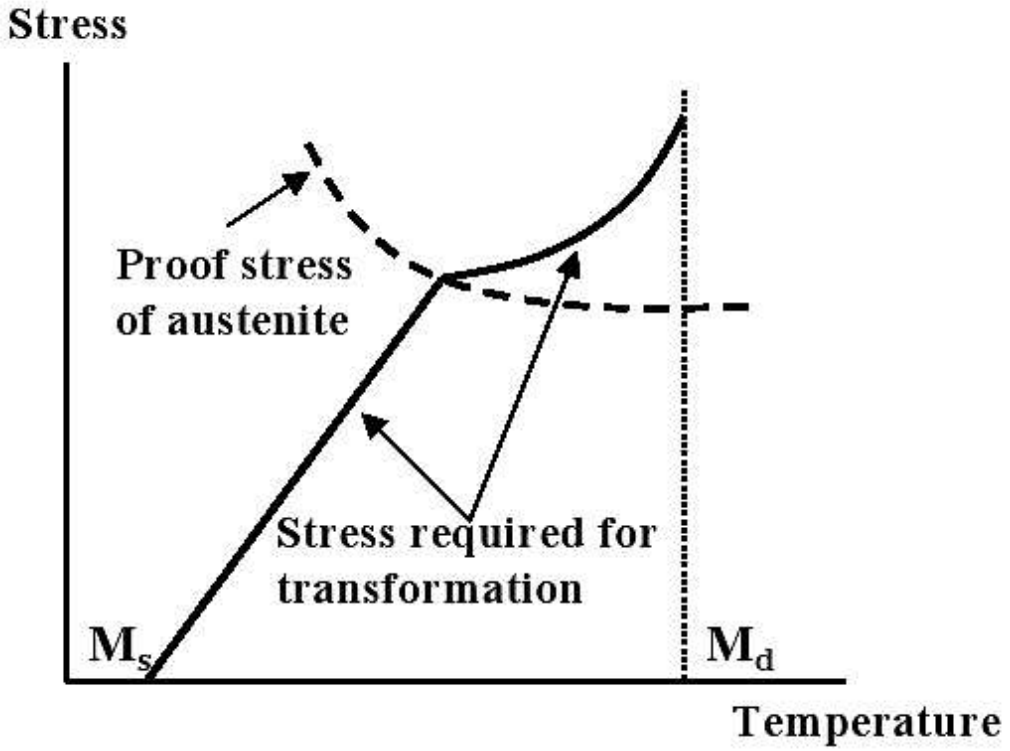

Figure 2.1: Stress requirement for martensitic transformation above M_S increases at higher temperatures; formation of martensite is not possible beyond M_d.

C	Si	Mn	Cr	Ni	Mo
0.31	1.92	2.02	8.89	8.31	3.8
0.25	1.96	2.08	8.88	7.60	4.04
0.25	1.90	0.92	8.80	7.80	4.00
0.25	-	-	-	24.4	4.10
0.23	-	1.48	-	22.0	4.00
0.24	-	1.48	-	20.97	3.57

Table 2.2: Typical chemical compositions (wt%) of early TRIP steels [Zackay *et al.*, 1967].

(Figure 2.2) due to changes in the stability of austenite to martensitic transformation; this is one of the key design issues.

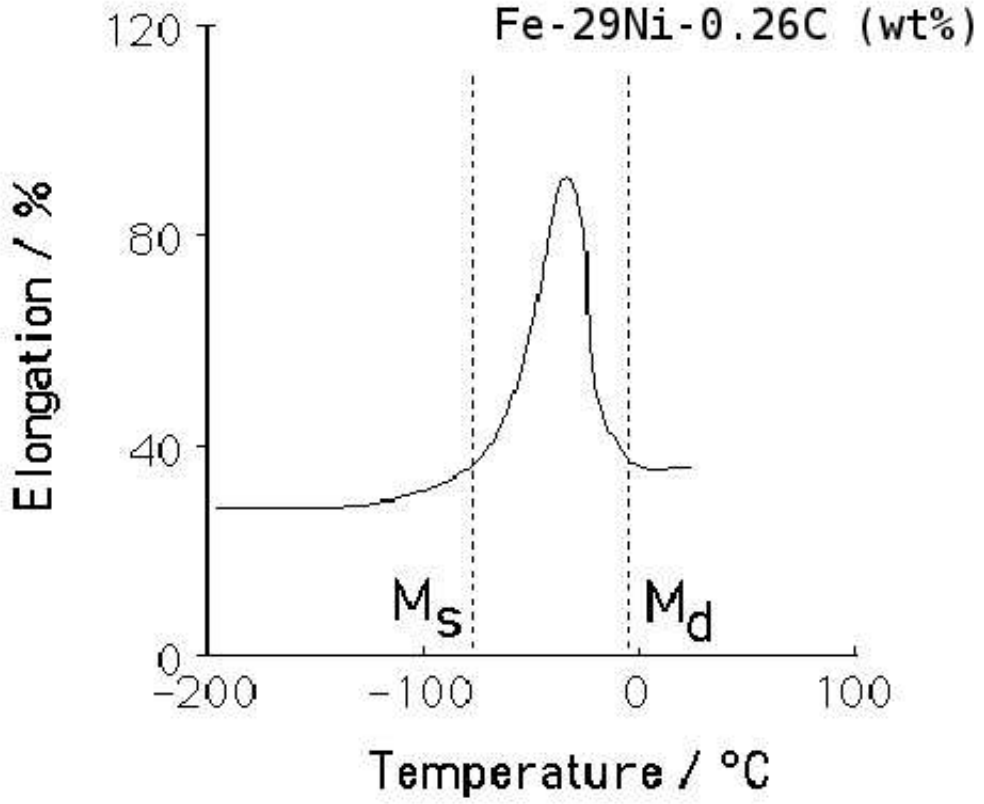

Figure 2.2: Mechanical properties of TRIP steels depend strongly on the test temperature. The elongation shows a maximum at an intermediate temperature between M_S and M_d [Tamura *et al.*, 1970].

2.2 Modern TRIP-assisted steels

In the 1980's, the TRIP effect was demonstrated in low-alloy steels made with 0.2 C, 1-2 Mn and 1-2 Si (wt%) [Matsumura *et al.*, 1987a; Takechi *et al.*, 1987]. The microstructures consisted of 50-60 vol.% allotriomorphic

ferrite, 20-30 vol.% carbide-free bainite, the remainder being high-carbon retained austenite with some martensite, Figure 2.3 [Jacques *et al.*, 2001b]. Such steels are henceforth referred to as TRIP-assisted to distinguish them from fully austenitic TRIP steels.

The TRIP-assisted alloys are lean and hence affordable (Table 2.3). They typically contain only 10-30 vol.% austenite [Hanzaki, 1994; Matsumura *et al.*, 1992; Sakuma *et al.*, 1991a; Sugimoto *et al.*, 1993, 1992a]. The microstructural evolution of these materials is described in the following section.

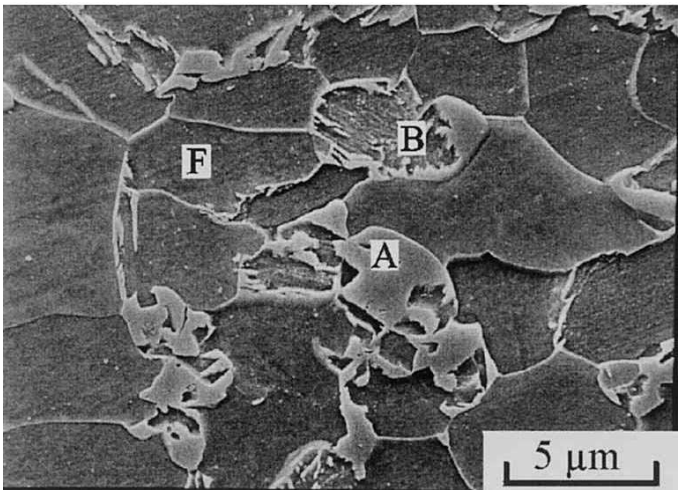

Figure 2.3: A typical multiphase microstructure of a modern TRIP-assisted steel, with allotriomorphic ferrite (F), carbide-free bainite (B) and retained austenite (A) [courtesy of Jacques].

2.3 Microstructural evolution

The microstructure of TRIP-assisted steel can be generated using both hot rolling and cold rolling. Hot rolling is generally carried out at temperatures where the steel is fully austenitic. After rolling, the material is cooled to

C	Si	Mn	Al	P	Nb	Mo	Cu
0.38	1.53	0.83		0.007			
0.18	2.0	1.5	0.037	0.015			
0.19	2.48	1.49	0.036	0.014			
0.11	0.59	1.55	1.5	0.012			
0.14	0.53	1.57		0.204			
0.22	1.55	1.55	0.028		0.035		
0.20	1.47	1.51	0.028	0.004	0.047	0.2	
0.20	1.6	1.6	0.028		0.041	0.3	
0.21	1.49	1.49	0.028	0.005	0.017	0.1	
0.14	1.49	1.51	0.04	0.0012			0.51

Table 2.3: Typical chemical compositions (wt%) of TRIP-assisted steels [Chen *et al.*, 2002; Hanzaki *et al.*, 1995; Hashimoto *et al.*, 2004; Jacques *et al.*, 2001b; Jiao *et al.*, 2002; Kim *et al.*, 2002; Matsumura *et al.*, 1987b; Sugimoto *et al.*, 1992a].

ambient temperature. The cooling rate is controlled so that austenite first transforms to allotriomorphic ferrite and then to bainite. However, a two-stage annealing treatment is required to produce the desired microstructure in cold rolled TRIP-assisted steels (Figure 2.4). The material is initially heated to a temperature in the $(\alpha+\gamma)$[1] phase region generating a mixture of ferrite and austenite, which subsequently decomposes to bainite at a lower temperature.

Austenite is retained in TRIP-assisted steels due to the *incomplete reaction phenomenon* associated with bainitic transformation [Bhadeshia, 2001]. Bainitic ferrite grows without diffusion but excess carbon subsequently partitions into the residual austenite (Figure 2.5). Diffusionless growth can only be sustained at temperatures below T_0, at which ferrite and austenite of identical chemical composition have the same free energy. It follows that in the

[1]The terms α and γ represent ferrite and austenite respectively.

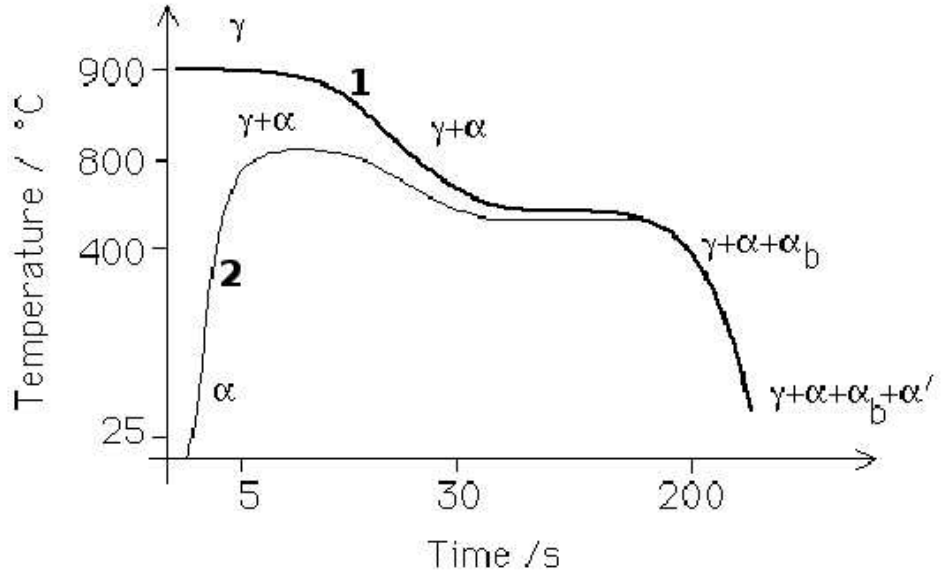

Figure 2.4: Schematic illustration of the two routes to generate the microstructure of TRIP-assisted steel, with typical temperature and time indicated. Curves 1 and 2 stand for the transformation from fully austenitic state after hot rolling and intercritical annealing after cold rolling respectively. The terms γ, α, α_b and α' represent austenite, allotriomorphic ferrite, bainitic ferrite and martensite respectively [Bhadeshia, 2001].

absence of carbide precipitation the bainite reaction stops when the carbon content in austenite equals the T_0' limit (considering the stored energy of bainite), as illustrated in Figure 2.6.

Some elements like silicon, aluminium and phosphorous retard cementite precipitation allowing the carbon to remain dissolved in austenite. The carbon-enriched residual austenite becomes stable against any further martensitic transformation during subsequent cooling [Andrews, 1965], and hence is retained. The pronounced effect of carbon in stabilising austenite is therefore exploited in retaining austenite, thus permitting the concentration of other solutes to be kept to a minimum.

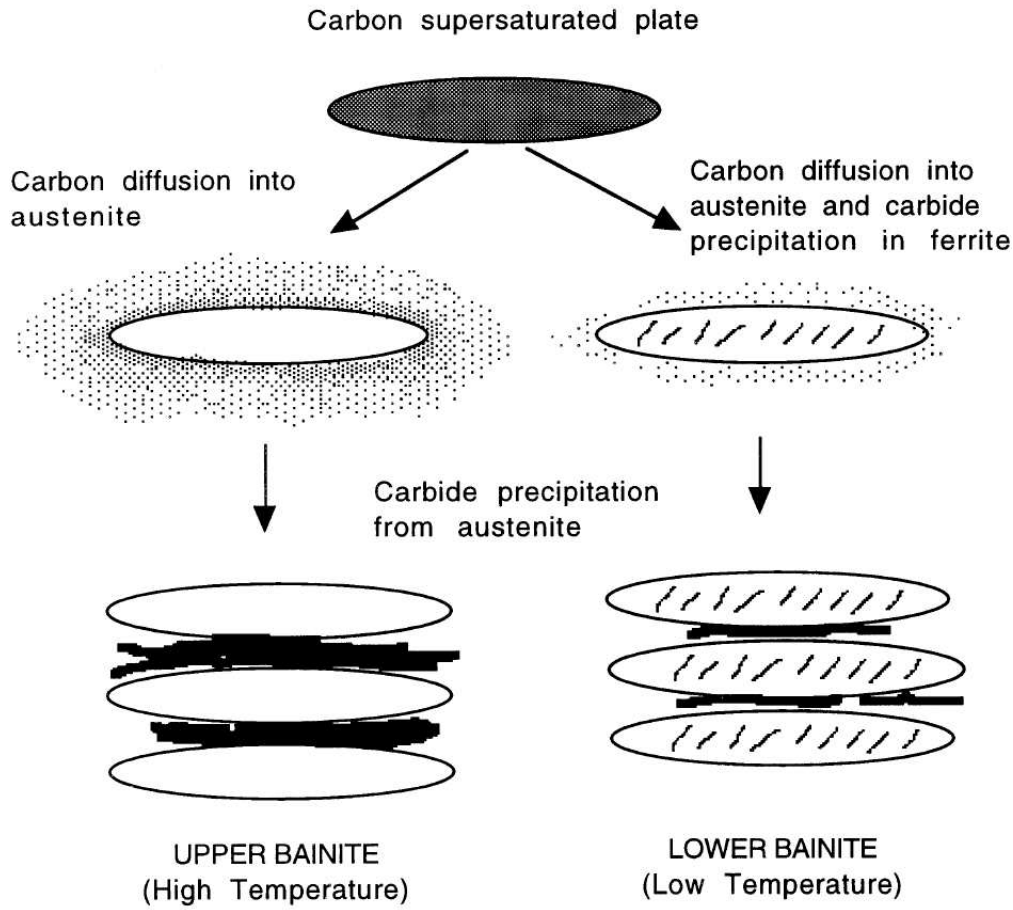

Figure 2.5: Schematic illustration of bainite reaction mechanism [Bhadeshia, 2001].

Microstructural evolution during the isothermal formation of bainite is identical for both hot and cold rolled TRIP-assisted steels. A typical transformation map is shown in Figure 2.7 [Jacques *et al.*, 2001b]. As the bainite reaction progresses, the residual austenite becomes enriched with carbon and gains stability against martensitic transformation during cooling. When the enrichment is inadequate at low holding times, the austenite may decompose partly into martensite during cooling. On the other hand, amount of un-

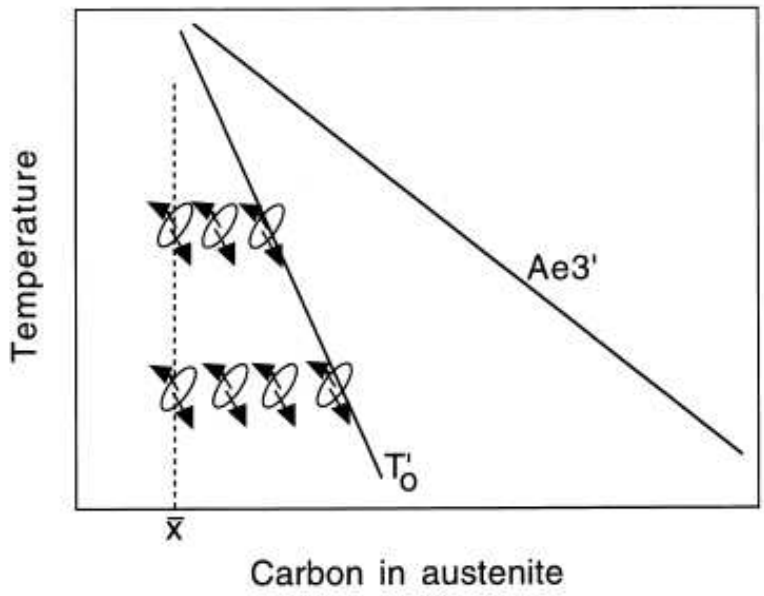

Figure 2.6: The incomplete reaction phenomenon: bainite reaction stops as carbon in austenite approaches T_0' limit, $\bar{x}$ is the bulk carbon content of the steel and A_e3' represents the paraequilibrium $(\alpha + \gamma)$-γ phase boundary [Bhadeshia, 2001].

transformed austenite decreases, as more bainite forms with greater holding time. It follows that the quantity of retained austenite becomes maximum at an intermediate holding time during bainite reaction.

One fascinating aspect of the bainite reaction is the sub-unit mechanism of growth [Bhadeshia, 2001]. In steels containing sufficient silicon or aluminium, bainite forms as an aggregate of ferrite plates separated by untransformed austenite. The individual plates are called *sub-units* while the aggregate is known as a *sheaf* (Figure 2.8). A sheaf of bainite therefore evolves by repeated nucleation of new sub-units predominantly at the tip of the pre-existing ones, rather on their sides.

But such a mechanism may not occur in TRIP-assisted steels because

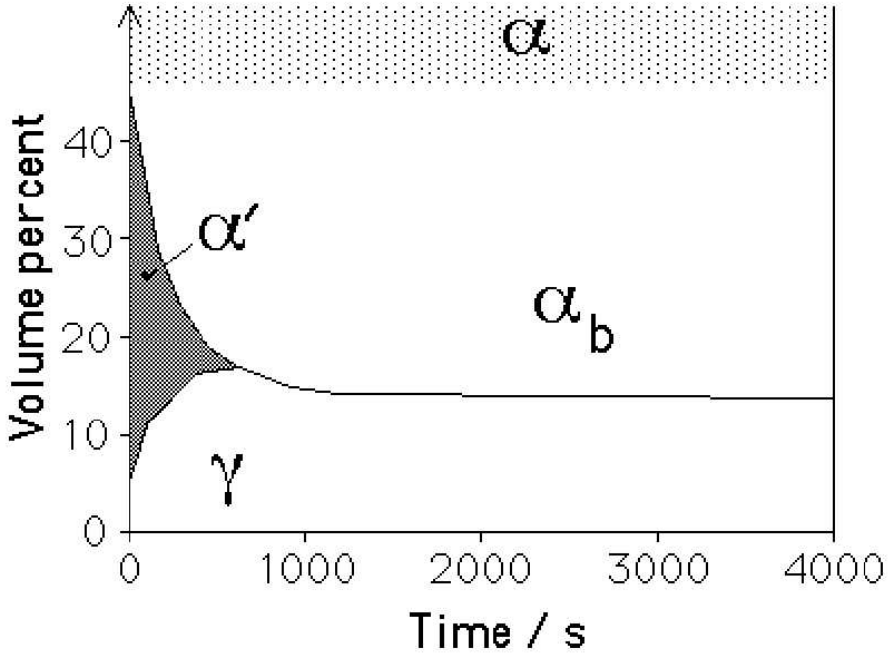

Figure 2.7: Typical microstructural evolution map during the bainite reaction. Retained austenite peaks at an intermediate holding time [Jacques *et al.*, 2001b].

of the size of the available austenite [Jacques, 2003]. Bainite in these steels consists of adjacent platelets that span the whole of the austenite grain (Figure 2.9). This is more likely to be observed in the cold rolled steels subjected to intercritical annealing than in hot rolled materials. Intercritical annealing produces very fine regions of austenite (about 1 μm) so that the space available for the sub-unit mechanism to operate is minimised.

Epitaxial ferrite is also more likely to be present in the microstructures of cold rolled steels than the hot rolled products. After intercritical annealing some ferrite may form during cooling to the bainite transformation temperature. This occurs by the movement of an existing austenite-ferrite boundary *i.e.*, epitaxial growth [Zaefferer *et al.*, 2004].

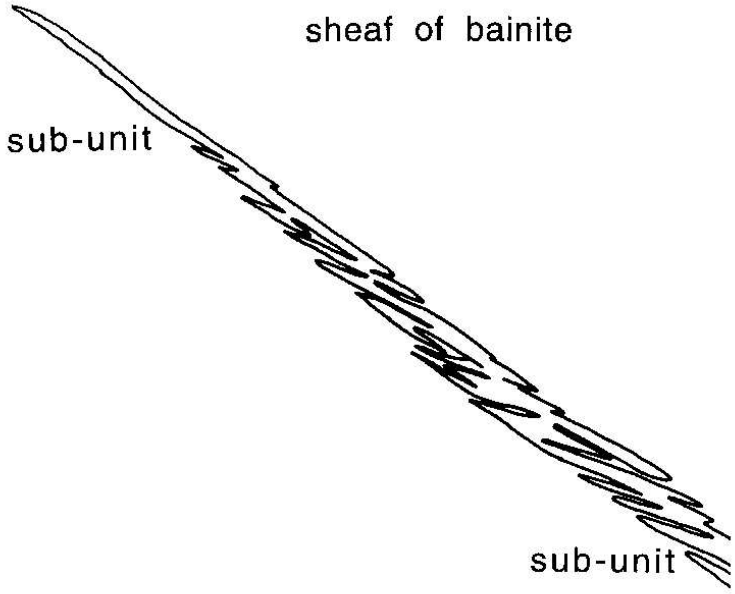

Figure 2.8: Schematic illustration of sub-units and sheaf of bainite [Bhadeshia, 2001].

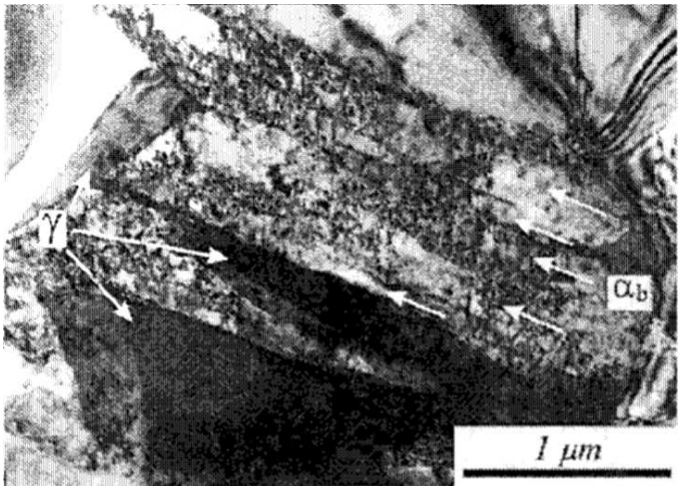

Figure 2.9: Bainite consisting of adjacent ferrite platelets in TRIP-assisted steels [courtesy of Jacques].

2.4 Alloying elements in TRIP-assisted steels

Solutes other than carbon are added for the following reasons:

- to optimise the fraction of retained austenite,
- to control cementite precipitation,
- to increase the hardness of ferrite and
- to increase the hardenability so that pearlite formation can be avoided before bainite reaction.

Carbon, manganese and silicon

Like carbon, manganese is an austenite stabiliser. Silicon although a ferrite stabiliser, helps to retain carbon-enriched austenite by suppressing cementite precipitation from austenite. Silicon also solid-solution strengthens ferrite and hence can enhance the overall strength of the steel.

An increase in manganese may compensate for any reduction in silicon [Sakuma *et al.*, 1991a; Shi *et al.*, 2002], but this shifts the T_0 curve to lower carbon concentrations, thereby limiting the amount of bainite that can form. Additionally, pronounced banding may occur in steels containing a large manganese concentration [Kim *et al.*, 2001].

Aluminium and phosphorous

Both aluminium and phosphorous inhibit cementite precipitation and hence can substitute for silicon [Mintz, 2003]. However, unlike silicon, aluminium does not strengthen ferrite. Steels in which silicon is replaced by aluminium may therefore be weaker [Girault *et al.*, 2001; Jacques *et al.*, 2001a].

Phosphorous, on the other hand, strengthens ferrite [Pichler *et al.*, 1998]. An addition of 0.1 wt% phosphorous leads to an increase of about 75 MPa in the strength of ferrite [Pickering, 1978].

Niobium and Molybdenum

Niobium in solid solution is reported to increase the quantity of retained austenite [Hanzaki *et al.*, 1995; Pereloma *et al.*, 1999]. The reason is not clear, as niobium is known to be a ferrite stabiliser. Fine precipitates of niobium carbides and complex NbMoC precipitates can also strengthen the ferrite [Hashimoto *et al.*, 2004].

Molybdenum is a solid solution strengthener of ferrite and retards pearlite formation. In low-silicon steels, its addition can lead to mechanical properties comparable to high-silicon steels *viz.* ultimate tensile strength in excess of 1000 MPa with a total elongation of about 36% [Bouet *et al.*, 1998a,b].

Copper

Copper, being an austenite stabiliser, helps to retain austenite [Im *et al.*, 2000a; Kim and Lee, 1999]. Besides solid solution strengthening, ϵ-Cu precipitates in ferrite can boost the overall strength [Kim *et al.*, 2002]. Thus copper can be thought to replace silicon in both the roles of retaining austenite and increasing strength of ferrite.

Boron

Small concentrations of boron are known to significantly improve hardenability. Boron-containing low-silicon steels have been found to contain sufficient

retained austenite and display a sensitive TRIP effect [Sadhukhan *et al.*, 2001].

2.5 Mechanical performance

TRIP-assisted steels are reputed for the superior uniform elongation compared to other similarly strong steels like dual phase steels. The latter with microstructures of 10-15 vol.% low carbon (C $<$ 0.3 wt%) martensite dispersed in ferrite have high strength [Rashid, 1979a,b]. But these steels lacked formability. Traces of untransformed retained austenite in the microstructures of these steels were indeed thought to enhance the ductility through TRIP effect [Goel *et al.*, 1985; Kim, 1988; Rao and Rashid, 1983; Sangal *et al.*, 1985].

As noted by Hassani and Yue [1999], TRIP-assisted steel can be imagined to be a modification of the dual phase steel. Substantially greater quantities of retained austenite in TRIP-assisted steels yielded even greater elongation (Figure 2.10), as compared to dual phase steels.

However, the TRIP-assisted steel does not seem to exhibit continuous yielding unlike the dual phase steel (Figure 2.10). Continuous yielding is advantageous in forming operations as this helps to avoid stretcher strain or *Lüder bands*. The gradual yielding of dual phase steels is mainly due to the free dislocations present in the ferrite grains. Formation of bainite, instead of martensite, in TRIP-assisted steels is not very effective to induce free dislocations in ferrite, resulting discontinuous yielding [Sakuma *et al.*, 1992]. It may be possible to avoid this by allowing some martensite to form during cooling after the isothermal formation of bainite [Choi *et al.*, 1988]. The dis-

continuous yielding of the intercritically annealed cold rolled TRIP-assisted steels could also be due to the strain ageing of ferrite at the temperature where bainite forms [Choi *et al.*, 1988]. The ageing of ferrite can occur due to the difference in the solubility of the interstitial solutes at the intercritical annealing temperature and the bainite formation temperature.

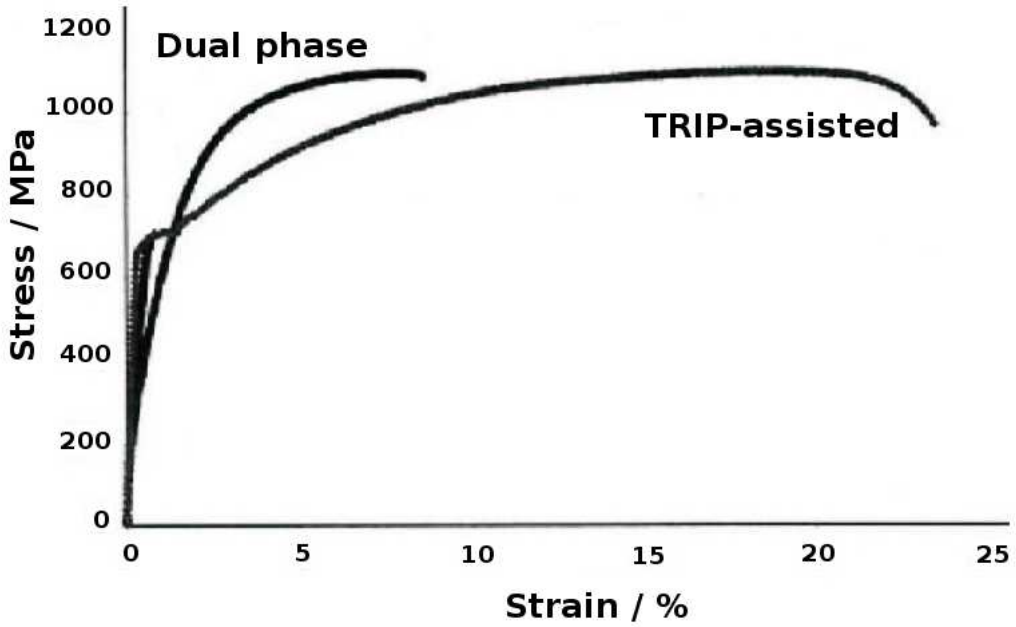

Figure 2.10: Superior elongation observed in a TRIP-assisted steel compared to a dual phase steel with similar strength level [Hassani and Yue, 1999].

The large uniform elongation in TRIP-assisted steels is mainly attributed to the strain-induced martensitic transformation of retained austenite. However, the transformation strains themselves can contribute at most 2% to the observed elongation given the small fraction of austenite present in these materials [Bhadeshia, 2002]. Other phases in the microstructure must also influence the overall mechanical behaviour. An interesting consequence of the strain-induced martensitic transformation of austenite has been

revealed by Jacques *et al.* [2001c]. The volume expansion due to martensitic transformation generates dislocations in adjacent ferrite (Figure 2.11). Freshly produced dislocations in the ferrite phase can then take part in the deformation process.

Martensite that forms in these steels inherits the high carbon content of the austenite. It is surprising that the freshly produced high-carbon martensite does not impair the ductility. Carbon embrittles martensite, a fact that seems to have been ignored in explaining the properties of these materials.

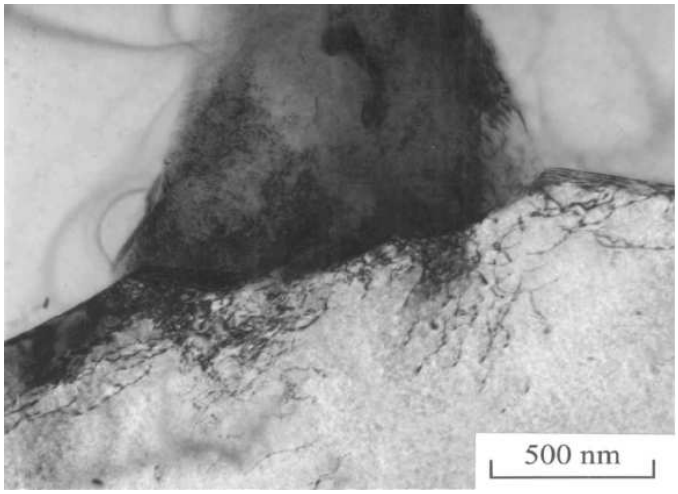

Figure 2.11: Dislocations generated in ferrite due to transformation of austenite during deformation [courtesy of Jacques].

2.6 Factors affecting performance

There are many factors that have been thought to control the mechanical properties of these steels, as summarised in this section.

2.6.1 Proportion of phases

TRIP-assisted steels consist of allotriomorphic ferrite, bainitic ferrite, retained austenite with or without traces of martensite. As reported by Choi *et al.* [2002], a high volume fraction of retained austenite improves elongation as well as the ultimate tensile strength of the steel (Figure 2.12).

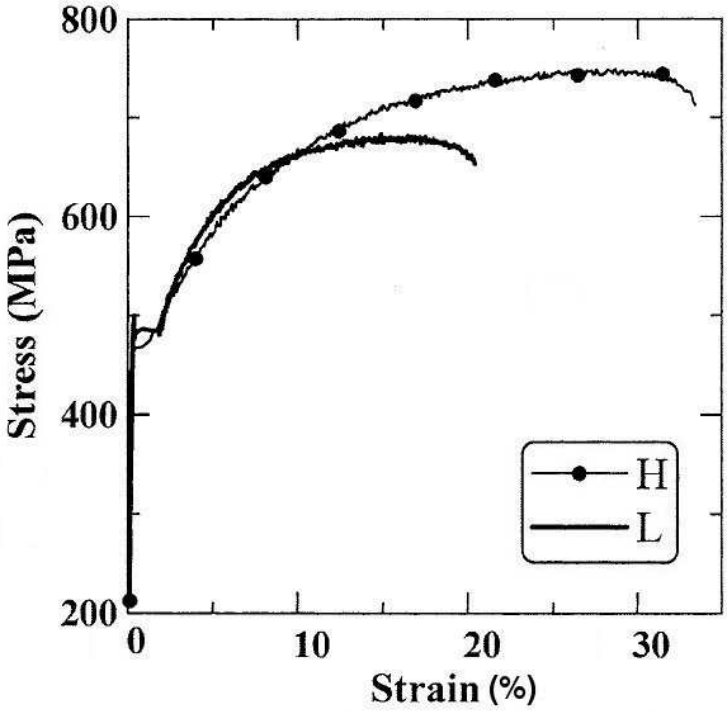

Figure 2.12: Higher UTS and uniform elongation obtained with H-type sample as compared to L-type, H-type sample contains higher austenite volume fraction than the L-type [Choi *et al.*, 2002].

However, a high retained austenite volume fraction implies less bainite which may adversely affect the strength. Similarly, high ferrite fraction during intercritical annealing finally results in less bainite, leading to a reduction in strength [Imai *et al.*, 1992].

Aluminium-containing steels contain more ferrite as compared to steels relying on silicon [Monohar *et al.*, 2002, 2003]. This is because in aluminium-containing steels, austenite starts transforming into allotriomorphic ferrite at a higher temperature and with a faster kinetics than in steels made with silicon [Manohar *et al.*, 2002]. A high ferrite fraction in the microstructure can reduce the overall strength of a steel made with aluminium.

Steels with reduced silicon content have been shown to possess properties similar to high-silicon steels by Jacques *et al.* [2001b]. This is due to the presence of some martensite in the low-silicon material.

It seems, phases other than retained austenite can influence the mechanical behaviour of these steels. However, most of the research has been focussed on the TRIP effect due to the strain-induced transformation of austenite.

2.6.2 Stability of retained austenite

The rate at which austenite transforms during deformation appears to be the highly emphasised factor affecting the properties. The austenite stability should be such that it transforms progressively during deformation, so that damage can be accommodated at all stages of deformation.

Increasing carbon content of austenite lowers the driving force for martensitic transformation. It is known that after isothermal bainite transformation, retained austenite is not homogeneously enriched with carbon [Schrader and Wever, 1952]. Regions in the vicinity of the bainite sheaves or the films of austenite trapped between bainite are rich in carbon. This may even lead to the observation of two different lattice parameters of austenite

formed in the same sample [Matas and Hehemann, 1961]. So austenite areas that are depleted of carbon, transform first during deformation. It follows, with increasing plastic strain, untransformed austenite may be observed to have a greater lattice parameter, because of the larger carbon content as shown in Figure 2.13 [Itami *et al.*, 1995].

Besides the carbon content, austenite stability can be also enhanced by a fine grain size. High stability of the retained austenite with fine grain size, dispersed in a ferritic microstructure obtained after intercritical annealing, was reported long back by Rigsbee [1979]. This is due to the absence of substructures in the austenite, for example stacking faults and other defects, that provide nucleation sites for martensitic transformation. Austenite in TRIP-assisted steels exists in two forms, isolated austenite grains in ferrite away from the bainitic phase and films of austenite in-between bainitic ferrite plates. The latter type of austenite is generally observed to be more stable during deformation than the former types [Basuki and Aernoudt, 1999; Koh *et al.*, 1998; Sugimoto *et al.*, 1993]. It is thus thought that isolated small austenite grains dispersed in ferrite actually contribute to the TRIP effect. This is illustrated in Figure 2.14.

By micromechanical modelling, Reisner *et al.* [1998] showed that the tendency for strain-induced transformation depends on the orientation of the austenite grains. Austenite with a random texture behaves similarly to the average of the sharp texture components.

The mechanical stability of retained austenite during deformation also seems to depend on the hardness of the other phases. The hardness increases in the order ferrite, bainite, austenite and martensite [Furnemont *et*

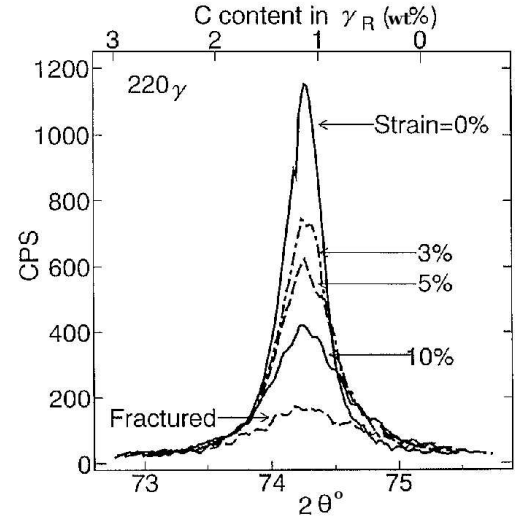

(a)

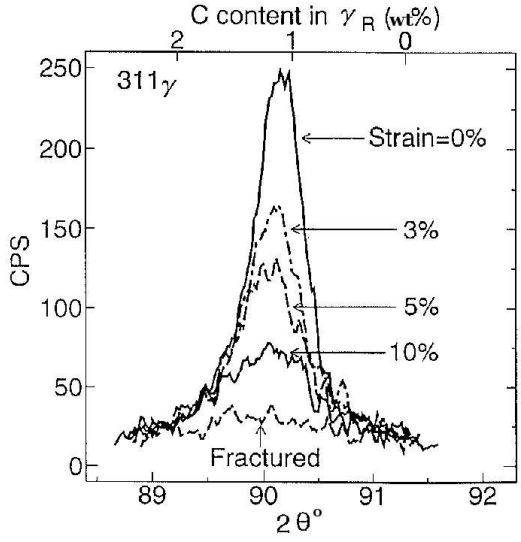

(b)

Figure 2.13: With increasing plastic strain, volume fraction of austenite decreases along with the increase in carbon content, which is apparent from the shift in the positions of the austenite, γ_R, peaks [Itami *et al.*, 1995].

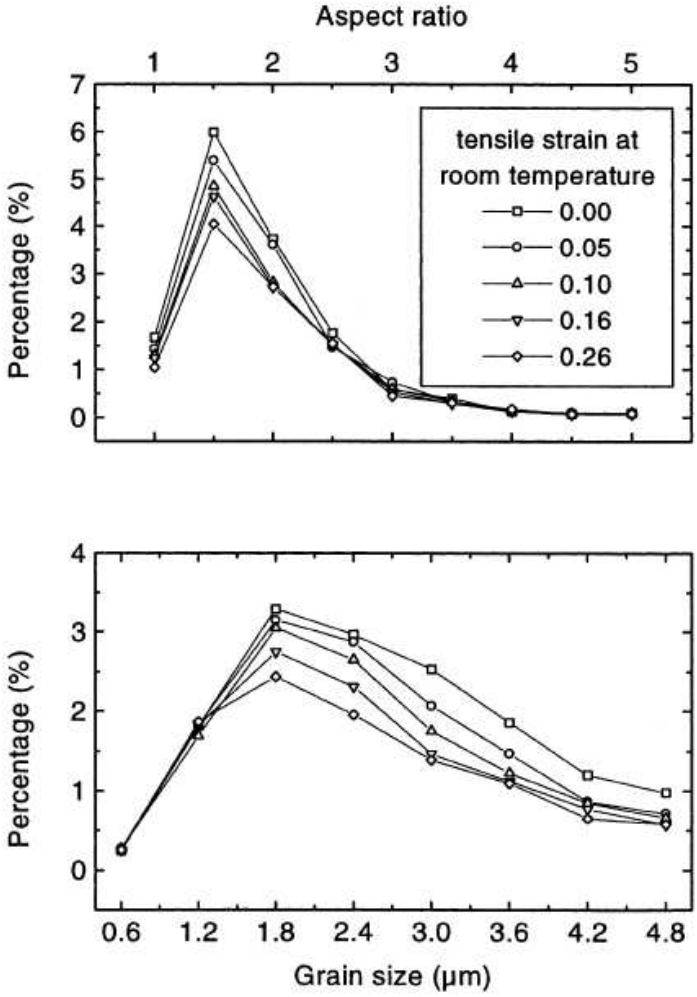

Figure 2.14: Effect of grain size and morphology of austenite on its stability, retained austenite with an aspect ratio larger than 2.5 and grain size finer than 1.2 μm remains unchanged with increasing tensile deformation [Basuki and Aernoudt, 1999].

al., 2002]. An increase in the hardness of ferrite will obviously delay the transfer of stress to the austenite and hence the onset of TRIP. This is the basis of the *composite effect* as proposed by Jacques *et al.* [2001d]. Steels with reduced silicon content are generally low in retained austenite fraction.

Nevertheless, it is possible to achieve favourable properties in these steels due to the presence of martensite strengthening the matrix hence delaying the onset of TRIP effect.

It follows that any increase in the hardness of the matrix phase can be beneficial for the mechanical properties. This is consistent with the promising properties of the steels containing phosphorus or copper, that strengthen the ferrite matrix. However, any increment of matrix strength may not always be beneficial. Sakuma *et al.* [1991b] showed that increasing carbon content from 0.1 wt% to 0.4 wt%, increases the volume fraction and stability of retained austenite. But this reduces the ferrite content, thereby increasing strength with an associated loss in ductility. This, of course, removes any advantage associated with TRIP steels.

Similarly, aluminium-containing steels may be expected to have inferior properties as compared to silicon containing steels due to softer ferrite matrix. However, due to higher carbon enrichment in the retained austenite, steels based on aluminium instead of silicon achieve better properties [De Meyer *et al.*, 1999a,b].

2.6.3 Test parameters

Temperature

Higher temperature increases the stability of austenite against martensitic transformation due to reduced driving force for transformation. Temperature can therefore exert a significant influence on the mechanical properties (Figure 2.15).

The ultimate tensile strength and total elongation, unlike the yield

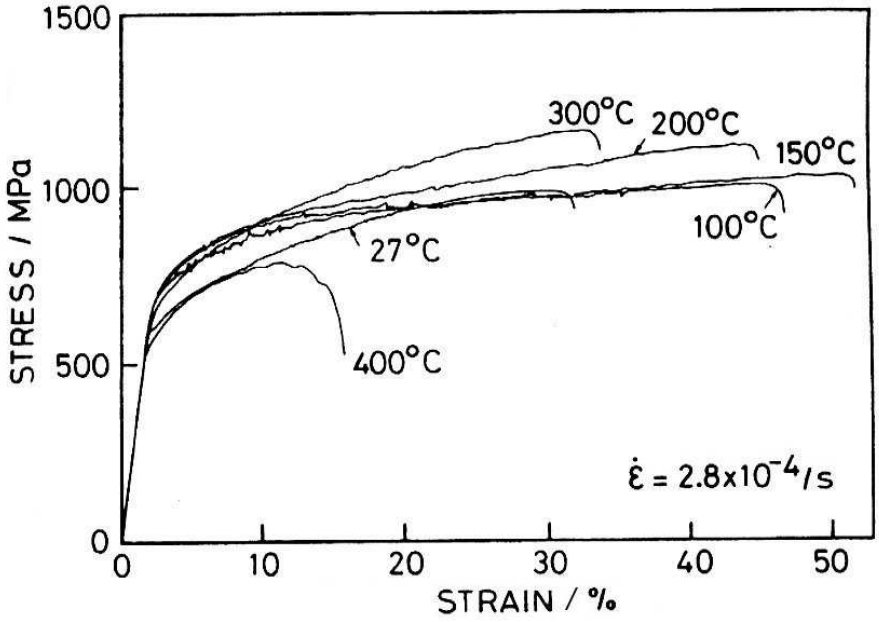

Figure 2.15: Effect of test temperature on the flow curve of TRIP-assisted steels [Sugimoto *et al.*, 1992b].

strength, appear to vary much more strongly with temperature. However, the properties seem to improve only upto a certain maximum temperature [Sugimoto *et al.*, 1993, 1992a]. This is consistent with the observed behaviour of the classical TRIP steels with a fully austenitic microstructure, as mentioned earlier.

Modern TRIP-assisted steels possess a multiphase microstructure, only 10-30 vol.% of which is austenite. The strength and elongation of the individual phases are also very likely to depend on the test temperature. These may all influence the temperature dependence of the overall mechanical properties. This aspect appears to have not been considered in understanding the mechanical behaviour of these steels.

Strain rate

Figure 2.16 shows the influence of the strain rate on the nature of the flow curves at different temperatures. An intermediate strain rate appears to maximise elongation, consistently at all the testing temperatures.

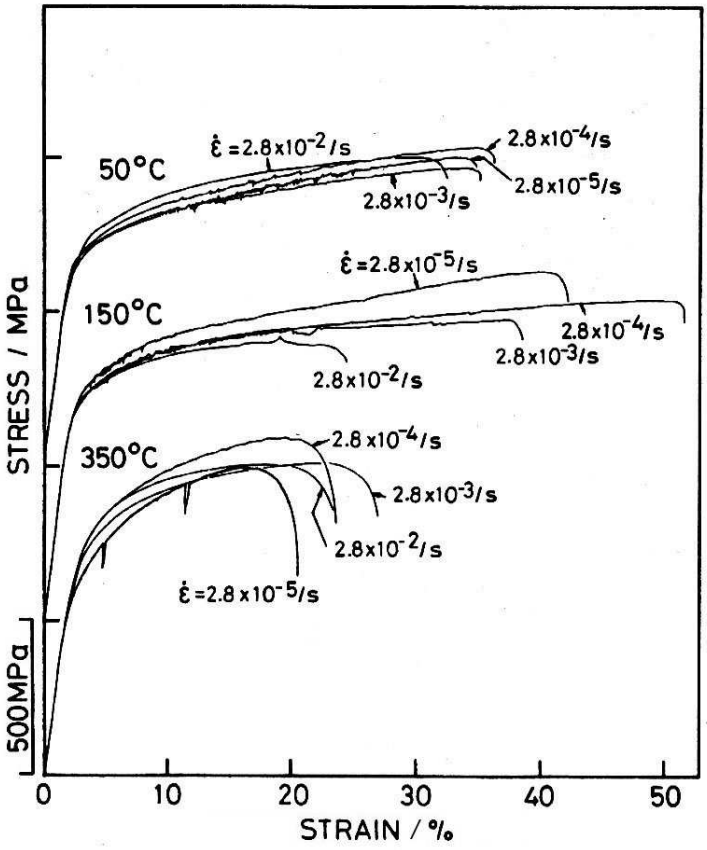

Figure 2.16: Effect of strain rate on the nature of the flow curve at different test temperatures [Sugimoto *et al.*, 1992b].

High strain rate tensile testing is often referred to as *dynamic mechanical testing*. The volume fraction, size, distribution and morphology of retained austenite have all been shown to affect the dynamic mechanical properties [Wei *et al.*, 2003]. Increasing strain rate from 10^{-3} to 2.5×10^{2} s^{-1}

raises both yield strength and ultimate tensile strength while the strain-hardening behaviour remains almost the same, as reported by Choi *et al.* [2002].

2.6.4 State of stress or strain

Unlike uniaxial tension or compression, deformation-induced martensitic transformation is always known to be suppressed by hydrostatic pressure. The stability of the austenite can therefore be enhanced by applying hydrostatic pressure during tensile test, resulting higher uniform elongation [Pyshmintsev *et al.*, 2002]. This may be important in hydroforming operations. Retained austenite in such a case would not be fully consumed during forming, thereby allowing the TRIP effect to be utilised for crash-worthiness in finished components.

Strain-induced martensitic transformation is retarded under plain-strain conditions relative to uniaxial loading [Im *et al.*, 2002]. This is due to lower applied stress and strain under plane-strain condition. By contrast, under biaxial stretching, the transformation is promoted relative to uniaxial testing, although the results vary with the sample orientation relative to the rolling direction [Streicher *et al.*, 2002]. This may be related to the texture of austenite grains [Reisner *et al.*, 1998].

To summarise, the strain-induced transformation of retained austenite has been considered to be the major factor influencing the mechanical performance. This is despite the fact that these steels possess multiphase microstructures, some 10-30 vol.% of which is only retained austenite. A moderately stable austenite appears to be the key to optimise ductility. Among

many factors, carbon content of the retained austenite influences its stability. Therefore not only the fraction of austenite, but also its carbon content appears to be a salient microstructural feature controlling the properties. It is best to have the austenite transforming progressively during deformation. The kinetics of this transformation has been a subject of much research, as described in the following section.

2.7 Strain-induced martensite formation

The martensitic transformation of austenite during deformation may occur due to stress or strain (Figure 2.1). The progress of strain-induced transformation is illustrated in Figure 2.17. Rapid transformation at first is due to the nucleation sites introduced by the deformation. However, an excessive strain can retard the transformation, eventually bringing it to a halt. This latter phenomenon is known as *mechanical stabilisation*, a characteristic feature of displacive transformations. By contrast, the effect of stress is purely thermodynamic.

There are several empirical models for the strain-induced transformation. One of these was proposed by Olson and Cohen [1975] to model the experimental data reported by Angel [1954],

$$f^{\alpha'} = 1 - \exp[-\beta\{1 - \alpha\epsilon\}^n] \tag{2.1}$$

where $f^{\alpha'}$ is the volume fraction of martensite obtained at a strain ϵ. The model contains two temperature dependent parameters, α and β. The former depends on the stacking fault energy of the steel, which in turn is affected by

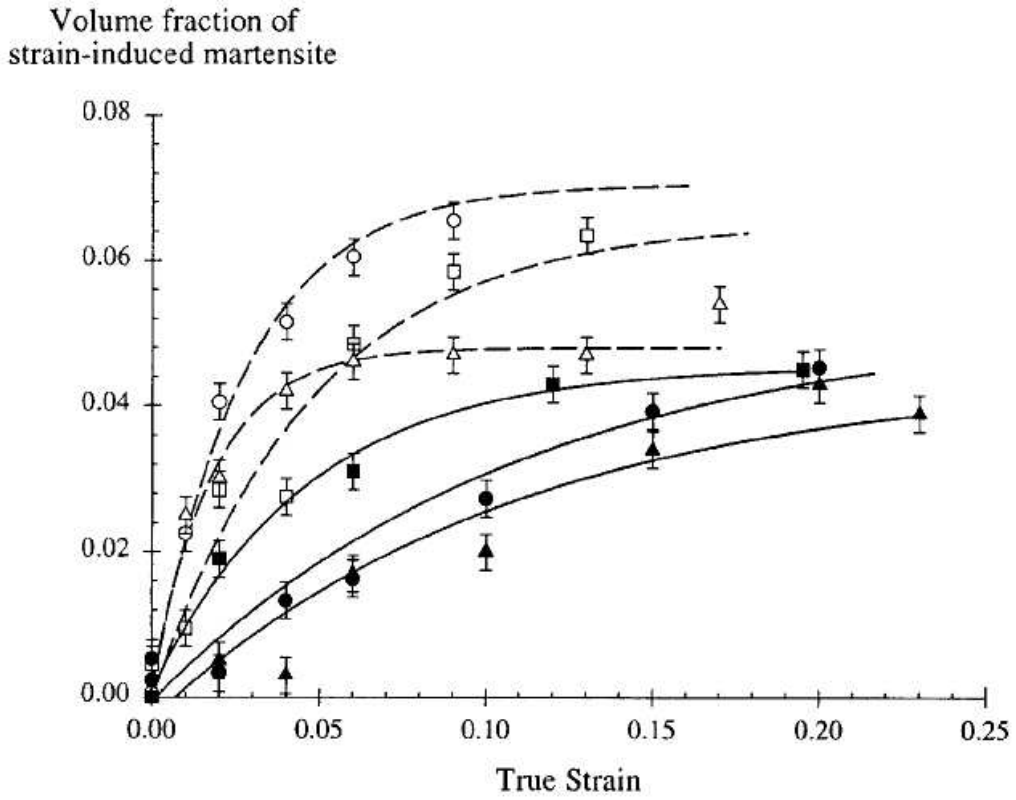

Figure 2.17: Kinetics of the strain-induced martensite formation, each curve represents a steel with different carbon content of the retained austenite [Jacques *et al.*, 2001c].

temperature. β defines the probability that a shear-band intersection creates a nucleation site, and therefore can be thought to depend on the chemical driving force, hence temperature. However, the exponent n in the model comes from fitting to experimental data. A value of 4.5 is appropriate for the steels studied by Angel.

Guimaraes [1972] studied a group of Fe-Ni-C alloys and proposed a similar exponential fit:

$$f^{\alpha'} = 1 - \exp(-k\epsilon^Z) \tag{2.2}$$

with empirical constants $k = 28$ and $Z = 3.7$.

A different parabolic type of dependence was proposed by Gerberich *et al.* [1970]:

$$f^{\alpha'} = A_2 \epsilon^{1/2} \tag{2.3}$$

where A_2 is an empirical constant.

As can be seen, none of these models include volume fraction of austenite and therefore exclude any possible interaction between the parent and the transformed phases. Angel [1954] and Ludwigson and Berger [1969] considered this and proposed the following model:

$$f^{\alpha'} = A_1 \epsilon^B V_\gamma \tag{2.4}$$

where A_1 and B are constants, with $B = 3$ for stainless steels.

All these models are formulated on the basis of the experimental data for fully austenitic steels. The strain-induced transformation of retained austenite in TRIP-assisted steel has been expressed by Sugimoto *et al.* [1992b] as

$$\ln(V_\gamma^0) - \ln(V_\gamma) = k\epsilon \tag{2.5}$$

where V_γ^0 is the original retained austenite volume fraction and V_γ is the volume fraction of the untransformed austenite at a plastic strain ϵ. The empirical constant k must be measured for each steel.

A novel way of describing strain-induced transformation of retained austenite in these TRIP-assisted steels has been proposed by Sherif *et al.* [2004], a development of the model of Sugimoto *et al.* [1992b]. The fraction of untransformed austenite is expressed as a function of plastic strain,

deformation temperature, chemical composition and the original amount of austenite. The final equation is given as,

$$ln(V_\gamma^0) - ln(V_\gamma) = k_1 \Delta G^{\alpha'\gamma} \epsilon \tag{2.6}$$

where k_1 takes a value of 0.002017 J mol^{-1}, independent of the steel composition.

All these models explain adequately the kinetics of strain-induced formation of martensite. But none takes into account the possibility of mechanical stabilisation at large plastic strains.

2.8 Special properties

2.8.1 Formability

Formability is defined as the ease with which an object having a complex geometry can be manufactured using the material. This can approximately be related to plasticity or ductility which tends to deteriorate with increasing strength. TRIP-assisted steels are unique in this respect, they exhibit better formability than several other steels of comparable strength [Konieczny, 2003; Sugimoto *et al.*, 1996].

Formability is not assessed by a single attribute but expressed as a combination of properties such as deep drawability, stretch formability, stretch flangeability and bendability. The state of stress is different in each of these forming operations, as illustrated schematically in Figure 2.18.

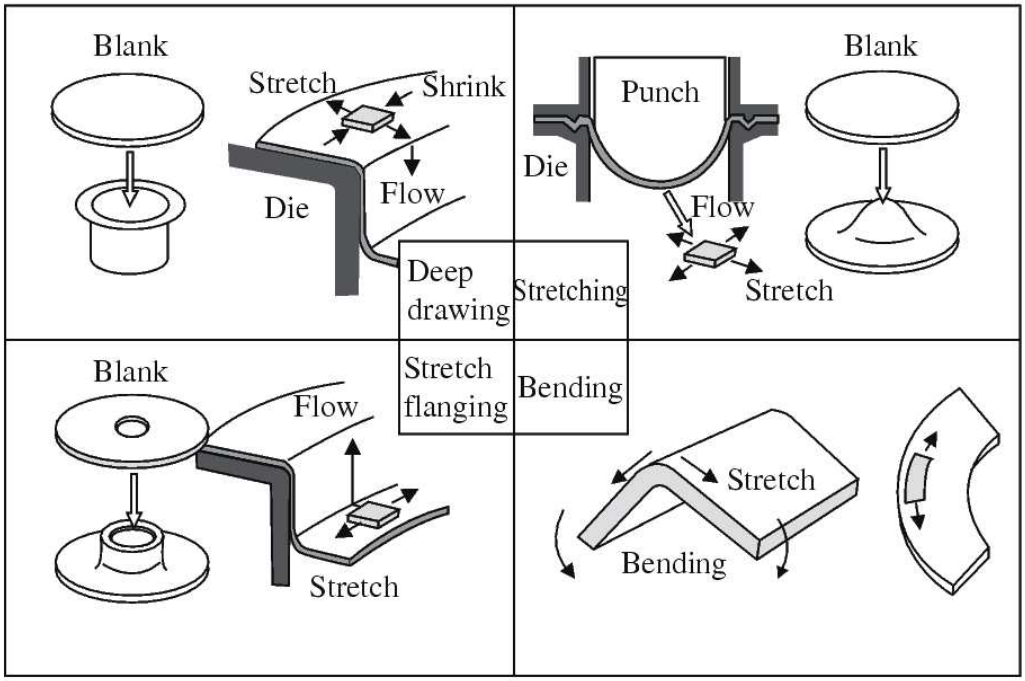

Figure 2.18: State of stress existing during different modes of forming operations [Takahashi, 2003].

Deep drawability

This is expressed by the Lankford parameter or r value, the ratio of true strain in the width direction to that in thickness direction. $\bar{r}$ is the average of r values measured on specimens obtained at different directions, namely at 0°, 45° and 90° to the rolling direction. A higher $\bar{r}$ value leads to better deep drawability. TRIP-assisted steels exhibit good deep drawability [Hiwatashi *et al.*, 1994; Nagasaka *et al.*, 1999a,b], due to the retarding influence of the hydrostatic pressure generated during the drawing operation on the strain-induced transformation of austenite.

Stretch formability

In this test, rectangular blanks marked with circular grids on the surface by electrochemical etching method are deformed under a punch until local fracture occurs. This is also sometimes referred to as Limiting Dome Height test [Im *et al.*, 2000b; Lee *et al.*, 2004, 2002a]. After the test, the circular grids turn into oval shape. The strain values on the major and the minor axes are measured and used to construct a Forming Limit Curve.

The maximum stretch height and the maximum stretch load are also measured. Good stretch formability is expressed by a high stretch height and a low stretching load [Sugimoto *et al.*, 1995; Sugimoto and Kobayashi, 1994]. Microstructures with isolated retained austenite islands in ferrite away from bainite have better stretch formability than networks of austenite.

Stretch flangeability

Stretch flangeability is a more complex property assessed by a two step process *viz.* (a) hole punching and (b) hole expanding [Sugimoto *et al.*, 1999]. A hole is first punched on the steel blank and then allowed to expand until cracks appear on the surface. The ratio of the increase in diameter of the hole to the original diameter is measured in this test.

The key to superior stretch flangeability is to maintain a high level of untransformed retained austenite on hole punching, with a large ductility through TRIP effect on hole expanding. Thus, stretch flangeability is mainly controlled by the stability of the retained austenite rather its volume fraction [Sugimoto *et al.*, 1999]. Carbon content and morphology of retained austenite as well as the temperature of operation are reported to have significant influence on stretch flangeability [Nagasaka *et al.*, 1996, 1998].

2.8.2 Crash-worthiness

One of the key requirements for automobile steels is crash-resistance. In a crash scenario, the strain rate may well exceed 250 s^{-1} and the prevailing state of stress or strain may be much more complex than uniaxial tension. Static and quasi-static tensile tests performed with a slow strain rate of about 0.005 s^{-1} are therefore not sufficient. Servo-hydraulic testing system, Split Hopkinson Bar, pneumatic tensile impact tester, dynamical tensile tests on impact loading, crash tests on welded double hat-shaped specimens are some examples of testing procedures for crash-resistance assessments [Wei *et al.*, 2003; Yan and Xu, 2003, 2002].

TRIP-assisted steels, like all other steels, exhibit a positive strain-rate sensitivity index, which means that an increase in strain rate increases the flow stress but elongation is reduced. However, superior elongation has been reported for TRIP-assisted steels even at high strain rate [Uenishi *et al.*, 2000; Wei *et al.*, 2002a,b], presumably due to the TRIP effect. A comparison on crash-worthiness of different types of steels can be found in Figure 2.19 [Uenishi *et al.*, 2000]. With crash-worthiness justified properly, these steels can be used as front or rear door side-impact bars in a passenger car.

2.8.3 Fatigue resistance

The importance of fatigue resistance is obvious for a steel to be used in automobile components that are routinely subjected to cyclic loading [Yan, 2002]. Prestraining has been identified to be the most effective factor increasing fatigue strength.

Fatigue strength increases significantly in steels having an allotriomor-

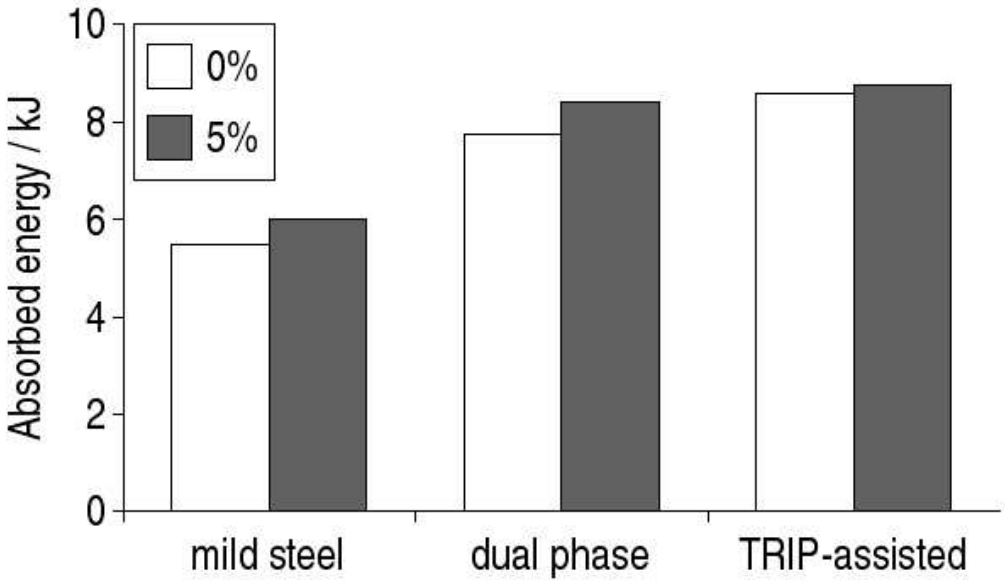

Figure 2.19: Superior crash-worthiness of TRIP-assisted steels compared to other types, the steels are tested with a prestrain of 0% and 5% in each case [Uenishi *et al.*, 2000].

phic ferrite matrix when compared to bainitic steels with retained austenite [Song *et al.*, 2003, 2001]. This is because of the higher compressive stress in the matrix of the former type of materials due to the strain-induced transformation of the retained austenite during prestraining.

Dual phase steels are known to exhibit high fatigue strength. Figure 2.20 illustrates comparable fatigue limit of TRIP-assisted steels with dual phase steels [Takahashi, 2003]. Besides solid solution hardening of ferrite with silicon, compressive residual stress due to the martensitic transformation during cyclic loading can act as an extra advantage in TRIP-assisted steels. These materials therefore appear to play a significant role in modern automobiles with lighter body weight but adequate safety.

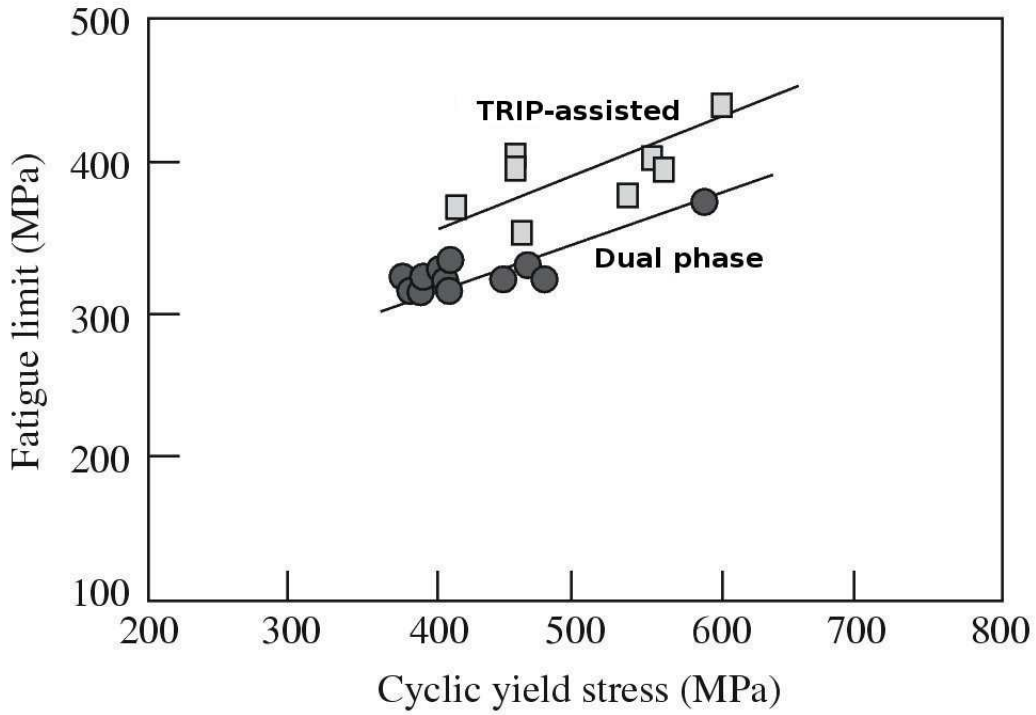

Figure 2.20: Effect of cyclic yield stress on fatigue limit of dual phase and TRIP-assisted steels [Takahashi, 2003].

2.8.4 Bake hardening

Bake hardening refers to the increase in strength of a steel sheet as a result of thermal ageing at an elevated temperature after a small amount of pre-straining. This offers a practical advantage of boosting the strength level of a formed component during the process of paint baking.

A nominal increase of about 25 MPa strength has been reported in each of two TRIP-assisted steel grades of 0.2C-1.5Si-1.5Mn (all in wt%) with and without 0.5 wt% addition of copper [Wang *et al.*, 2004]. After the baking treatment at a temperature of 170°C for 1200 s, some retained austenite transforms to bainite with simultaneous increase in carbon content of the

untransformed austenite. Retained austenite in these steels has indeed been shown to undergo decomposition into a mixture of ferrite and cementite when exposed to high temperature [Sugimoto *et al.*, 1992b]. The increase in strength expected from the increase in carbon content of retained austenite has been observed to negate the decrease in strength due to the loss of austenite forming bainite. The bake hardening has thus been ascribed to the ferritic matrix of these steels.

2.9 Limitations

The attractive mechanical properties of TRIP-assisted steels make them suitable for the manufacture of new-generation passenger cars. However, there are many problems encountered during the processing of these materials due to the high silicon content.

Use of thinner gauge sheets of high-strength steels in automobile components necessitates protection against corrosion using zinc coatings through hot-dip galvanising process [Mintz, 2001]. This consists of dipping the steel in a molten zinc bath maintained at a temperature of around 450°C, at which iron and zinc share great affinity and allow an alloy to form, whereas pure zinc prevails at the surface. The final product is a steel surface protected with a zinc coating.

The cold rolled sheets are initially heated to a temperature in the (α+γ) phase region. This is followed by another dwelling at a lower temperature of some 400°C. In between these two stages, the sheet is passed through a molten zinc bath for galvanising. A typical process cycle is depicted in Figure 2.21.

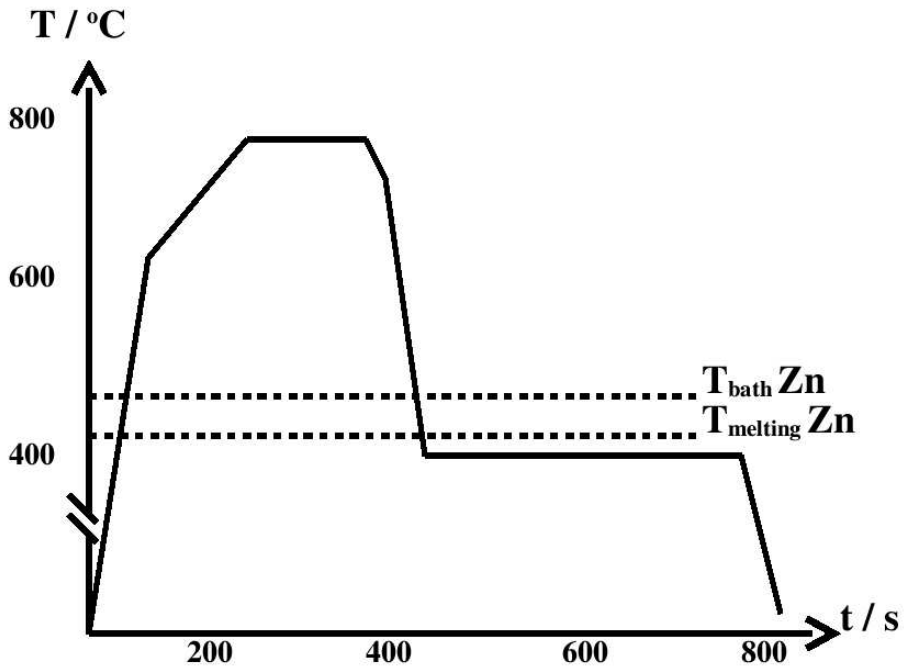

Figure 2.21: Schematic illustration of a typical continuous galvanising line.

Silicon causes problems during the galvanising operation [Mahieu *et al.*, 2002b; Mintz, 2001; Pichler *et al.*, 2003, 2002]. The intercritical annealing is carried out in a furnace maintained with low oxygen partial pressure before hot-dip galvanising. Under this condition, iron does not get oxidised but silicon can still be oxidised preferentially. This gives rise to a sheet surface with poor wetability in molten zinc.

Silicon also affects the nature of the surface scale formed in a hot rolled material. During hot rolling, the steel is exposed to air at high temperature. This leads to surface oxidation. Normally the oxide layer consists mainly of FeO. But in TRIP-assisted steels, the surface scale changes to complex oxides such as Fayalite (Fe_xSiO_y). This reduces the surface quality and affects the rolling properties adversely by changing the friction coefficient.

Silicon is added in these steels mainly to inhibit cementite precipitation during bainite formation. This can also be achieved by adding aluminium or phosphorous instead of silicon. Materials have therefore been developed replacing silicon partly or fully by aluminium or phosphorous [De Meyer *et al.*, 1999a,b; Girault *et al.*, 2001; Jacques *et al.*, 2001a; Pichler *et al.*, 1998]. Phosphorous however imposes the risk of embrittlement due to grain-boundary segregation. This probably restricts its addition to some 0.2 wt% maximum in these steels.

Substitution of silicon with aluminium helps by modifying the surface oxide [Mahieu *et al.*, 2002b, 2001a; Maki *et al.*, 2001]. Aluminium-containing steels exhibit better wetabilitiy than those made with silicon after processing in a furnace with low dew point prior to galvanising [Maki *et al.*, 2003]. The dew point of the annealing atmosphere affects the rate of oxidation of the elements segregated to the surface and thereby exerts an influence on wetability.

2.10 Other variants

Silicon-containing steels with fully bainitic microstructures possess retained austenite which transforms to martensite during deformation. Therefore these alloys also rely on TRIP for the properties. The properties are excellent despite the presence of austenite mainly as thin films interspersed with bainitic ferrite [Bouet *et al.*, 2000]. This is not in accordance with the advantage associated with the fine granular austenite in contrast to the thin films of austenite as observed for the conventional TRIP-assisted steels [Basuki and Aernoudt, 1999; Koh *et al.*, 1998; Sugimoto *et al.*, 1993].

Exciting combination of mechanical properties has also been reported by Sugimoto *et al.* [2004] in fully bainitic steels containing carbon in the range of 0.1-0.6 wt% and 1.5 wt% each of silicon and manganese. Mechanical behaviour of these steels were investigated at different temperatures. In the temperature range 0°C to 75°C, development of mechanical properties has been mainly ascribed to the TRIP effect. However, in the temperature range 200°C to 300°C, steels containing carbon in excess of 0.4 wt% showed strain-induced bainitic transformation and dynamic strain-ageing, rather than strain-induced formation of martensite.

Steels with fully bainitic microstructures have been found to display better stretch flangeability than the conventional TRIP-assisted steels [Sugimoto *et al.*, 2002a, 2000]. Further enhancement of the properties has also been observed in steels with annealed martensite as the matrix phase [Sugimoto *et al.*, 2002b].

2.11 Summary

Modern TRIP-assisted steels are lean in chemical composition. Nevertheless, it is possible to retain some 10-30 vol.% of austenite in ferrite-rich microstructures of these alloys. This is achieved by exploiting the fact that addition of silicon or aluminium helps inhibiting the precipitation of cementite during bainite formation and hence allows carbon to remain dissolved in the untransformed austenite. Silicon, however, degrades the surface quality of the product and also makes the processing difficult, due to the formation of adherent surface scale. Replacing silicon by aluminium is thus generally thought as a practical solution to make these steels.

The steels record superior uniform elongation, compared to dual phase steels of similar strength, and hence are suitable for the manufacture of cars with lighter body weight yet adequate safety. However, TRIP-assisted steels are generally found to suffer from discontinuous yielding unlike dual phase steels.

The large uniform elongation of TRIP-assisted steels is mainly attributed to the strain-induced transformation of the retained austenite into martensite. Retention of austenite in these alloys is due to the carbon enrichment. Martensite that forms also inherits the high carbon content of the austenite and should therefore be brittle. This does not reconcile with the remarkable elongation observed in these steels.

The rate of strain-induced transformation of austenite appears to be the key to optimise ductility of these materials. The stability of austenite should be such that it transforms into martensite progressively during deformation. Carbon content of the retained austenite, among many other factors, influences its stability. Therefore, not only the volume fraction of retained austenite but also its carbon content appears to be salient in controlling the properties. It is therefore important to understand the variation of these parameters as function of the processing conditions and chemical compositions of these steels.

Role of plastic strain in austenite on subsequent transformation into martensite is ambivalent. Strain creates defects that can act as additional nucleation sites for transformation. However, an excessive defect density due to large plastic strains can inhibit the growth of martensite plates, ultimately leading the transformation to a halt. This is called mechanical stabilisation.

The properties of TRIP-assisted steels are generally thought to rely on the strain-induced transformation of austenite. Hence it is essential to understand if there is any contention of mechanical stabilisation in these steels. However, there exists no quantitative theory for predicting the onset of mechanical stabilisation.

These steels are often subjected to different complex tests for assessing formability. The results are often interpreted in terms of the strength-elongation product but without proper justification. There has been no proper attempt in understanding the relationship between the forming properties and the tensile properties.

Chapter 3

Brittle martensite

Modern TRIP-assisted steels are generally believed to rely on stress or strain-induced martensitic transformation of retained austenite to achieve properties. The carbon concentration of the retained austenite is usually in excess of 1 wt%. Martensite that forms in these materials inherits the high carbon content of austenite and remains in freshly produced untempered condition. This is therefore expected to be brittle, but the mechanical properties, especially formability, of these materials are nevertheless impressive. This does not reconcile with the apparent brittleness of the high-carbon martensite. The purpose of work presented in this chapter is to explain this contradictory behaviour.

3.1 Hypothesis

Martensite that forms from the high-carbon austenite in the TRIP-assisted steels actually exists in a composite microstructure. This can be imagined to be similar to a uniaxially aligned, discontinuous, brittle-fibre composite

material, with the brittle martensite plates embedded in a ductile austenite matrix. During loading, axial stress is transmitted from the matrix into the fibre via shear loading of the cylindrical surface of the fibre, τ, [Cox, 1952].

This load transfer causes the tensile stress in the fibre to rise to a maximum value, σ_P, half way along the length of the fibre. If σ_P exceeds the fracture strength, σ_F, then the fibre breaks. However, if the fibre is short, end effects prevent the maximum stress in the fibre from reaching σ_F. The fibre then remains intact. The critical fibre length below which it does not fracture is designated l_C. Fibres longer than l_C tend to break into segments of length l_C.

It is proposed here that load transfer into the hard martensite becomes similarly difficult as the scale of the martensite in a relatively soft matrix decreases. In other words, the martensite will not crack easily if its size is reduced below some critical value. Naturally, work-hardening comes into this scenario so that sufficient load should eventually be transferred into the martensite to cause fracture. However, the stage at which this occurs ought to be delayed when the martensite is fine.

3.2 Experiments

Material and heat treatment

A steel with the chemical composition of Fe-0.98C-1.46Si-1.89Mn-1.26Cr-0.26Mo wt% was selected. The bulk composition of the alloy represents the high-carbon austenite, hence the martensite, that exists in the modern TRIP-assisted steels. The alloy was homogenised at 1200°C for 48 h. Cylindrical

samples of length 12 mm and diameter 8 mm were made out of this steel and sealed in quartz tubes containing a partial pressure of argon for heat treatment in an air furnace.

The sealed samples were austenitised at 1200°C, 1100°C, 1000°C and 950°C for 10 minutes in order to generate a range of austenite grain sizes for subsequent transformation into martensite during quenching in water. Another set of samples was cooled slowly by switching off the furnace following the same austenitising conditions. This was done in order to obtain a clear definition of the austenite grain boundaries. One more sample was heated to 1200°C for 10 minutes followed by soaking at 950°C for another 10 minutes before finally quenching to room temperature.

Metallography

Cross sections of the quenched samples were polished using standard metallographic techniques. They were then examined in unetched states using optical microscopy to characterise any cracks. The distances between adjacent cracks in the individual plates of martensite were measured using a graticule fitted to the microscope.

The quenched samples were etched using 10 wt% aqueous sodium metabisulfite solution to reveal the martensitic microstructures. The apparent martensite plate lengths measured on two-dimensional sections were determined in a similar way as the distance between cracks.

The furnace cooled samples were etched with boiling alkaline sodium picrate solution (made with 2 g picric acid, 25 g NaOH and 100 mL distilled water) to reveal the austenite grain size as a function of the austenitising temperature; the size was characterised using the lineal intercept ($\overline{L}$) method.

3.3 Results and discussion

Etched surfaces of the quenched samples revealed the dark-etched lenticular plates of martensite with untransformed regions of austenite, as presented in Figures 3.1-3.4. A significant amount of untransformed austenite can be seen in each sample. This is due to the high carbon content of the alloy.

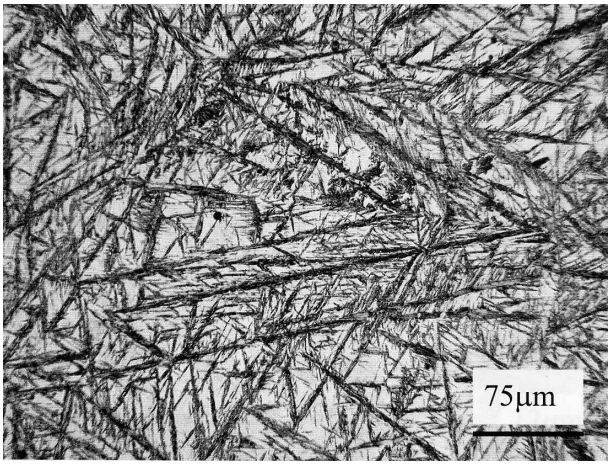

Figure 3.1: Micrograph of the sample quenched after austenitising at 1200°C.

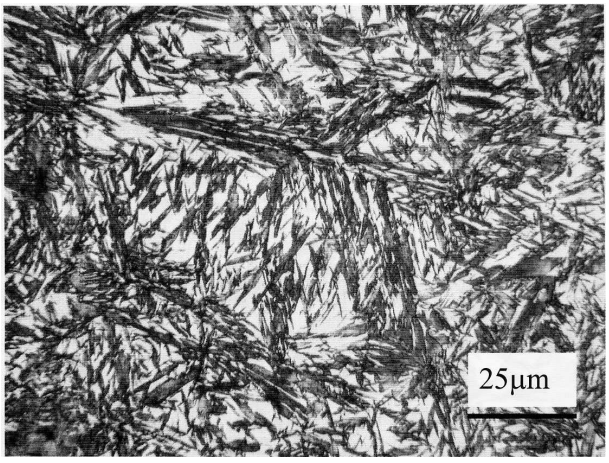

Figure 3.2: Micrograph of the sample quenched after austenitising at 1100°C.

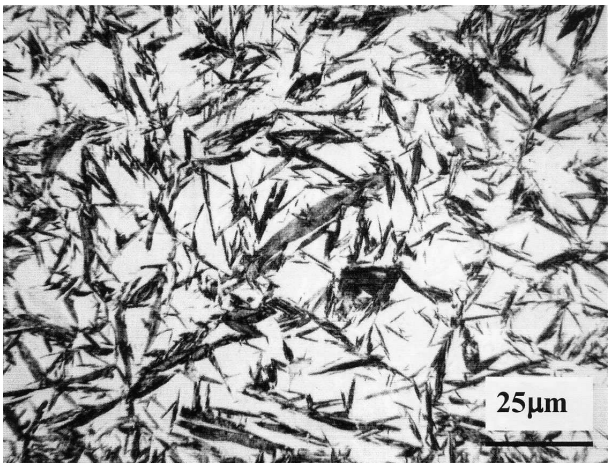

Figure 3.3: Micrograph of the sample quenched after austenitising at 1000°C.

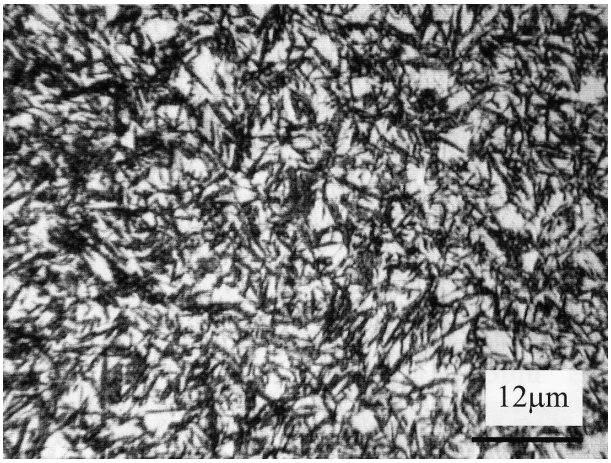

Figure 3.4: Micrograph of the sample quenched after austenitising at 950°C.

Martensite plates exist with a distribution of plate lengths in each of the samples. Growth of the initial plates is restricted only by the austenite grain boundaries, while those formed subsequently are also stopped by the pre-existing plates. New plates forming during the progress of transformation therefore tend to be finer than the earlier ones, the coarsest ones in each sample being given by the prior austenite grain size. The microstructures of

these samples therefore get refined at lower austenitising temperatures that lead to finer prior austenite grain sizes (Table 3.1).

Austenitising temperature (°C)	Mean lineal intercept (μm)	% Error
1200	410	13
1100	124	20
1000	65	18
950	25	26

Table 3.1: Variation of austenite grain size with austenitising temperature, error represents $\pm 1\sigma$.

Quenched samples in the polished but unetched conditions were examined using an optical microscope to observe any cracks. Samples austenitised at 1200°C and 1100°C revealed cracks across the coarser plates in periodic arrays. In general, the finer plates were found to be less susceptible to cracking. Only a few isolated cracks were observed in the sample quenched from 1000°C and the plates, in general, were observed to be singly-cracked. The sample quenched from 950°C was found to be free of any cracks. Micrographs obtained from the polished and the etched surfaces of the samples quenched from 1200°C and 1000°C are presented in Figures 3.5 and 3.6 respectively.

The cracking of the martensite plates observed in these experiments is presumably due to the quench stresses. These stresses might be thought to increase with higher austenitising temperatures and thus could affect the observation. To eliminate any possible role of this differential quench stresses, one sample was austenitised at 1200°C for 10 minutes and soaked at 950°C for another 10 minutes before finally quenching in water. Similar microcracks as the sample directly quenched from 1200°C were also observed in this sample, as depicted in Figure 3.7.

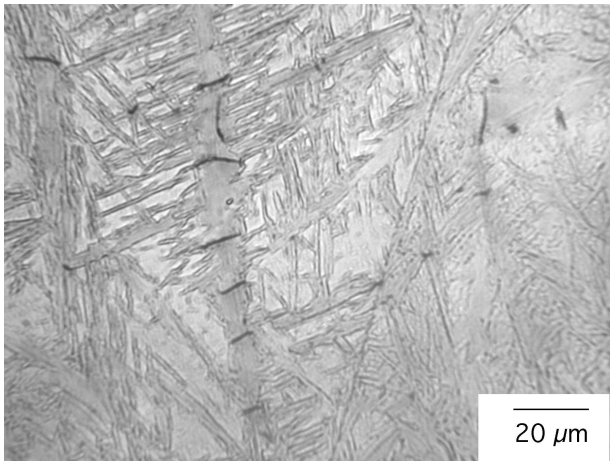

(a)

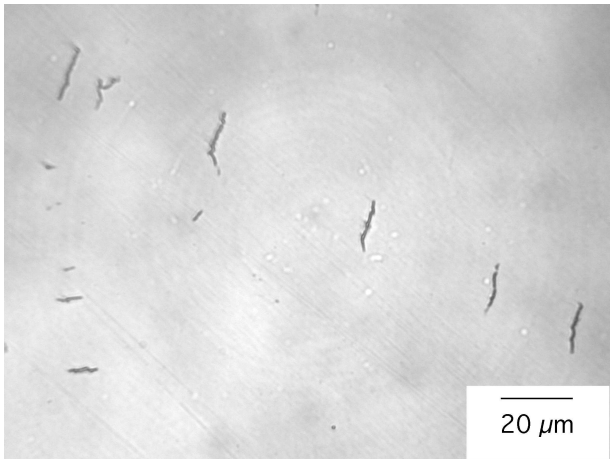

(b)

Figure 3.5: Microcracking in the sample austenitised at 1200°C: (a) etched sample; (b) periodically cracked plate in unetched sample.

The apparent distances between two adjacent cracks in individual fragmented plates of martensite in the samples austenitised at 1200°C and 1100°C were measured using optical metallography. These measurements follow a distribution as depicted in Figure 3.8. The distances are designated l_a to

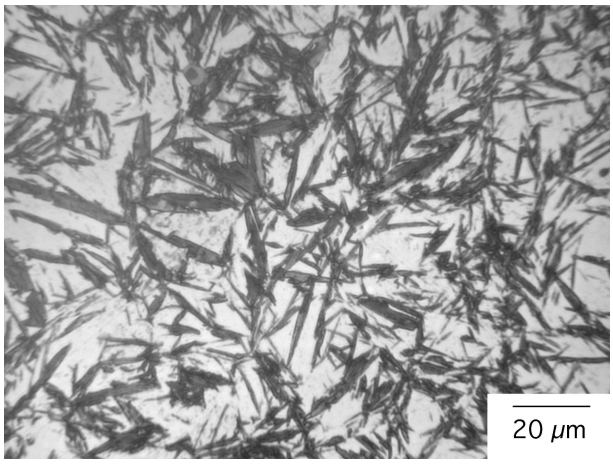

(a)

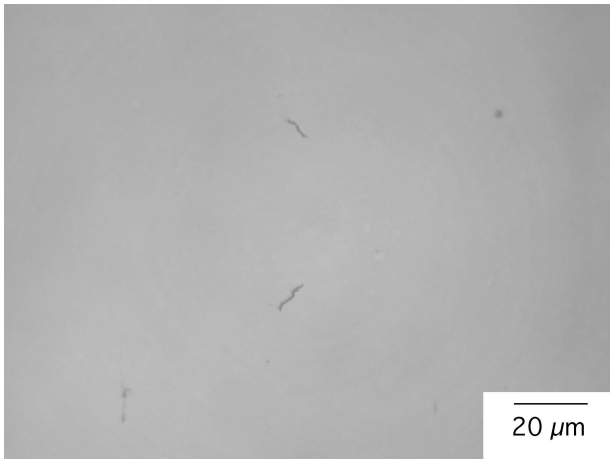

(b)

Figure 3.6: Microcracking in the sample austenitised at 1000°C: (a) etched sample where cracks are difficult to detect; (b) occasional cracks visible in unetched sample.

emphasise that they are apparent measures because stereological effects are not taken into account. The mean values for these measurements were found to be $\overline{l}_a = 58\,\mu$m and $\overline{l}_a = 38\,\mu$m for the samples austenitised at 1200°C and

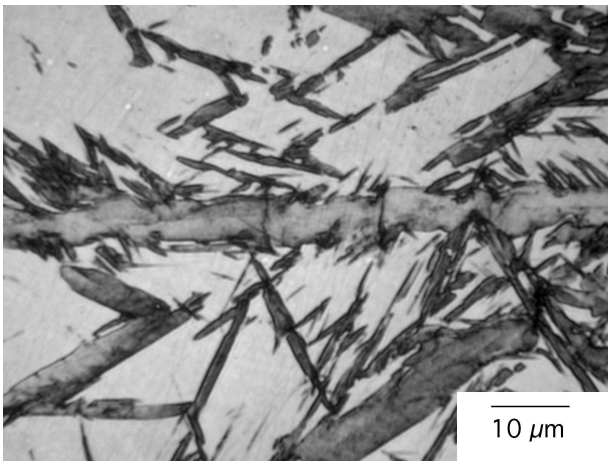

Figure 3.7: Microcracking in the sample austenitised at 1200°C and soaked at 950°C before quenching.

1100°C respectively.

The minimum value observed in all the measurements, within experimental error, was found to be $\simeq 10\,\mu$m. This is more relevant than the mean value in the present context. If it is assumed that the critical stress transfer length $l_C = 10\,\mu$m, then an austenite grain size which is somewhat less than this value would avoid quench cracking of the type explored in this work. One difficulty is that cracks were not detected in the T_γ =950°C sample with a prior austenite grain size of $25\,\mu$m, which is greater than l_C. It is possible that the cracks exist but have been missed because the sample contains few plates of length greater than l_C. Therefore, the plate length distributions were also measured for each sample.

The apparent lengths of approximately 180 martensite plates from each sample were measured using optical metallography. In all cases the plates were chosen at random by arbitrarily translating the stage across a cursor which identified the plate to be measured. The size distributions are illus-

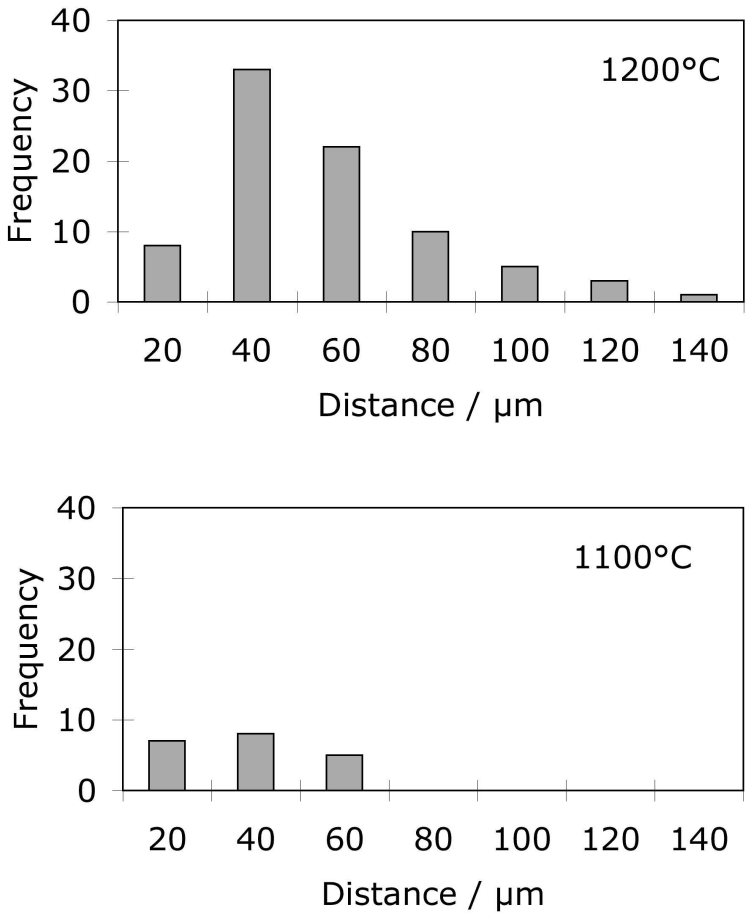

Figure 3.8: The frequency of observation versus the apparent distance between cracks on individual martensite plates in the samples with the coarsest microstructures ($T_\gamma = 1200$ and 1100°C).

trated in Figure 3.9, plotted on identical scales to facilitate comparisons.

It is evident that a coarse grain size tends to have a more uniform distribution of plate sizes (Figure 3.9(a)) whereas the smallest plates dominate when the austenite grain size is reduced (Figure 3.9(d)). This is consistent with the work by Guimaraes and co-workers on the heterogeneity of martensitic transformation when the austenite grain size is small [Guimaraes and

Saavedra, 1984; Guimaraes and Gomes, 1978]. Some austenite grains transform via a burst of martensite, while others remain fully austenitic. Such bursts can be expected to lead to a greater preponderance of fine plates. By contrast, coarse grained microstructures transform uniformly with the majority of austenite grains participating, thus allowing a gradual evolution of microstructure as the sample is cooled.

3.4 Simulating microstructural evolution

The objective in this section is to theoretically compute the evolution of martensite plate size distribution. As mentioned earlier, formation of martensite plates partitions the parent austenite grain into several compartments. Untransformed regions of austenite naturally decrease in size with more plates of martensite forming. Thus with the progress of transformation, new martensite plates form with reduced plate lengths generating a distribution of plate sizes. This concept, as proposed originally by Fischer [1949], has been used here to calculate the theoretical distribution of martensite plate lengths:

At n^{th} instant (n varying as $1, 2, 3, \ldots$), the number of austenite pockets available for transformation, N, is given by

$$N = 2^{n-1} \tag{3.1}$$

This is taken as the number of martensite plates forming at that instant, assuming only one martensite plate forms from a given pocket.

The volume of each of the austenite pockets at the n^{th} instant, V_n, is

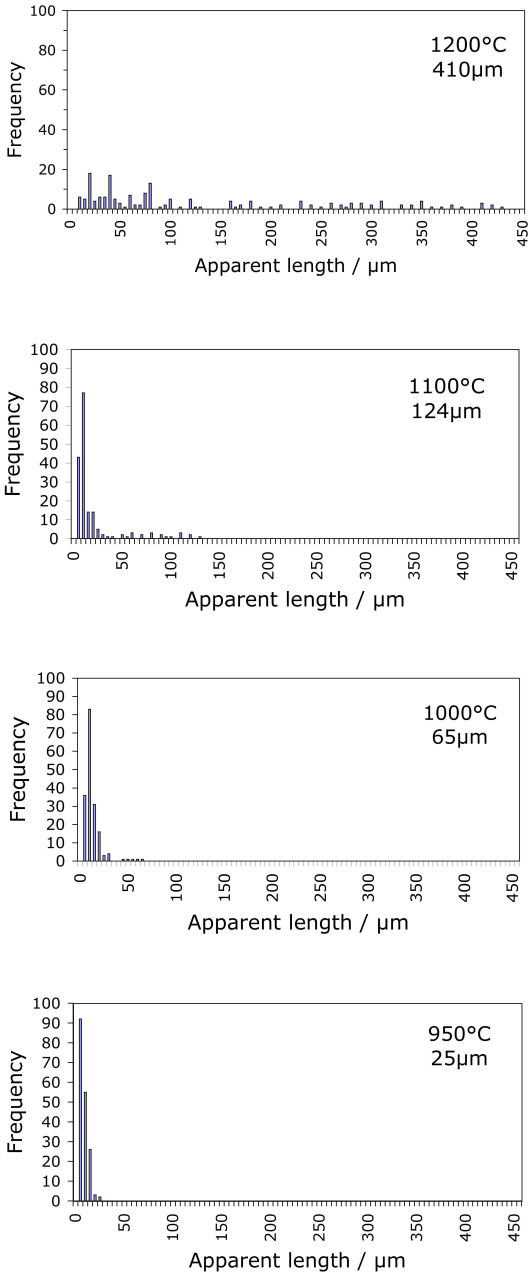

Figure 3.9: The distribution of apparent martensite plate lengths (T_γ and $\overline{L}_\gamma$ values stated). The distributions are all on the same scale to allow comparisons to be made. The bin size on the horizontal scale is 5 μm.

given by

$$V_n = \frac{V_0}{2^{n-1}} \tag{3.2}$$

where V_0 is the original volume of austenite grain. The volume of austenite pockets can be converted into mean lineal intercept, invoking the relationships $L = 1.69a$ and $V = 11.314a^3$ for truncated octahedral grains, where L is the mean lineal intercept, V is the volume and a is the edge length of the unit cell [Mark, 1956].

This results in the following equation relating L_n to V_n at n^{th} instant:

$$L_n = (0.4266V_n)^{\frac{1}{3}} \tag{3.3}$$

This can be considered to be the length of any martensite plate forming at that instant.

There is, however, one limitation of the above formulation. Volume of the pre-existing martensite plates has not been taken into account while calculating the volume of austenite available for transformation, V_n, at the n^{th} instant. Shape of the martensite plates are generally considered to be thin circular discs with a finite volume given by $\pi r^2 c$; $2r$ being the length of the plate and c, the semi-thickness, which is assumed to be $0.05r$. The total martensite plate volume is thus subtracted from the instantaneous austenite pocket volume in order to calculate the *effective* austenite volume.

Knowing the initial mean lineal intercept of the austenite grain size, it is now possible to obtain a theoretical variation in the martensite plate length using the above methodology. The theoretical and the experimental plate length distributions obtained with different prior austenite grain sizes

are presented in Figure 3.10.

The calculated and measured curves compare well, in terms of the influence of the initial austenite grain size and with respect to their general shapes. However, the absolute reduction in length is much greater with the calculated curves. This is because equation 3.1 implies that the number of plates N that form in each generation n is given by $N = a^{n-1}$ with $a = 2$. This leads to a rapid increase in N and a correspondingly rapid decrease in the plate length as n increases. Thus, whereas each point in the calculated curve can represent N plates of identical length, every point in the measured curve is a different plate. The gradual variation in the measured plate length distribution implies that $a < 2$.

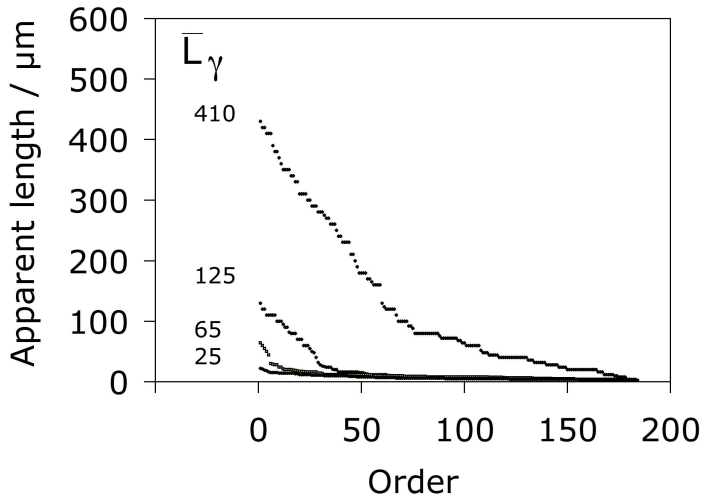

(a)

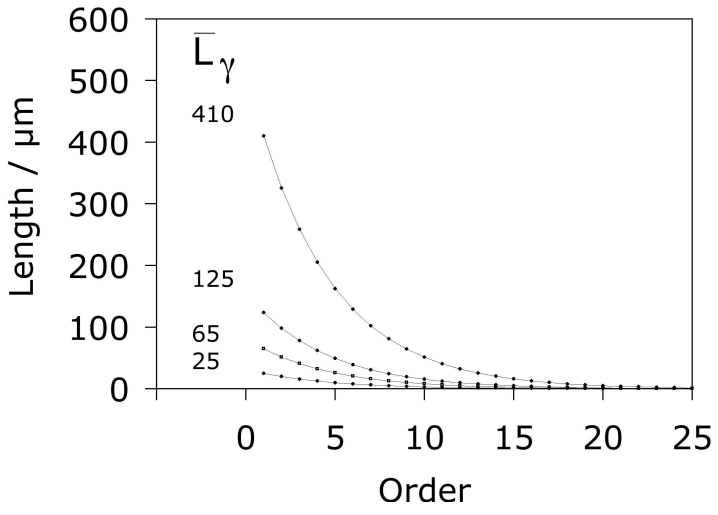

(b)

Figure 3.10: (a) The experimentally measured apparent lengths of martensite plates arranged in the sequence in which they are assumed to form. (b) The corresponding curves for the calculated length versus the order in which the plates form.

3.5 Martensite in TRIP-assisted steels

In TRIP-assisted steels, austenite is retained because of its carbon enrichment following the bainite reaction. Partial decomposition of the untransformed austenite into martensite during cooling after bainite reaction is not unlikely. This is because the distribution of carbon in untransformed austenite after the bainite reaction is mostly heterogeneous [Matas and Hehemann, 1961]. Areas near the bainitic ferrite-austenite interface are richer in carbon than those away from it. The austenite away from the interfaces may transform into martensite on cooling to ambient temperature. Indeed there is evidence of martensite, albeit traces, formed during heat treatment of these materials [Jacques *et al.*, 2001d; Zaefferer *et al.*, 2004]. The austenite in TRIP-assisted steels is in a finely divided state with a grain size of about 1 μm [Jacques, 2003]. It therefore follows that martensite forming in these fine regions of austenite is likely to be devoid of microcracks.

Similarly, the high-carbon martensite produced during plastic deformation of TRIP-assisted steels can also be expected to resist cracking because of the fine plate size. However, the cracking of martensite plates discussed in Section 3.3 results from the quench stresses. The nature of these stresses is arbitrary and has not been characterised.

Further studies were thus carried out with the following objectives:

- To investigate the cracking tendency of the martensite plates during controlled straining.
- To study the nature of the martensite formed during deformation of austenite.

3.6 Experiments

Material

The alloy used for the experiments described in Section 3.3 was modified with nickel to depress the M_S temperature below room temperature. A model developed by Capdevila *et al.* [2003] was used to study the effect of adding nickel on the M_S temperature of Fe-1C-1.5Mn-1.5Si (wt%) alloy (Figure 3.11). From this, it appears that about 8 wt% nickel can depress the M_S temperature of the alloy sufficiently below room temperature. The alloy can therefore be expected to be fully austenitic when quenched to room temperature after austenitising at a higher temperature.

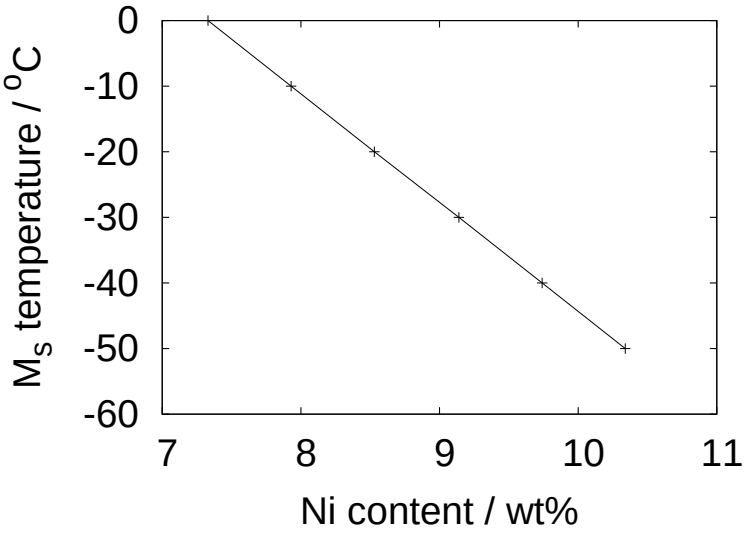

Figure 3.11: Calculated effect of Ni addition on the M_S temperature of Fe-1C-1.5Mn-1.5Si (wt%) alloy.

The chemical composition of the modified alloy was analysed to be Fe-0.91C-8.42Ni-1.58Mn-1.55Si-1.15Cr-0.23Mo (wt%). Calculations using MTDATA [2005] with the SGTE database reveal austenite to exist as a single

phase at 1100°C (Figure 3.12). Austenite, ferrite, cementite and liquid phases were allowed to exist in equilibrium for the calculations. The alloy was therefore homogenised at 1100°C for 48 h before further experiments.

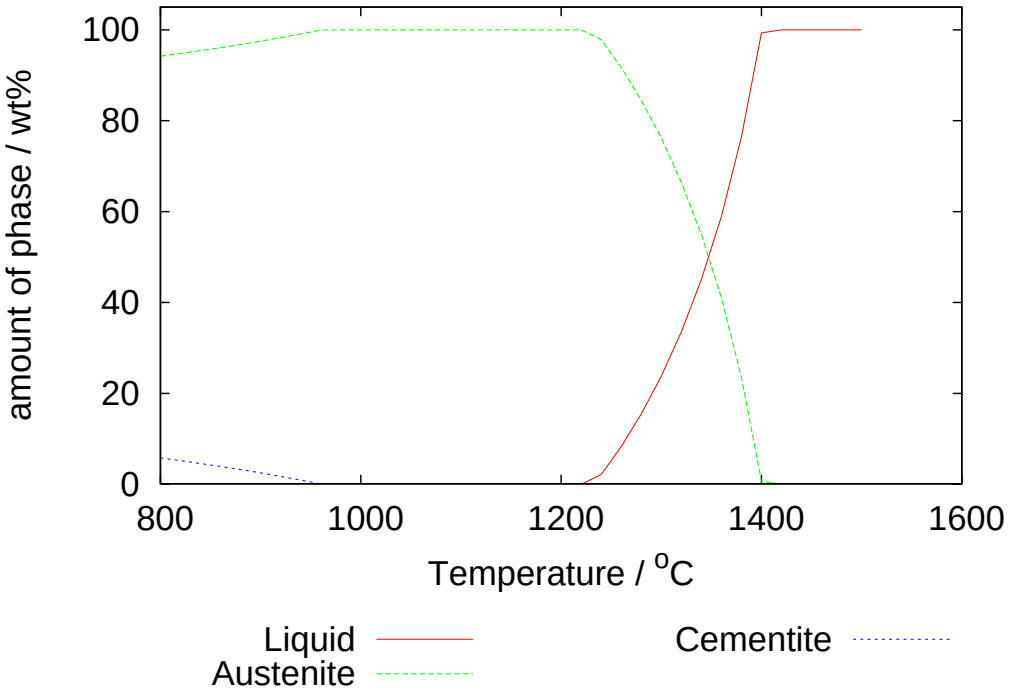

Figure 3.12: Diagram showing the calculated temperature range at which austenite exists as the single phase in the modified alloy.

Heat treatment

Cylindrical samples of length 10 mm and diameter 5 mm were made out of the Fe-C-Ni alloy. These samples were then sealed in quartz tubes containing a partial pressure of argon for heat treatment in an air furnace. The sealed samples were austenitised at 1100°C for 10 minutes before quenching in water at room temperature. One set of samples was further quenched in liquid nitrogen to produce martensite.

Compression tests

The heat-treated samples were subjected to compression experiments. In these tests, samples with initial diameter d_0 and height h_0 were compressed to a height h. Compression strains were then measured as the percentage reductions in the height of the samples. From the constancy of volume criterion, the diameter of the compressed samples, d, is expected to be larger than the initial diameter and is given by the relation $d^2h = d_0^2h_0$. The portion of the sample in the mid-height region is free to flow outward. However, friction at the contact surfaces of the samples with the anvils restricts the material flow at the ends.

The differential flow of material leads to a barrelled profile of the compressed specimen with non-uniform strain distribution across the sample dimensions. This can be minimised with the use of lubricants at the contact surfaces of the samples with the anvils. The lubricant grease used in the present work consists of silicone oil and lithium soap. The chance of barrelling is also reduced in samples with a higher h_0/d_0 ratio [Dieter, 1988]. But there is a practical limit of the $h_0/d_0 \approx 2$ (which is used for the samples in this work), beyond which the samples may buckle during deformation.

Tests were performed at room temperature as well as at -50±1°C. The crosshead velocity used was 0.0017 mm s^{-1}. The martensitic samples were compressed at room temperature to two different strain levels *viz.* 3% and 7%. A strain of about 30% was applied in case of the austenitic sample compressed at a temperature of -50±1°C.

Metallography

The compressed samples were sectioned along the vertical direction. These sections were then polished, etched with 2% nital and observed using optical microscopy.

3.7 Results and discussion

Figure 3.13 depicts the microstructure of the sample quenched in liquid nitrogen. The micrograph reveals dark-etching lenticular plates of martensite along with untransformed austenite. This is similar to the microstructures presented in Figures 3.1-3.4. However, microcracking of the martensite plates of the type illustrated in Figures 3.5-3.6, was not observed in Figure 3.13. This is despite the comparable scales of the microstructures. It is possible that quenching in liquid nitrogen from room temperature does not induce enough stress to crack the martensite plates, unlike quenching in water after soaking at high temperatures. The addition of nickel might also be thought to have reduced the characteristic brittleness of the high-carbon martensite formed in the present alloy.

Martensitic samples produced by quenching in liquid nitrogen were further subjected to compression tests. Figure 3.14 presents the microstructures of the compressed samples. The plates of martensite are seen to contain arrays of parallel cracks across the plate length. This is similar to the microcracks observed in Figure 3.5. Furthermore, the larger plates are found to be preferentially cracked over the smaller ones (Figure 3.14(a)). This is consistent with the earlier quenching experiments that revealed a greater

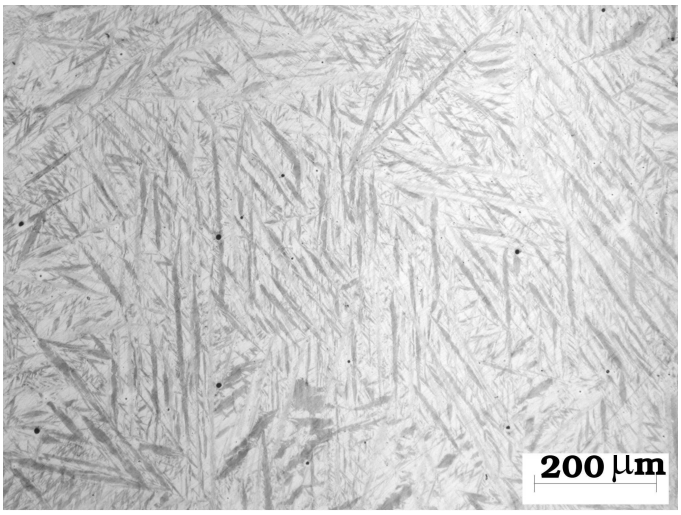

Figure 3.13: Plates of athermal martensite formed without any microcracks in the present alloy.

propensity of the coarser martensite plates to crack (Section 3.4). Cracks were more frequent following higher plastic deformation (Figure 3.14(b)). Sometimes cracks were also visible along some portions of the martensite-austenite interfaces in the 7% strained sample. The apparent distance between adjacent cracks was also measured in these samples, Figure 3.15. This is found to follow a similar distribution as that observed in Figure 3.8.

Figure 3.16 presents the micrographs obtained from the sample quenched at room temperature and then compressed by 30% at -50±1°C. Figure 3.16(a) reveals clearly the dark-etching small lens shaped martensite plates formed during straining of the austenite. Strain-induced martensite retained the lenticular shape but the individual plates are much finer in size than expected from the prior austenite grain size. Martensite plates cannot traverse across strong obstacles like grain boundaries, twin boundaries or other pre-existing martensite plates. In the present situation, growth of the

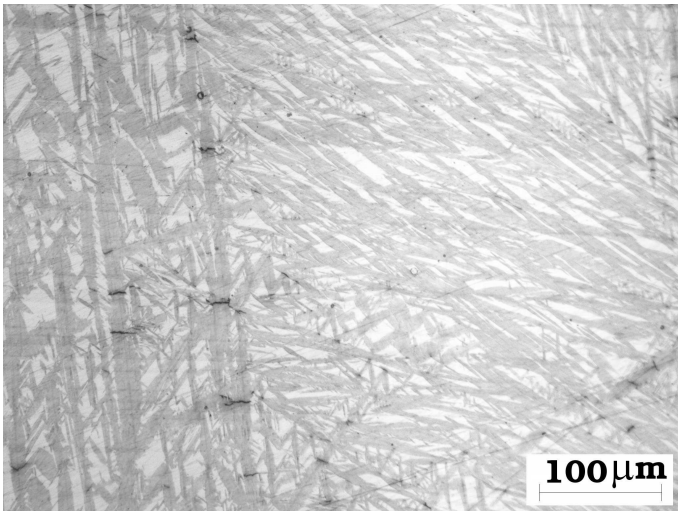

(a)

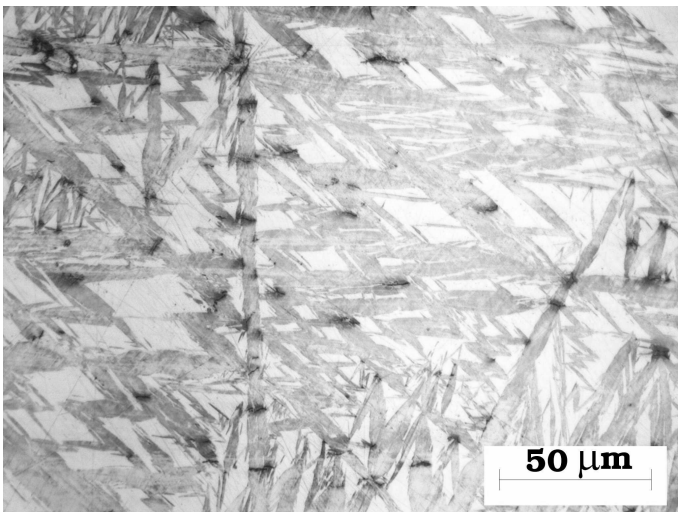

(b)

Figure 3.14: Cracking of martensite plates after (a) 3% and (b) 7% reduction in height of the martensitic samples.

martensite plates appears to be stifled by the defects produced due to plastic strain in austenite. Hence the plates tend to grow only upto limited sizes.

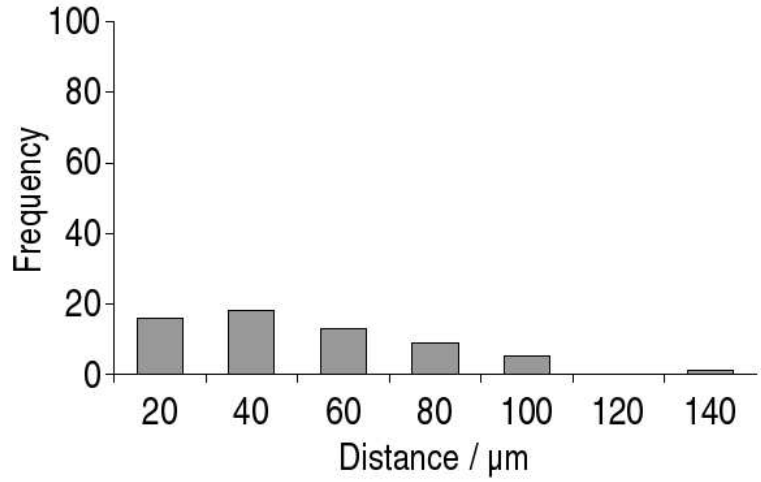

(a)

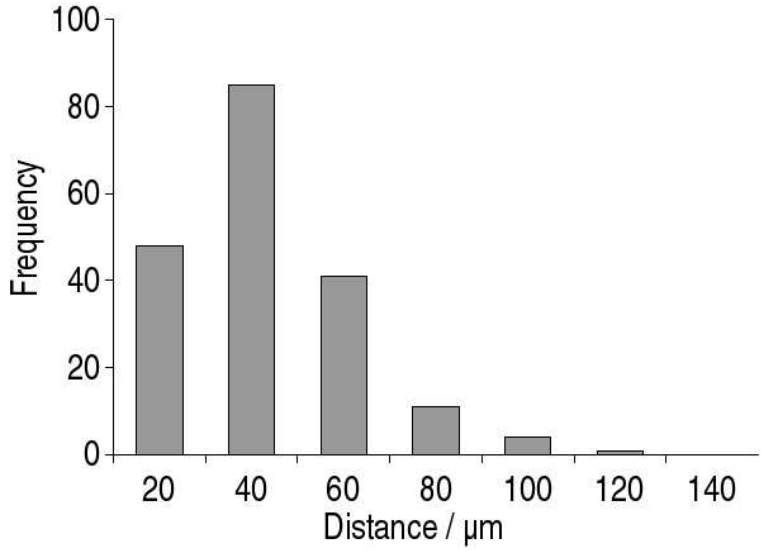

(b)

Figure 3.15: The frequency of observing cracks versus the apparent distance between cracks on martensite plates after (a) 3% and (b) 7% reduction in height.

The plates were also observed to be free of cracks.

A notable feature of the microstructure is the particular alignment of the martensite plates along the two preferred directions (Figure 3.16). This is due to the effect of stress on transformation [Patel and Cohen, 1953]. Martensite is known to form on some specific crystallographic planes of austenite known as habit planes. Without any external stress, transformation takes place on all the possible habit planes. This therefore does not lead to any bias in the microstructure. By contrast, martensite tends to form on only some specific habit planes under the influence of stress. This explains the particular alignment of the martensite plates along some preferred directions in the micrographs presented in Figure 3.16.

Figure 3.16(b) depicts that martensite is formed in one of the two grains visible in the micrograph, while there is no sign of transformation in the other grain. This may be due to the role of stress as described above. The resolved shear component of the external stress on the habit planes actually leads to transformation in steels, where the volume expansion due to transformation is small. Transformation becomes possible only above some critical magnitude of the resolved shear stress. The orientation of the individual austenite grains must influence the magnitude of the resolved shear stress on the crystallographic planes. Therefore it is not unlikely that some grains may not be favourably oriented for transformation under the influence of stress, as observed in Figure 3.16(b). The other possibility could be the heterogeneous nature of the compressive strain. All the grains might not be strained to the same extent under compression. This may also be responsible for no transformation to occur in one of the two grains visible in Figure 3.16(b).

3.8 Summary

High-carbon martensite is known to be a brittle phase. Yet it does not appear to be a liability in the TRIP-assisted steels reputed for good mechanical properties, especially formability. This apparent anomaly can be explained considering the role of martensite plate size on the brittleness. It has been demonstrated that the finer martensite plates are better able to resist cracking under stress or strain. It is the fine grain size of austenite that allows the high-carbon brittle martensite to form in these materials without endangering the mechanical properties.

It has been also shown that the plates of martensite formed during straining of austenite remain fine in size. This is probably due to the defects, created in austenite due to strain, that stifle the growth of martensite. The small plates of strain-induced martensite are observed to form only along some preferred directions. This is due to the effect of the accompanying stress. The fine-sized ordered martensite plates that form during the straining of austenite can be expected to be resistant to cracking. Untempered martensite that forms in the TRIP-assisted steels is therefore not expected to have any adverse effect on the mechanical performance, despite its high carbon concentration.

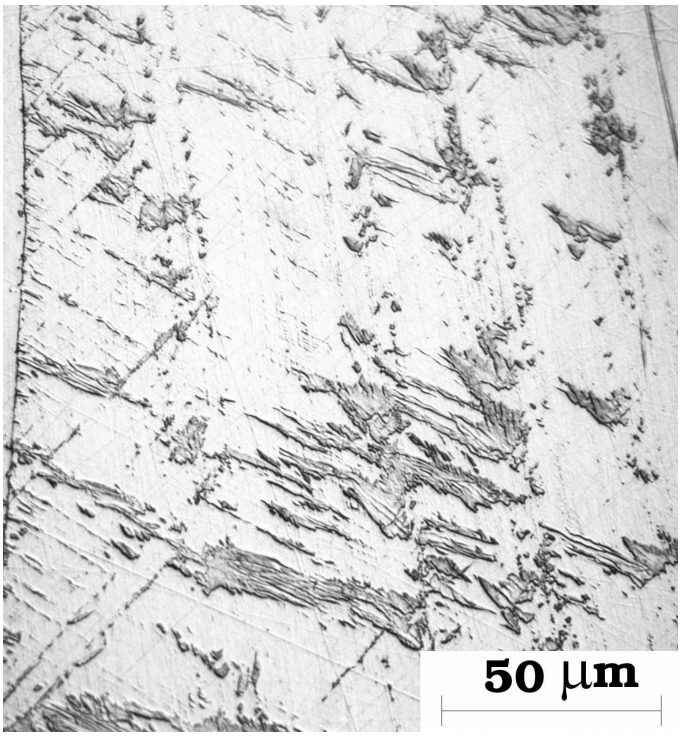

(a)

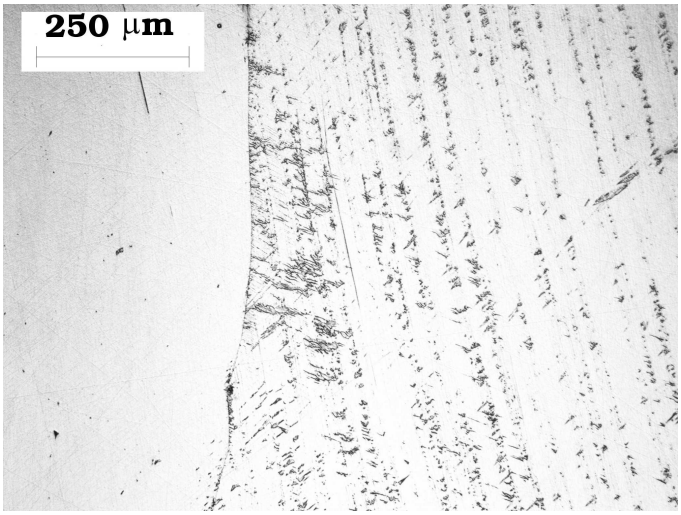

(b)

Figure 3.16: Martensite plates formed during straining of the austenitic sample; (a) showing preferred alignments of the plates, (b) revealing the preferential transformation in one of the two adjacent grains of austenite.

Chapter 4

Microstructural Modelling

Allotriomorphic ferrite, carbide-free bainite and retained austenite are constituents of the microstructure of TRIP-assisted steels. These phases can be produced beginning either with hot rolled or cold rolled steel. The austenite after hot rolling transforms to allotriomorphic ferrite and subsequently to bainite. However, a two-stage annealing process is necessary after cold rolling to produce the desired microstructure. During bainite formation, untransformed austenite gets enriched with carbon and is therefore retained at ambient temperature. Processing conditions as well as the chemical composition of the steel influences both the volume fraction and carbon content of retained austenite. The present chapter deals with an attempt to model the microstructure of TRIP-assisted steels using neural network techniques.

4.1 Neural network modelling

Neural network analysis represents a general method of regression that fits a non-linear function to experimental data. This can help quantify complex

phenomena involving many variables. The subject has been reviewed by Bhadeshia [1999a]. In linear regression, the product of each input variable x_i and a weight w_i is added to a constant θ to obtain the output y,

$$y = \sum_i w_i x_i + \theta \tag{4.1}$$

The weights and the constants can be imagined to be varied systematically until a best-fit expression of the output is reached as a function of the input variables. The difficulties with such a regression are:

1. A specific relation has to be chosen prior to the analysis.
2. The regression equation thus derived applies across the entire input space.

These difficulties can be overcome by making the network non-linear, setting the sum of the products to the argument of a hyperbolic tangent function,

$$y = \sum_j W_j h_j + \theta', \text{with } h_j = \tanh(\sum_i w_{ij} x_i + \theta_j) \tag{4.2}$$

where W_j is a weight and θ' is a constant. The hyperbolic tangent function introduces flexibility, non-linearity and the form of the function also varies in the input space. The strength of the function depends on the weights w_{ij}.

One major limitation of the non-linear regression method is the possibility of overfitting the data, as illustrated in Figure 4.1. This can be verified easily by testing the model with some unseen data. The experimental dataset can be divided randomly into two parts *viz.* training dataset and test dataset. After the model is created using the training dataset, its performance can be checked using the test dataset.

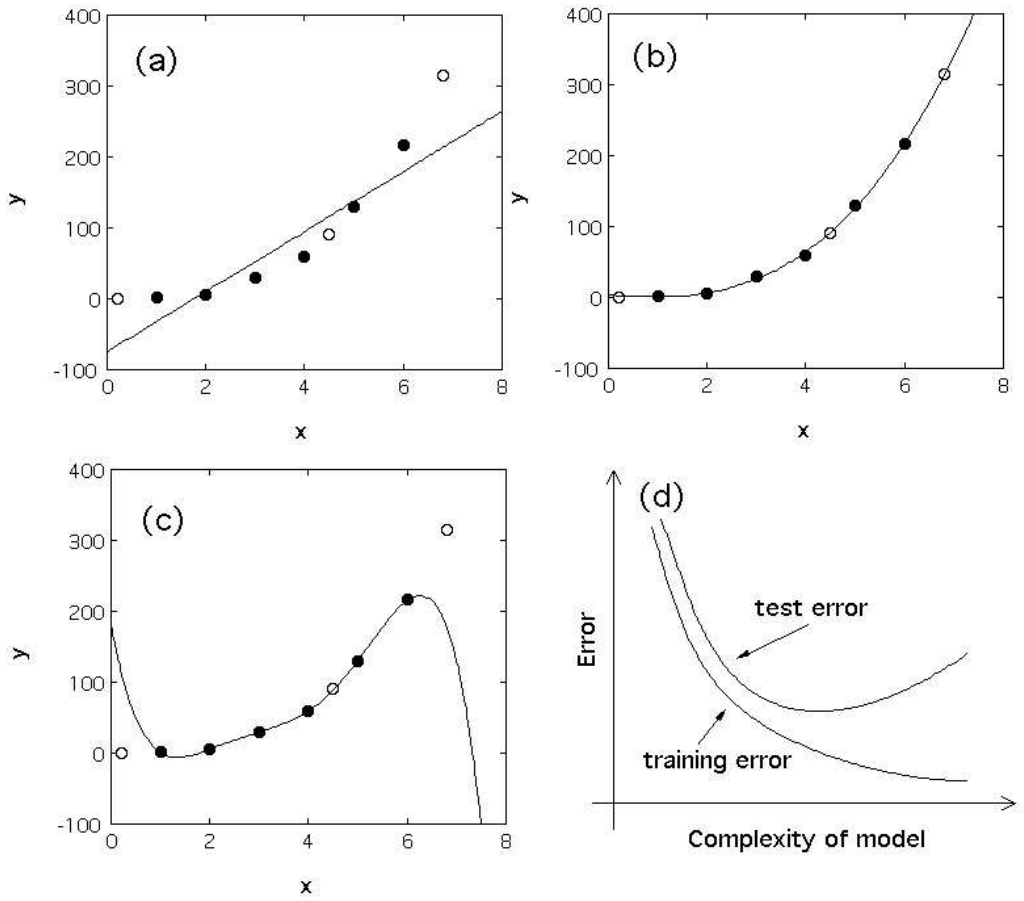

Figure 4.1: Modelling noisy data in a case where y should vary with x^3. The filled points represent training data, and the circles the testing data. (a) A simple linear function. (b) A cubic polynomial with optimum representation of both the training and test data. (c) A fifth order polynomial which does not generalise properly. (d) Variation in the test and training errors as a function of the model complexity [Bhadeshia, 1999a].

Figure 4.1(a)-(c) illustrates an imaginary case of modelling a dataset where y varies as a function of x^3. A linear function is too simple whereas an overcomplex function fails to generalise. The optimum behaviour is described in Figure 4.1(b). The best model is chosen by the minimum in the test error, as the training error tends to decrease continuously with increasing model

complexity (Figure 4.1(d)).

Modelling uncertainty

An important aspect of neural network modelling is the uncertainties associated with the predictions. The overall error in the predicted values of the output, E_D, can be calculated by comparing the predicted values (y_n) against the dataset values (t_n) as,

$$E_D \propto \sum_n (t_n - y_n)^2 \tag{4.3}$$

If all the important input variables are not considered in the analysis, E_D tends to increase. E_D represents only an overall perceived level of noise in the output and does not describe the uncertainties of the modelling process itself. The best-fit functions with the most probable weights may not necessarily describe the uncertainties in regions of the input space with noisy or sparse data.

Neural networks used in Bayesian framework allow the calculation of error bars representing the uncertainty in the fitting parameters [MacKay, 2003]. This invokes the possibility of fitting or extrapolating many functions into uncertain regions of the input space, still maintaining an optimum fit in regions having good quality data. A probability distribution of sets of weights is then used to define the fitting uncertainty. It follows that the error bars tend to increase in magnitude when data are noisy (A) or sparse (B), as illustrated in Figure 4.2.

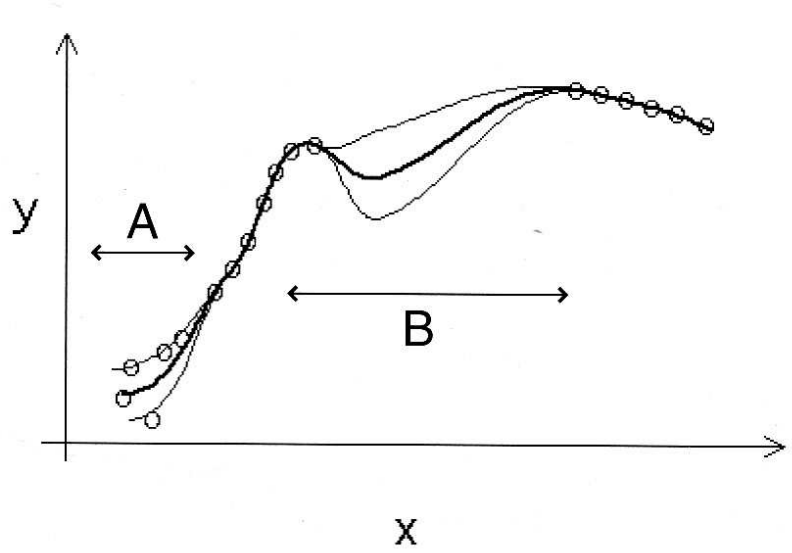

Figure 4.2: The uncertainty in defining a fitting function when data are noisy (A) or sparse (B). The thinner lines represent error bounds due to uncertainties in determining the weights [Bhadeshia, 1999a].

4.2 Model for retained austenite fraction

4.2.1 Database

The cold rolled steel is initially heated to a temperature in the $(\alpha + \gamma)$ phase region (intercritical annealing), to form ferrite and austenite. The material is then cooled rapidly to a lower temperature at which austenite transforms to bainite. Parameters of this two-step heat treatment along with the chemical composition were taken as input variables to the model, as shown in Table 4.1[1]. Figure 4.3 presents the distribution of the data points in the input space for each variable.

[1]Data used are due to Chen *et al.* [2002]; De Meyer *et al.* [1999a]; Itami *et al.* [1995]; Jacques *et al.* [2001a,b,c, 1999]; Kim *et al.* [2002, 2001]; Lee *et al.* [2002b]; Matsumura *et al.* [1992, 1987b]; Nakagaito *et al.* [2003]; Pichler *et al.* [1998]; Sakuma *et al.* [1993, 1991a]; Traint *et al.* [2002, 2000]

Inputs	Min.	Max.	Average	S.D.
Carbon / wt%	0.0950	0.3920	0.2102	0.1020
Manganese / wt%	0.6000	1.9900	1.4057	0.2796
Silicon / wt%	0.0400	2.1000	0.9619	0.5369
Aluminium / wt%	0.0000	2.0000	0.2979	0.5236
Phosphorus / wt%	0.0000	0.2040	0.0223	0.0401
Molybdenum / wt%	0.0000	0.1400	0.0043	0.0218
Copper / wt%	0.0000	0.5100	0.0065	0.0573
IA temperature / °C	730	840	778.2653	25.7829
IA time / s	60	450	213.2143	110.8414
IT temperature / °C	300	525	404.2347	39.5554
IT time / s	0	5400	441.3673	588.7228
Output	Min.	Max.	Average	S.D.
Retained austenite / vol.%	0.1267	27.0710	10.3805	5.8054

Table 4.1: Data used for the retained austenite fraction model, IA: intercritical annealing and IT: isothermal transformation to bainite, S.D.: standard deviation.

4.2.2 Model characteristics

The model was trained using 80% of the dataset values. The remainder was used to test the performance of the model with unseen data. Figure 4.4 compares the normalised predicted values with the corresponding normalised database value during training and testing steps respectively. Normalisation of the variables is carried out as follows

$$x_n = \frac{x - x_{min}}{x_{max} - x_{min}} - 0.5 \tag{4.4}$$

where x_n is the normalised value of the variable x, with x_{min} and x_{max} as the minimum and the maximum values respectively. The performance of the model can be seen to be satisfactory both during the training and testing stages.

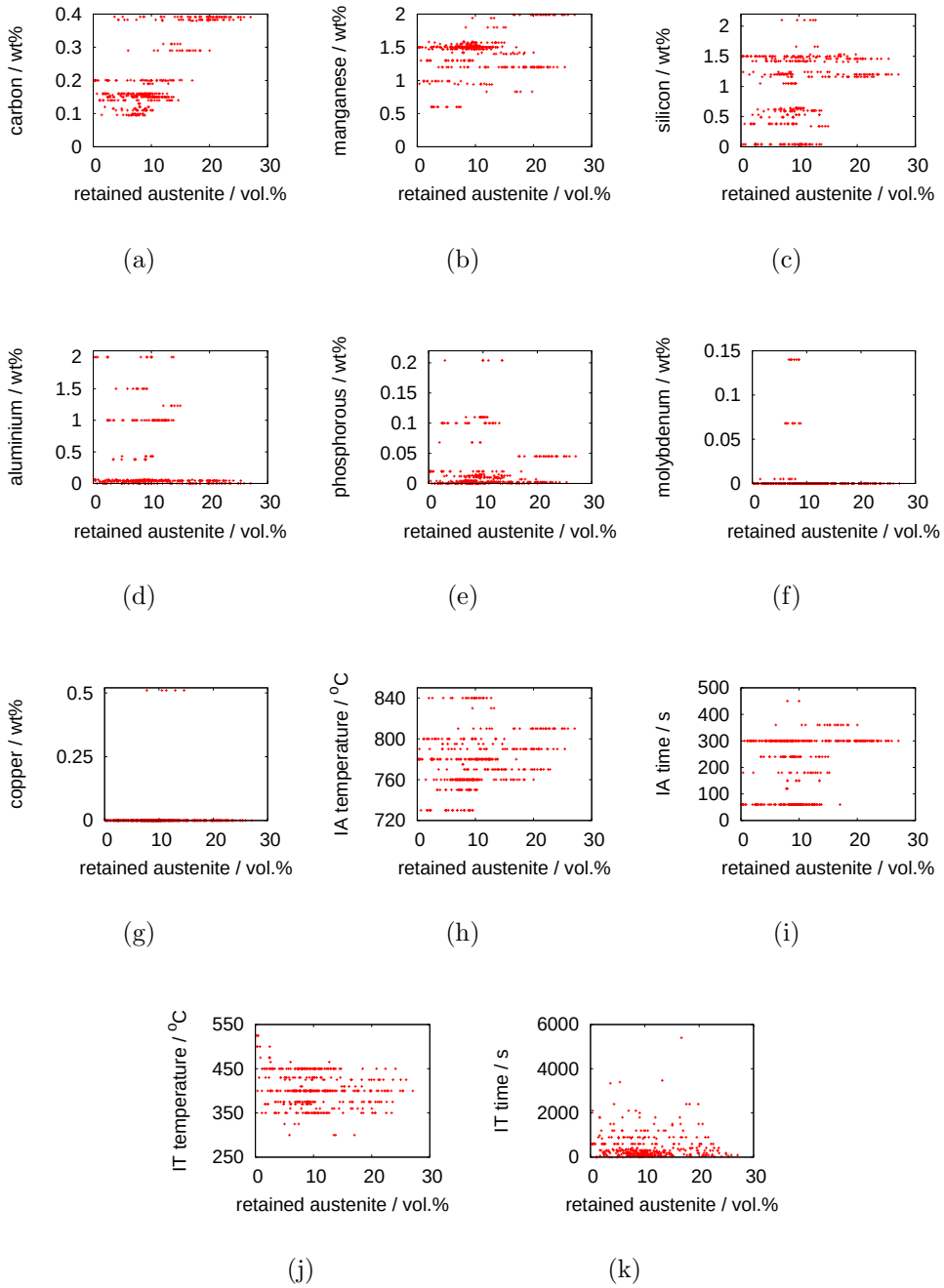

Figure 4.3: Distribution of data in the input space for the retained austenite fraction model

Figure 4.5(a) illustrates the reduction in noise with increasing number of hidden units. The final model is formed as a committee of models, which is selected on the basis of the observed minimum in the test error on combining increasing numbers of networks (Figure 4.5(b)).

Figure 4.6 presents the significances of each of the input variables as perceived by the models in the final committee. Bainite reaction time appears to be the most important factor controlling the retained austenite content in the microstructure.

4.2.3 Model predictions

Predictions were made by varying input variables over a base steel composition of 0.2C-1.5Mn-1.0Si-0.5Al-0.02P-0Mo-0Cu (all in wt%), intercritical annealing parameters of 780°C, 300 s and bainite transformation conditions as 400°C, 500 s. Both carbon and manganese are known to be austenite stabilisers [Pickering, 1978]. Therefore as expected, both carbon and manganese are beneficial for increasing austenite fraction (Figure 4.7(a)-(b)). Similarly, the addition of copper to these steels can also increase austenite content [Kim *et al.*, 2002] (Figure 4.7(f)). This is probably because copper reduces the driving force, ΔG, for the transformation of austenite to ferrite. Therefore these elements seem to affect the retained austenite content through the thermodynamic stability of austenite over ferrite.

Additionally, silicon, aluminium and phosphorous are known to help retain austenite by suppressing cementite formation during the bainite reaction. Figure 4.7(c) depicts this role of silicon on increasing retained austenite fraction. However, with 1 wt% silicon, the addition of aluminium up to about

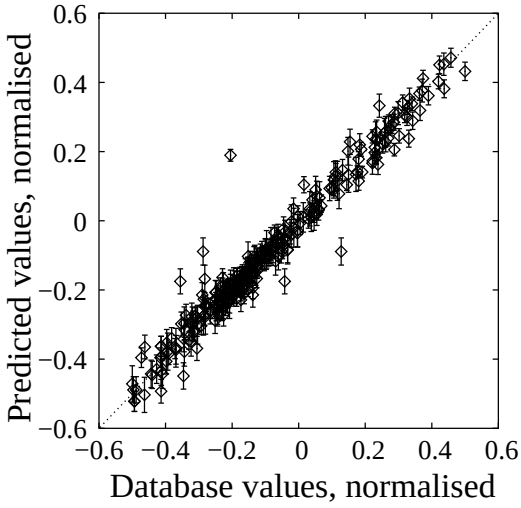

(a)

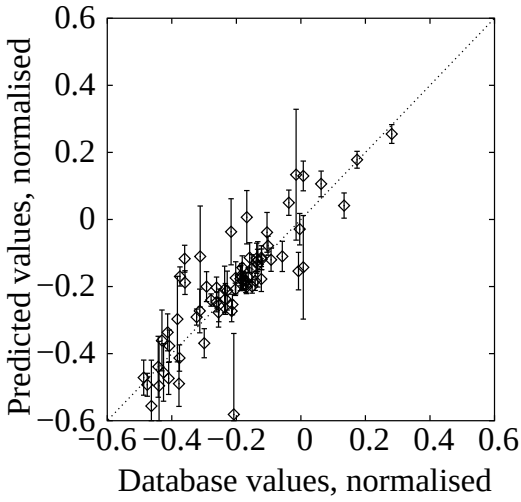

(b)

Figure 4.4: Model predictions compared with the actual database values during (a) training and (b) test.

1 wt% does not appear to have any marked effect on the retained austenite fraction (Figure 4.7(d)). Predictions with higher aluminium content are as-

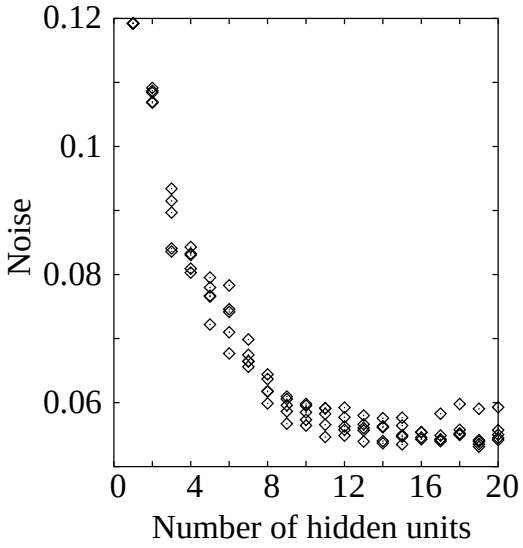

(a)

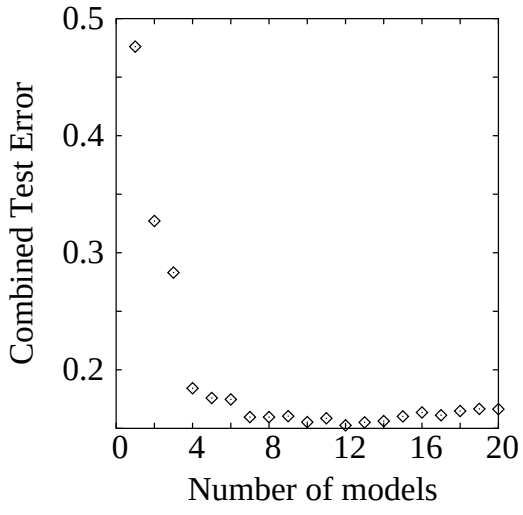

(b)

Figure 4.5: (a) Variation of noise (σ) with increasing hidden units. (b) Variation of the combined test error with number of models in committee.

sociated with large uncertainties suggesting more data are necessary in this range of the input space. Molybdenum increases hardenability and therefore

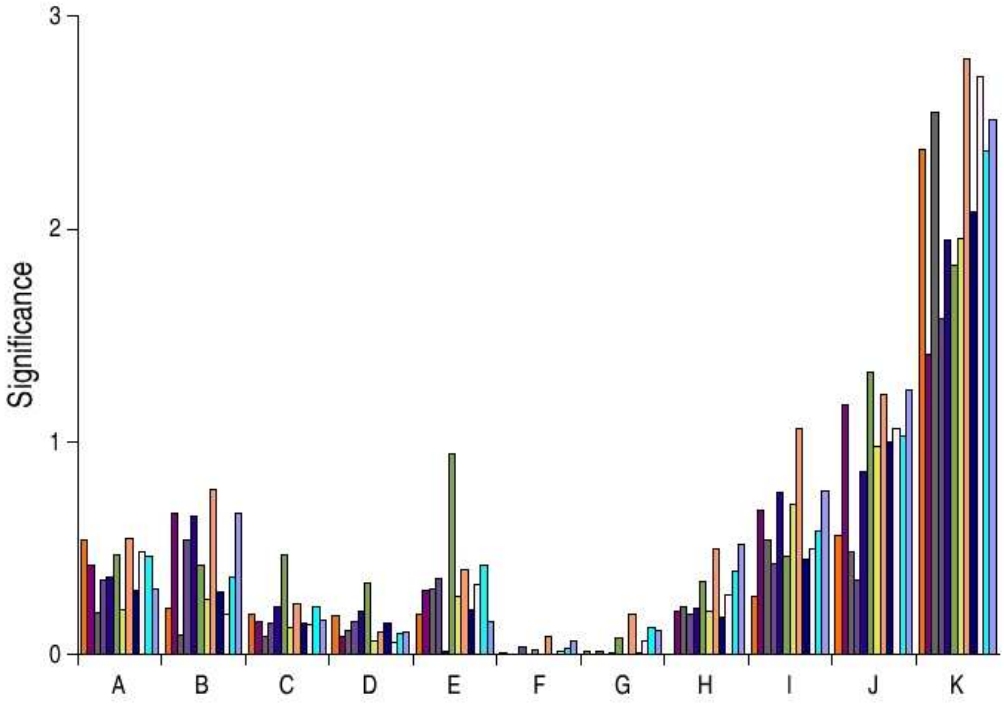

Figure 4.6: Significances of the input variables (A-K) for the retained austenite fraction model, A: carbon, B: manganese, C: silicon, D: aluminium, E: phosphorous, F: molybdenum, G: copper, H: intercritical annealing temperature, I: intercritical annealing time, J: bainite transformation temperature and K: bainite transformation time.

is likely to increase retained austenite fraction. Figure 4.7(e) depicts only a very subtle effect of molybdenum on increasing retained austenite fraction, with large uncertainties.

Figure 4.8(a) depicts the variation of retained austenite fraction with intercritical annealing temperature. It is generally believed that higher intercritical annealing temperature produces more austenite but with less stability (due to lower carbon content) whilst stability increases but the amount of austenite decreases at lower temperatures [Gallagher *et al.*, 2003]. Therefore, an intermediate annealing temperature is generally considered to max-

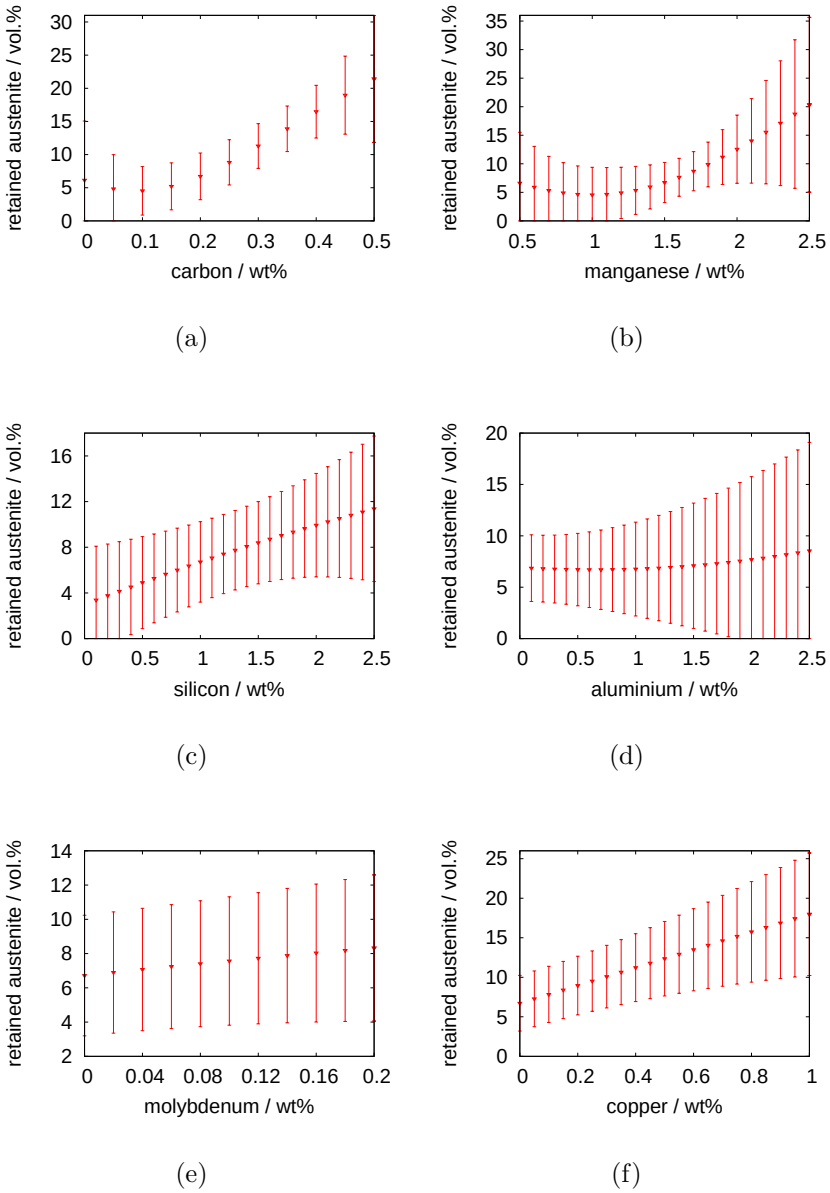

Figure 4.7: Effect of the alloying elements on retained austenite fraction: (a) carbon, (b) manganese, (c) silicon, (d) aluminium, (e) molybdenum and (f) copper.

imise retained austenite content in the final microstructure. However, Kim *et al.* [2001] reported higher retained austenite content with an intercritical

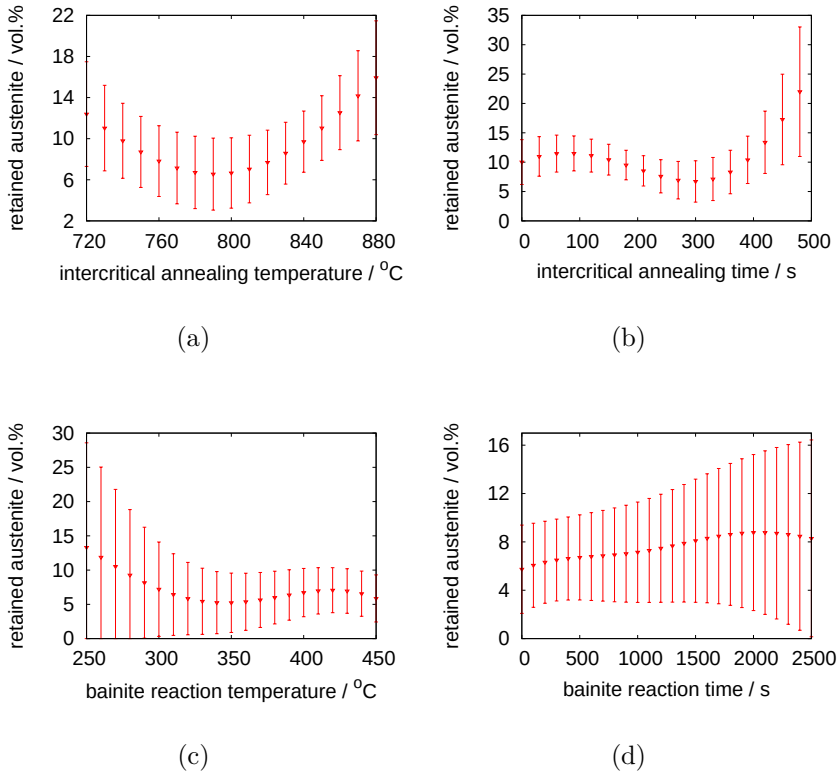

Figure 4.8: Effect of heat treatment parameters on retained austenite fraction: (a) intercritical annealing temperature and (b) time; (c) bainite transformation temperature and (d) time.

annealing temperature lower than the intermediate. This was ascribed to the greater stability of the austenite produced at a lower intercritical annealing temperature. Predictions from the present model suggest, either a high or a low intercritical annealing temperature for obtaining greater retained austenite content (Figure 4.8(a)).

Unlike interstitial carbon, the diffusion of substitutional solutes needs longer times. Increasing intercritical annealing time favours more efficient partitioning of the substitutional solutes like manganese in austenite. Man-

ganese, like carbon, stabilises the austenite. This can therefore increase the retained austenite content in the final microstructure (Figure 4.8(b)).

The effect of bainite reaction temperature and time on retaining austenite is depicted in Figure 4.8(c)-(d). Lower bainite transformation temperatures mean a slower rate of bainite formation. For a given transformation time, the amount of bainite formed is less at lower transformation temperatures. This will leave more untransformed austenite. Also, transformation ceases with higher carbon enrichment in the untransformed austenite at lower temperatures (T_0 criterion of the incomplete reaction phenomenon). Thus austenite becomes more stable at lower transformation temperatures. But this cannot be expected at an intermediate time. It is therefore likely that the increasing trend of retained austenite content with lower bainite formation temperatures arises from the larger amount of untransformed austenite due to the slower bainite reaction kinetics.

As the bainite transformation progresses, the residual austenite gets enriched with carbon. This imparts stability against subsequent martensitic transformation, thus increasing the retained austenite content (Figure 4.8(d)). On the other hand, the amount of untransformed austenite decreases with increasing time. It follows that the amount of retained austenite will be maximum at an intermediate time depending on transformation temperature [Jacques *et al.*, 2001b; Nakagaito *et al.*, 2003]. Figure 4.9 illustrates this effect in a 0.2C-1.5Mn-1.5Si (wt%) steel with intercritical annealing parameters 780°C and 300 s. Retained austenite fraction maximises at an intermediate bainite reaction time for both the transformation temperatures of 350°C and 375°C.

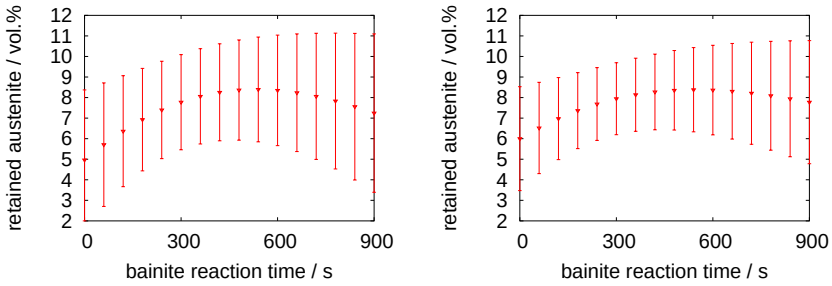

(a) (b)

Figure 4.9: Variation in retained austenite volume fraction with bainite reaction time at transformation temperature of (a) 350°C and (b) 375°C.

4.3 Model for carbon in retained austenite

4.3.1 Database

Data used for the model made for predicting the carbon content of retained austenite are presented in Table 4.2[2]. Figure 4.10 presents the distribution of each of the input variables against the output.

4.3.2 Model characteristics

As expected, increasing the number of hidden units reduces the noise level (Figure 4.11(a)). However, the test error does not tend to decrease continuously with increasing model complexity (Figure 4.11(b)). The optimum number of models in the committee was found to be seven, when the test error is minimum. The model appears to perform reasonably well, during

[2]Data used are due to De Meyer *et al.* [1999a]; Itami *et al.* [1995]; Jacques *et al.* [2001a,b,c, 1999]; Kim *et al.* [2002]; Matsumura *et al.* [1992, 1987b]; Nakagaito *et al.* [2003]; Wang *et al.* [2004]; Zaefferer *et al.* [2004]

Inputs	Min.	Max.	Average	S.D.
Carbon / wt%	0.1100	0.3920	0.2676	0.1150
Manganese / wt%	0.8300	1.6600	1.3019	0.1813
Silicon / wt%	0.3400	1.9900	1.2150	0.5284
Aluminium / wt%	0.0000	1.5000	0.1879	0.3982
Phosphorus / wt%	0.0000	0.0400	0.0025	0.0058
Copper / wt%	0.0000	0.5100	0.0051	0.0506
IA temperature / °C	730	830	773.2778	25.9773
IA time / s	60	360	286.9697	50.8797
IT temperature / °C	350	450	392.6263	28.4305
IT time / s	0	9725	578.7222	991.3905
Output	Min.	Max.	Average	S.D.
Carbon in retained austenite / wt%	0.49	1.8793	1.1949	0.3836

Table 4.2: Data used to model the carbon content of retained austenite, IA: intercritical annealing and IT: isothermal transformation to bainite, S.D.: standard deviation.

both the training and testing step (Figure 4.12(a)-(b)).

Figure 4.13 shows the model-perceived significance of each of the input parameters. Bainite reaction time appears to exert the strongest influence on the carbon content of retained austenite.

4.3.3 Model predictions

Predictions were made varying each input parameter over a base composition of 0.2C-1.5Mn-1.0Si-0.5Al-0.02P-0Cu (wt%); intercritical annealing parameters of 780°C, 300 s and bainite transformation conditions of 400°C, 500 s. Figures 4.14(a)-(d) demonstrate that the results for carbon, aluminium and silicon are uncertain while manganese shows an inverse trend. Manganese shifts the T_0 curve to lower carbon contents and hence reduces the carbon content of retained austenite.

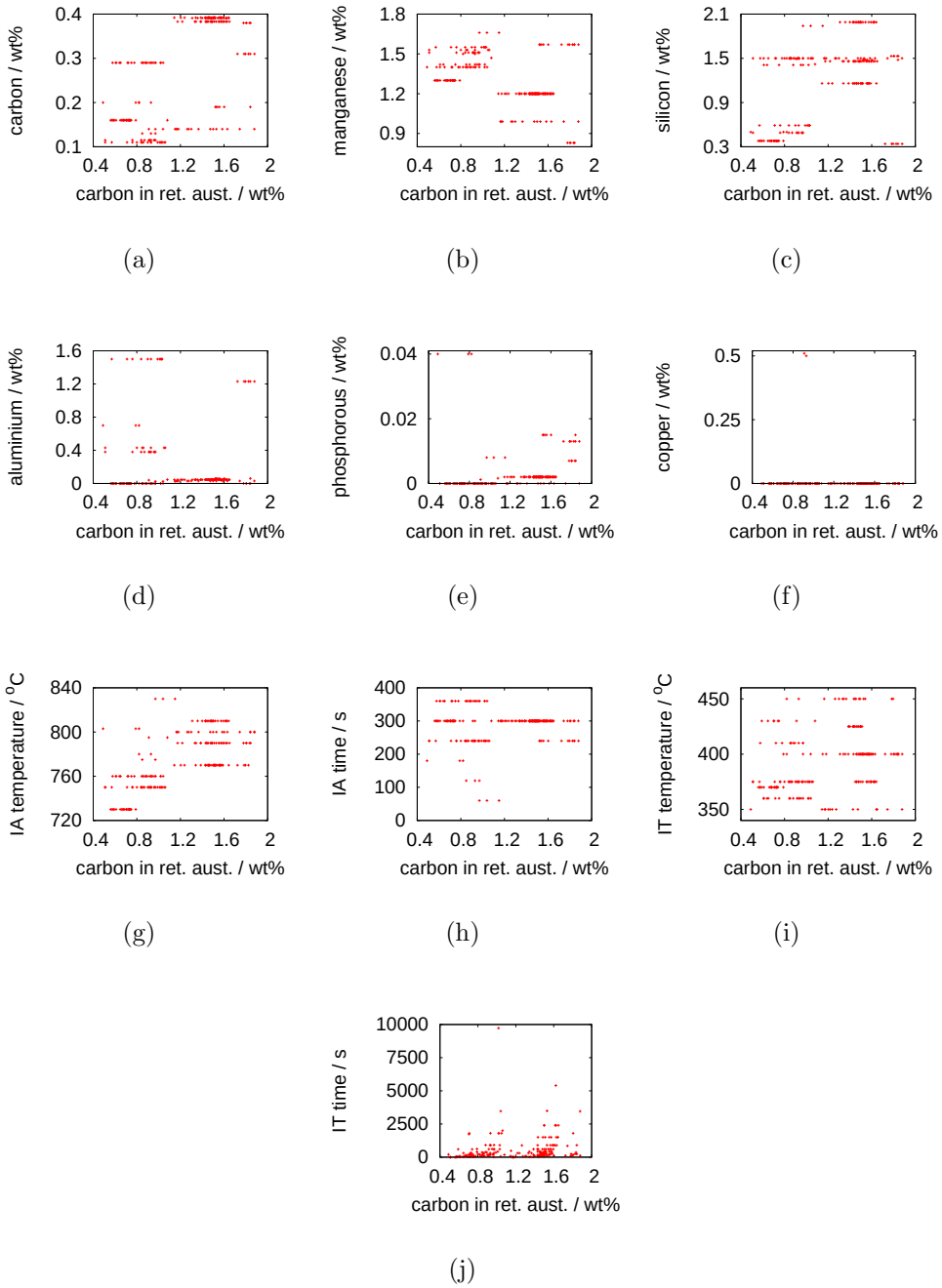

Figure 4.10: Distribution of data in the input space for the carbon content of retained austenite model.

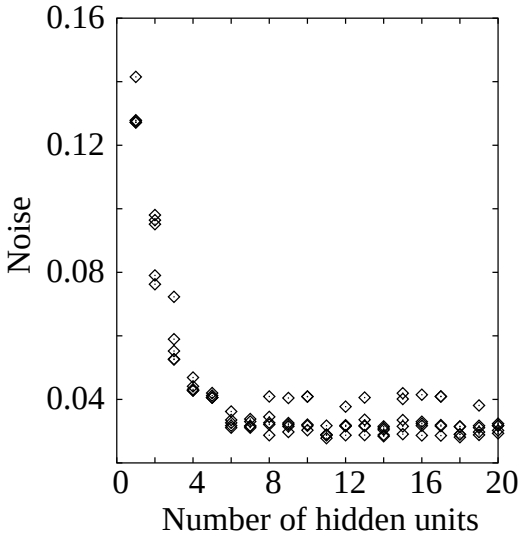

(a)

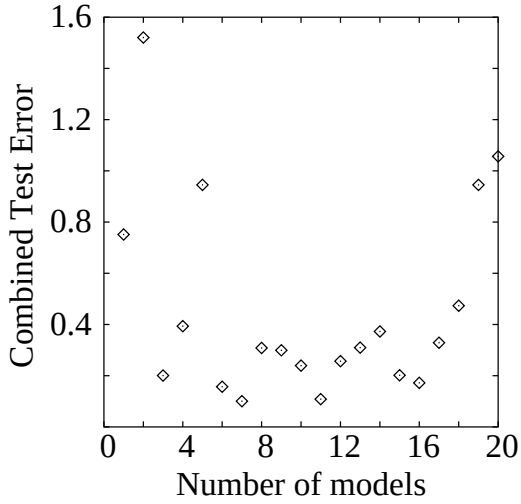

(b)

Figure 4.11: (a) Variation of noise (σ) with increasing number of hidden units. (b) Variation of test error with number of models in the committee.

Carbon may also be expected to have a similar effect as manganese. But this is apparently missing in Figure 4.14(a). The concentration of car-

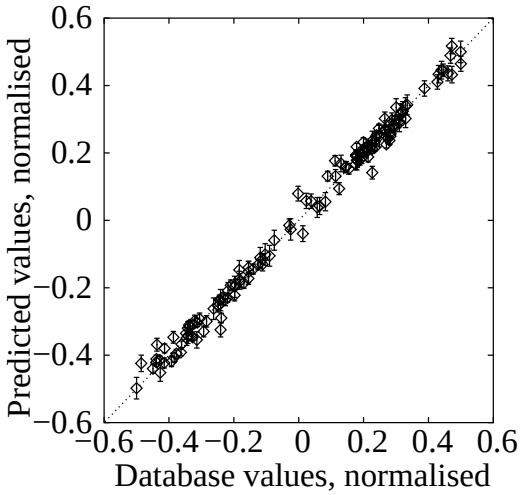

(a)

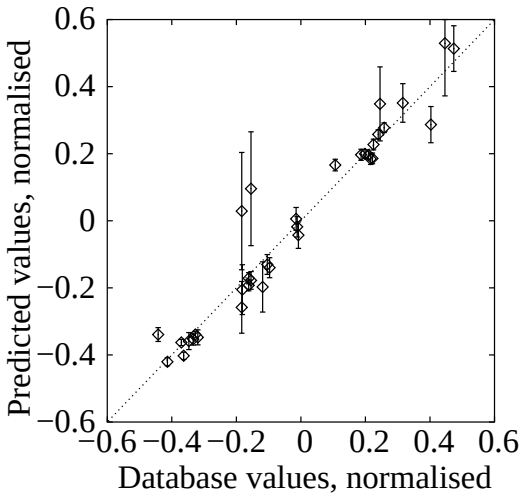

(b)

Figure 4.12: Model predictions compared with the actual database values during (a) training and (b) test.

bon in austenite before bainite formation is not the same as that of the bulk steel composition. During intercritical annealing, carbon in austenite

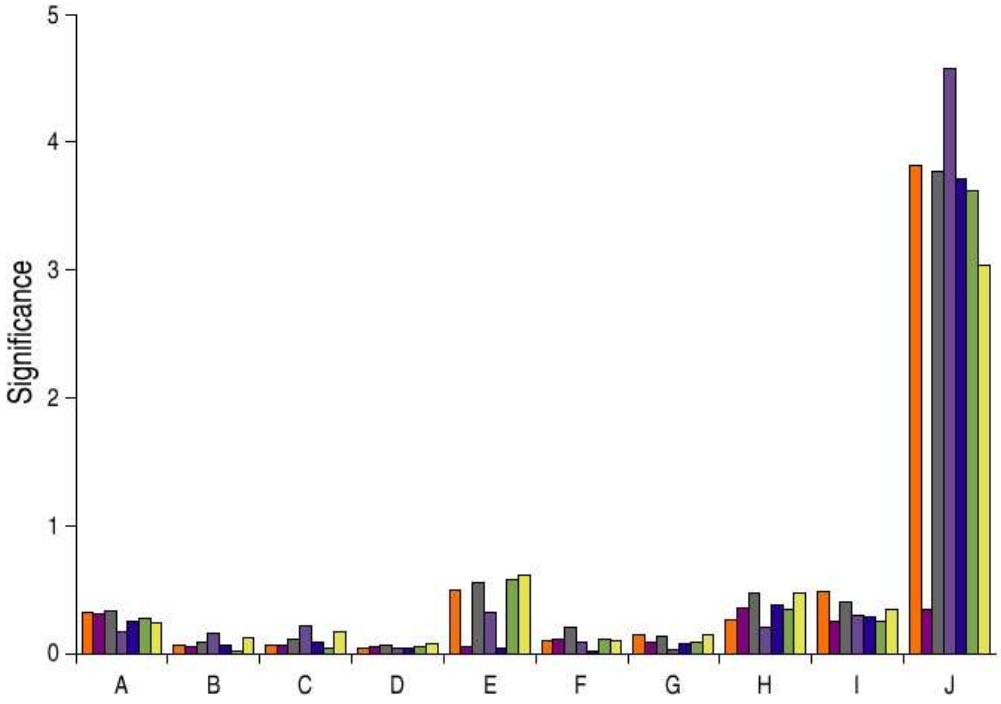

Figure 4.13: Significances of the input parameters (A-J) to the models for predicting carbon content of retained austenite, A: carbon, B: manganese, C: silicon, D: aluminium, E: phosphorous, F: copper, G: intercritical annealing temperature, H: intercritical annealing time, I: bainite transformation temperature, J: bainite transformation time.

increases due to ferrite formation. However, manganese in the austenite formed during intercritical annealing is most likely to remain same as that of the bulk composition. This is because partitioning of manganese requires a longer time than partitioning of carbon. It seems that carbon enrichment of retained austenite is affected by the bulk manganese concentration but not bulk carbon content of the steel. It may therefore be inferred that carbon enrichment in retained austenite is affected by the factors that can alter bainite reaction kinetics. This is also apparent from the effect of the heat treatment parameters on the carbon content of retained austenite, as illus-

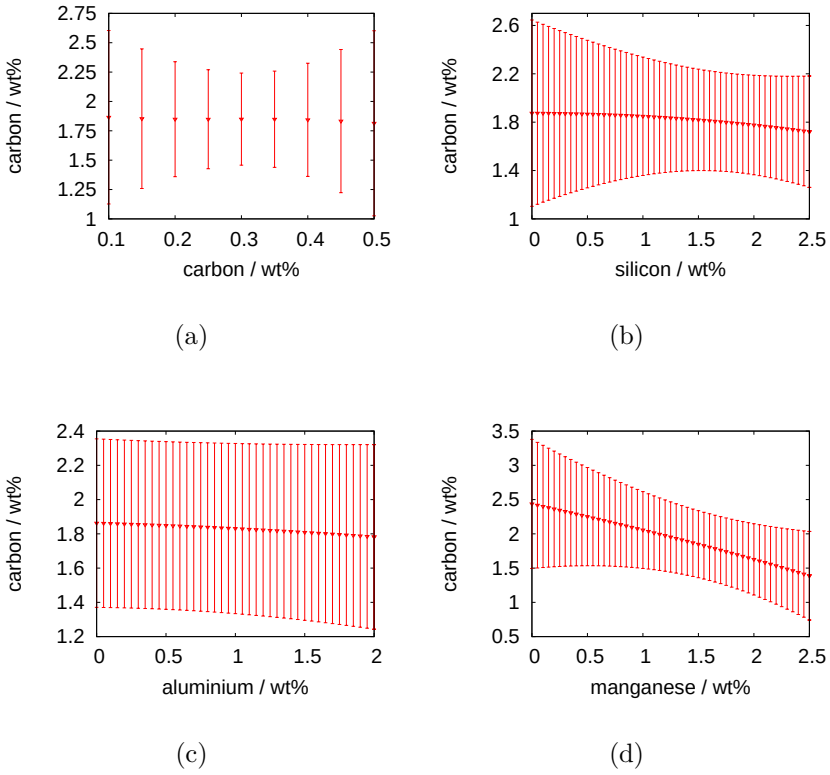

Figure 4.14: Effect of alloying elements on the carbon content of retained austenite: (a) carbon, (b) silicon, (c) aluminium and (d) manganese.

trated in Figure 4.15.

Austenite formed at a higher intercritical annealing temperatures is leaner in carbon. This can accelerate the subsequent transformation to bainite, resulting in rapid carbon enrichment of the residual austenite (Figure 4.15(a)). Similarly, with a longer holding period during the intercritical annealing, austenite gets enriched more with carbon and manganese, hence gaining stability. Subsequent transformation of austenite to bainite becomes sluggish, which explains the lower carbon enrichment at longer holding times of intercritical annealing (Figure 4.15(b)).

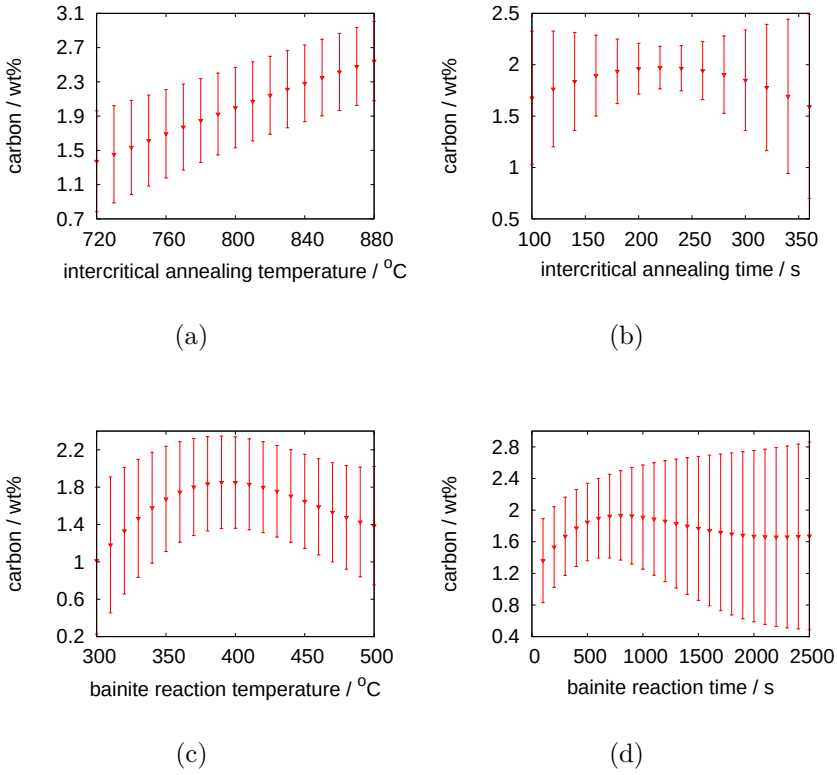

Figure 4.15: Effect of heat treatment conditions on the carbon content of retained austenite: intercritical annealing (a) temperature and (b) time; bainite transformation (c) temperature and (d) time.

Bainite transformation at a lower temperature should result in more carbon content of the retained austenite (as expected from T_0 criterion). This is observed up to a particular temperature, below which the carbon content appears to fall, as can be seen in Figure 4.15(c). At low temperature, transformation kinetics can be slow. Therefore the progress of bainite formation may not be sufficient to enrich the retained austenite with carbon. With an increase in bainite reaction time, carbon in retained austenite increases initially (Figure 4.15(d)). However, prolonged holding times may

result in some marginal loss of carbon, possibly due to cementite precipitation. Predictions for longer holding times are however associated with large uncertainties, limiting confidence in the predicted behaviour. More experiments are necessary in this region to confirm the predicted behaviour and its cause.

Figure 4.16 depicts the variation of carbon in retained austenite with progress of bainite reaction at two different temperatures for 0.2C-1.5Mn (wt%) steel made with either 1.5 wt% silicon or aluminium. Carbon in retained austenite appears to attain a maximum value at an intermediate time for both the steels at both temperatures. The maximum carbon content is higher at the lower transformation temperature for each steel. Furthermore, the maximum carbon content is higher for the aluminium-containing steel than that made with silicon. Both these predictions can be accounted for by the T_0 criterion of bainite transformation theory and can therefore be judged to be reasonable.

4.4 Summary

Neural network techniques have been adopted to create models for predicting the retained austenite fraction and its carbon content as a function of processing parameters and composition of TRIP-assisted steels.

Elements that tend to stabilise austenite over ferrite appear to increase the final retained austenite content. Retention of austenite is due to the carbon enrichment of the residual austenite after bainite formation. Therefore the rate of bainite formation seems to have a strong influence on retaining higher austenite fraction. Any factor that alters the rate of bainite transfor-

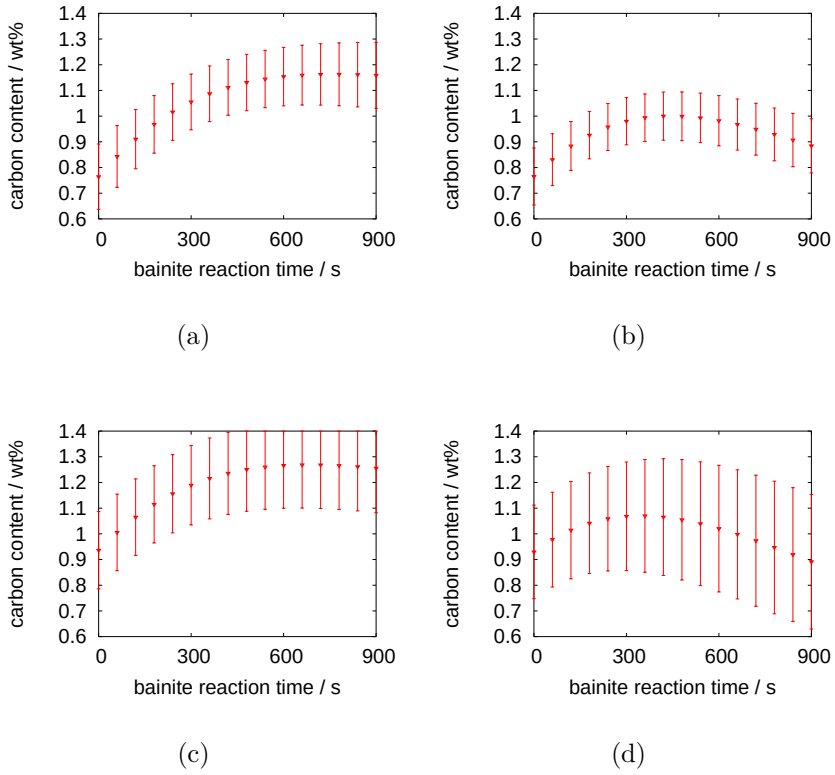

Figure 4.16: Variation in carbon content of retained austenite with bainite reaction time for 0.2C-1.5Mn-1.5Si (wt%) steel at transformation temperature of (a) 375°C and (b) 425°C; for 0.2C-1.5Mn-1.5Al (wt%) steel at transformation temperature of (c) 375°C and (d) 425°C.

mation affects retained austenite content in these steels.

The carbon content of retained austenite is primarily controlled by the extent of bainite transformation. However, the maximum carbon enrichment of the retained austenite can also be influenced by altering the T_0 point, with suitable alloying additions or the bainite formation temperature.

The model for retained austenite fraction was further used to formulate an optimum combination of silicon and retained austenite contents in these steels, as explained in the following Chapter.

Chapter 5

δ-TRIP steel

In TRIP-assisted steels, silicon helps to retain austenite by suppressing the precipitation of cementite. The carbon partitioned into the austenite, following the formation of bainite, remains there and permits it to be retained at room temperature. However, there is no quantitative theory to estimate the exact concentration of silicon necessary to prevent cementite. The silicon can be detrimental to the surface properties of automobile steels. So it is important to optimise both the silicon and the retained austenite contents.

The work presented in this chapter began with the aim of finding an optimum combination of silicon and retained austenite but the computational methods used gave surprising and interesting results. This stimulated experiments which led to the discovery of a new concept in TRIP-assisted steels.

To describe the story in a logical manner, the optimisation technique is explained first. This exploits the neural network model presented in Chapter 4. The final part deals with the design and testing of a steel with a radically different microstructure.

5.1 Optimisation

Numerical models can be used to optimise the chemical composition and process parameters of a material in order to achieve the appropriate microstructure or properties [Murugananth *et al.*, 2004]. This is done by the repeated interrogation of the numerical model in order to attain a specific output, in a process called optimisation (Figure 5.1).

The first step is to identify the target, the design variables *i.e.*, the input variables of the numerical model that are to be varied and the parameters which should not be altered during the calculations. An initial set of input variables is chosen and is used to evaluate the output parameter. The difference between the calculated output and the target is then used as a fitness for purpose parameter. If the fitness is not satisfactory, the optimiser algorithm decides the direction in which the design variables should be varied and the whole process is then repeated. The process terminates once the required degree of fitness is attained.

Optimisation methods are classified as linear or non-linear, based on the function relating the variables of the model [Nelder and Mead, 1965]. In practice, linear functions are seldom observed. Sequential quadratic programming, downhill simplex methods, genetic algorithms represent some of the non-linear methods of optimisation [Epogy, 2003].

Genetic algorithm

Genetic algorithms carry out the optimisation by mutation or recombination and selection [Epogy, 2003]. A point is first chosen in the design space. A family of points is subsequently generated around the initial one. This

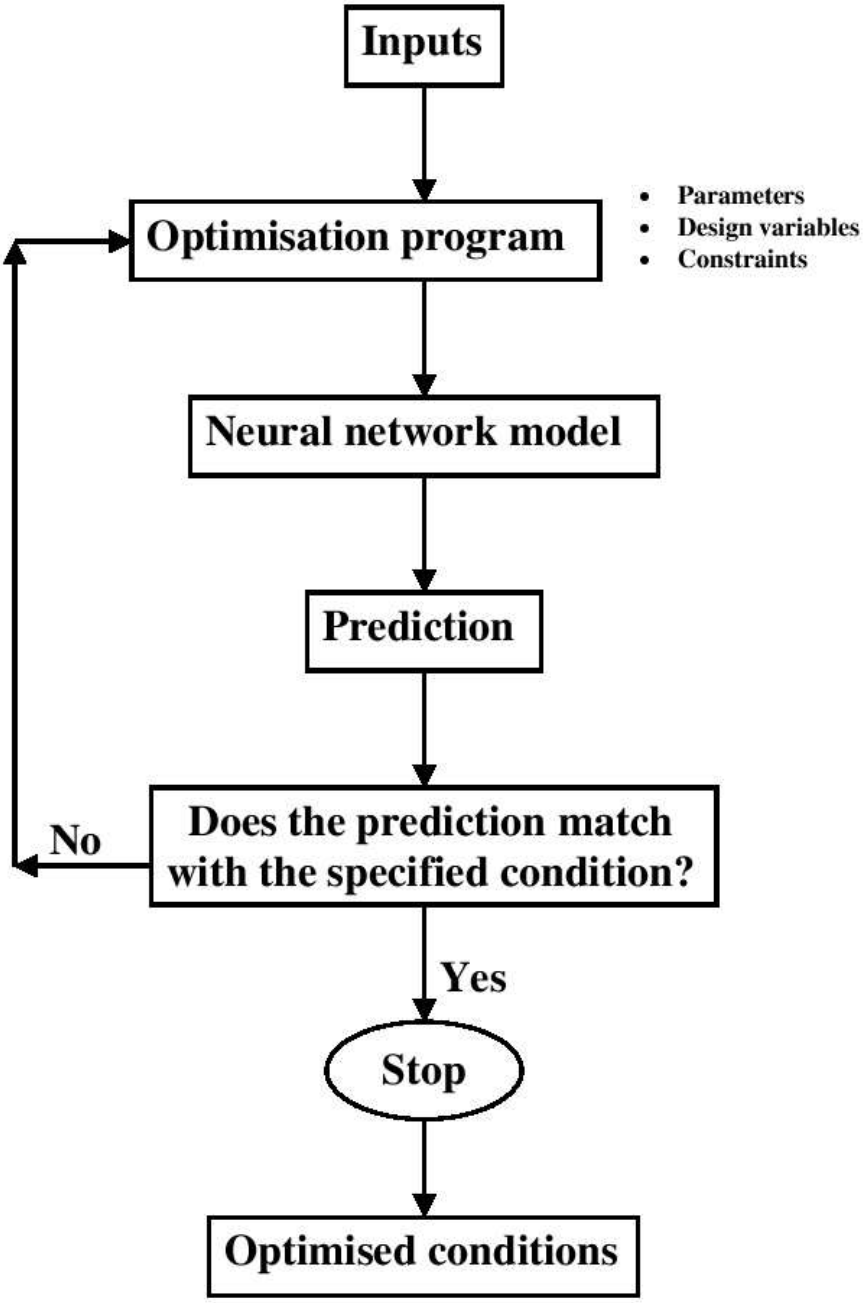

Figure 5.1: Flow diagram of the optimisation process.

is called mutation. By contrast, in the recombination process, values are exchanged between a random number of points. These are done in such a

way so that the points move in a direction allowing the objective function to be optimised. The best of all the points is finally selected as the solution.

5.2 Optimised TRIP-assisted steel

A genetic algorithm was used in the present work to formulate an optimum chemical composition of TRIP-assisted steel, given the objective of maximising the retained austenite fraction and keeping the silicon addition to a minimum. A neural network model was created relating the retained austenite fraction to the concentrations of different alloying elements and the process parameters of these materials, as described in Chapter 4. The model was coupled with commercial software, Epogy [2003], to carry out the optimisation process. The coupling and optimisation was carried out at Nanyang Technological University, Singapore by Dr M. Murugananth.

Concentrations of all the alloying elements, except phosphorous, were allowed to vary. The intercritical annealing temperature and the isothermal bainite reaction temperature were also chosen as design variables. However, the dwell time at these temperatures was kept constant. The uncertainty in the model prediction was considered as a constraint, with a maximum permitted value of 20%.

The algorithm converged to an alloy with the chemical composition Fe-0.4C-2Mn-0.5Si-2Al-0.5Cu-0.02P (wt%), with a microstructure estimated to contain 41±20 vol.% of retained austenite, after intercritical annealing at 840°C followed by bainite transformation at 300°C.

The alloy is rich in carbon, manganese, aluminium and copper. Each of these elements is known to help retain austenite [Girault *et al.*, 2001; Jacques

et al., 2001a; Kim and Lee, 1999; Sakuma *et al.*, 1991a; Shi *et al.*, 2002]. The concentrations of these elements were therefore increased by the algorithm while reducing the silicon content, as required by the objective. The result obtained therefore appears to be physically meaningful.

5.3 Thermodynamic calculations

Amounts of various phases in equilibrium as a function of temperature were calculated for the optimised alloy using MTDATA with the SGTE database. Ferrite, austenite, cementite and liquid were allowed to exist. The results are presented in Figure 5.2. The alloy starts to solidify by forming ferrite, which reaches a maximum of about 85 wt%. This is called δ-ferrite. Austenite starts to form thereafter with the amount of δ-ferrite decreasing. However, the calculations indicate that austenite can never exist as a single phase in the alloy. With cooling, the amount of austenite increases and attains a maximum of about 80 wt% before it starts to decompose to allotriomorphic ferrite.

Figure 5.2 also reveals the alloy to exist as a mixture of about 54 wt% austenite and 46 wt% ferrite at 840°C, the predicted intercritical annealing temperature for the optimum alloy. The chemical composition of the austenite formed at 840°C was calculated to be Fe-0.67C-2.54Mn-0.53Si-1.35Al-0.013P-0.51Cu (wt%). Temperatures at which the austenite can be expected to start transforming into bainite and martensite were calculated using the MAP_STEEL_MUCG73 program to be 354°C and 160°C respectively. Both the predicted intercritical annealing and the bainite reaction temperature of 300°C therefore appear reasonable.

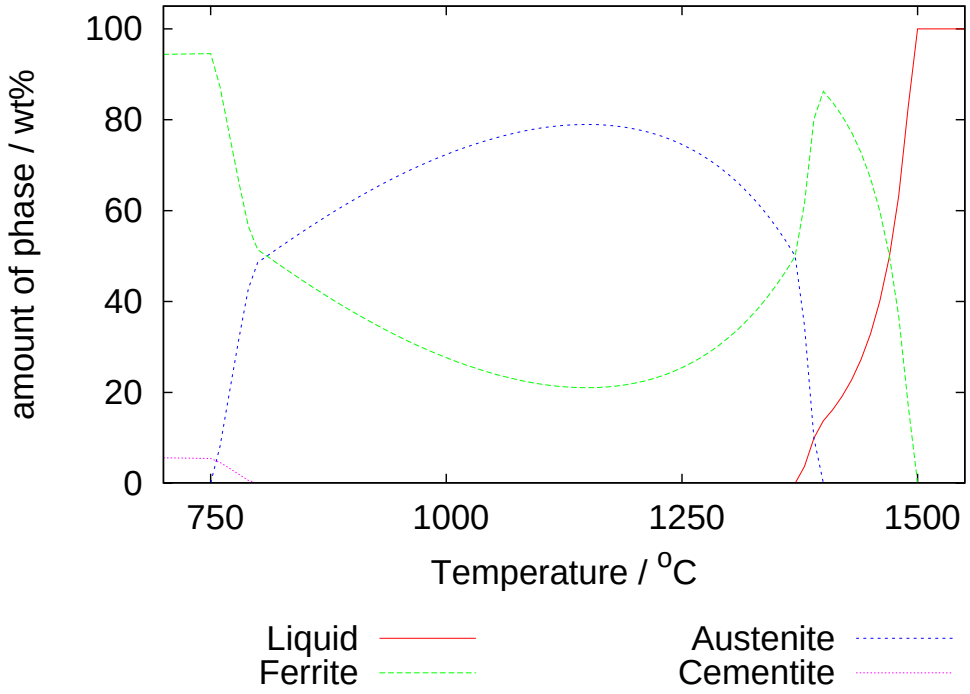

Figure 5.2: Calculated amounts of different phases as a function of temperature for the optimised alloy.

Retention of austenite in these steels is due to its carbon enrichment after the bainite reaction. Bainitic ferrite grows without any diffusion but excess carbon subsequently partitions to the residual austenite [Bhadeshia, 2001]. The reaction can be sustained till the free energy of the austenite becomes equal to that of the ferrite. This happens when the mole fraction of carbon in residual austenite becomes x_{T0}. This is calculated by the MAP_STEEL_MUCG73 program to be 0.0497 (*i.e.*, 1.115 wt%) at 300°C, for the austenite formed during intercritical annealing at 840°C.

The initial mole fraction of carbon in a fully austenitic sample, $\bar{x}$, can be related to the final volume fractions and carbon content of the bainitic

ferrite and austenite as,

$$\bar{x} = v_\alpha x_\alpha + v_\gamma x_\gamma \tag{5.1}$$

where v_α and v_γ are the volume fractions of bainite and austenite in the microstructure with mole fractions of carbon x_α and x_γ respectively.

The mole fraction of carbon in the austenite formed at 840°C is calculated to be 0.0312. Substituting $\bar{x} = 0.0312$, $x_\gamma = 0.0497$ and assuming $x_\alpha = 0$ in the above equation, the volume fraction of austenite remaining untransformed after bainite reaction at 300°C is calculated to be 0.628. Assuming the densities of bainite and austenite do not vary significantly, the calculations suggest the final weight fraction of retained austenite to be 0.628. However, in the present case, the initial weight fraction of austenite in the material before the bainite reaction was only 0.54. Thus the final retained austenite weight fraction, and hence also the volume fraction, can be expected to be 0.339. This austenite is expected to contain 1.115 wt% carbon and hence to be stable against further decomposition into martensite. The thermodynamic calculation therefore seems to be in reasonable agreement with the predictions made by the genetic algorithm.

Figure 5.2 indicates that the optimum alloy can never be fully austenitic. This could be due to the aluminium which stabilises δ-ferrite and forms γ-loop in the phase diagram. This is not generally desirable as it prevents the steel from becoming fully austenitic. However, TRIP-assisted steels in any case contain allotriomorphic ferrite which can, in principle, be substituted with δ-ferrite. This defines a new class of steels, designated δ-TRIP. Experiments were therefore carried out using alloys based on the optimum composition with the objective of using the δ-ferrite to design a

new microstructure and to test the properties.

5.4 Experiments

Materials

Based on the optimised composition, four alloys designated A, B, C and D were made in laboratory with chemical compositions as shown in Table 5.1. Alloy A was prepared in a vacuum melting furnace and in a small quantity of some 50 g. This was made simply to establish proof of concept. The other three alloys were made as 50 kg ingots in air-melting furnace. The three larger melts were made because it was difficult to get the desired composition.

Alloy	C	Mn	Si	Al	P	Cu
A	0.41	2.42	0.46	1.57	0.26	0.42
B	0.36	1.96	0.73	2.22	0.022	0.52
C	0.42	1.91	0.62	2.30	0.022	0.53
D	0.43	1.90	0.63	2.16	0.022	0.52

Table 5.1: Chemical compositions of the alloys made for experiments.

Heat treatment

Samples of alloys A and B in the as-cast condition were sealed in quartz tubes containing a partial pressure of argon for heat treatment in an air furnace. One set of the alloy A samples was tempered at 300°C for 1 h, 2 h and 4 h respectively. Samples of the alloys A and B were also subjected to two-step heat treatment, involving initial heating to a temperature in the (α+γ) phase region followed by an isothermal dwell at a lower temperature, in order to

obtain bainite. Details about the heat treatment parameters are described in the following section.

Characterisation procedures

Microstructures of the samples in both as-cast and heat-treated conditions were characterised using optical and field emission gun scanning electron microscopy (FEGSEM). Samples were polished using standard metallographic techniques and etched with 2% nital solution. The electron microscope was operated at a 10 kV accelerating voltage.

X-ray diffraction tests of the samples were carried out with a scan range of 40°-120° at 0.5° intervals and a 5 s dwell at each step. Cu-K_α radiation was used and the operating voltage and current were set at 40 kV and 40 mA respectively. Samples were polished, etched with 2% nital and then once again just fine polished before finally putting into the diffractometer.

Mechanical tests

The bulk hardnesses and the microhardness of the constituent phases were recorded with 10 kg and 50 g load respectively.

Uniaxial tensile tests were carried out with the heat-treated samples of the alloy B, at room temperature and 100°C. Specimens were machined from the heat-treated blocks with circular cross-section of 5 mm diameter and 30 mm gauge length. The samples were deformed with a strain rate of 2.8×10^{-5} s^{-1}. An extensometer of 10 mm gauge length was attached to the specimen tested at room temperature. However, this could not be used for the high temperature test. Samples cut from near the fracture surfaces were used for X-ray diffraction studies in order to measure the fraction of austenite remaining at fracture.

5.5 Results and discussion

Alloy A

Figure 5.3 presents the equilibrium phase fractions as a function of temperature for alloy A, as calculated using MTDATA with the SGTE database. This predicts significant quantities of δ-ferrite to be retained during solidification of the alloy. The microstructures of the alloy in the as-cast condition are presented in Figure 5.4, showing light-etching elongated grains of ferrite. The morphology is that of dendrites of δ-ferrite formed directly from the liquid during solidification. The micrographs also reveal a dark-etching residual phase, the nature of which is not clear from Figure 5.4. FEGSEM images, presented in Figure 5.5, indicate this residual phase to be martensitic.

The microhardnesses of δ-ferrite and the residual phase in the as-cast microstructure and the bulk hardness values are presented in Table 5.2. The high hardness of the residual phase is consistent with that of the high-carbon martensite [Bhadeshia and Honeycombe, 2006].

Phase	**Hardness / HV**
δ-ferrite	296±20
Residual phase	801±57
Bulk	412±25

Table 5.2: Microhardness of the constituent phases and the bulk hardness of the as-cast sample. The values represent the average of 20 readings in each case and the error bar represents one standard deviation.

The hardness data of Table 5.2 were used to estimate the volume fractions of the constituent phases in the as-cast sample using a rule of mixtures. Assuming the microhardnesses of the δ-ferrite and the residual martensitic

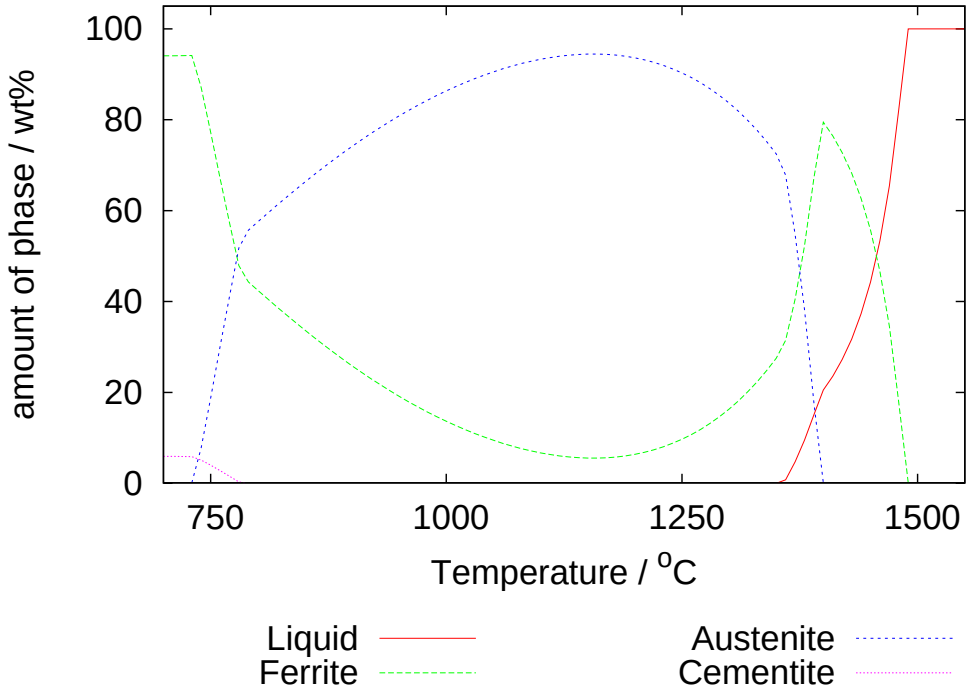

Figure 5.3: Calculated amounts of phases in equilibrium for alloy A.

phase are H_1 and H_2 respectively, the bulk hardness, H_b, of the sample can be expressed as:

$$H_b = vH_1 + (1 - v)H_2 \tag{5.2}$$

where, v is the volume fraction of δ-ferrite. A point count method was also used to measure the phase fractions. Assuming that the densities of the two phases are not significantly different, the measurements effectively represent the weight fraction of each phase, as presented in Table 5.3. Errors reported in the point count measurements represent $\pm 1\sigma$.

Figure 5.3 indicates a maximum of about 80 wt% δ-ferrite to form at 1400°C in equilibrium with liquid. Austenite forms on further cooling, leading to a decrease in the δ-ferrite content. Table 5.4 shows the calculated

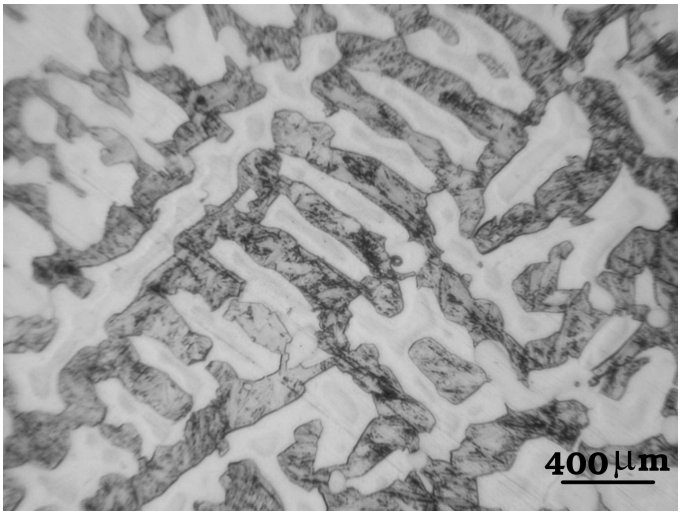

(a)

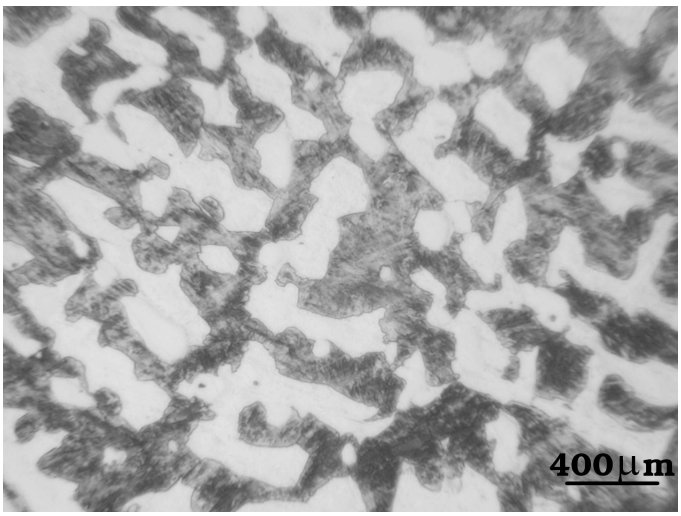

(b)

Figure 5.4: Optical micrographs of alloy A in the as-cast condition.

phase fractions and the chemical composition of the δ-ferrite and the liquid existing in equilibrium at 1400°C. The experimentally determined fraction of δ-ferrite in the as-cast microstructure appears comparable with that cal-

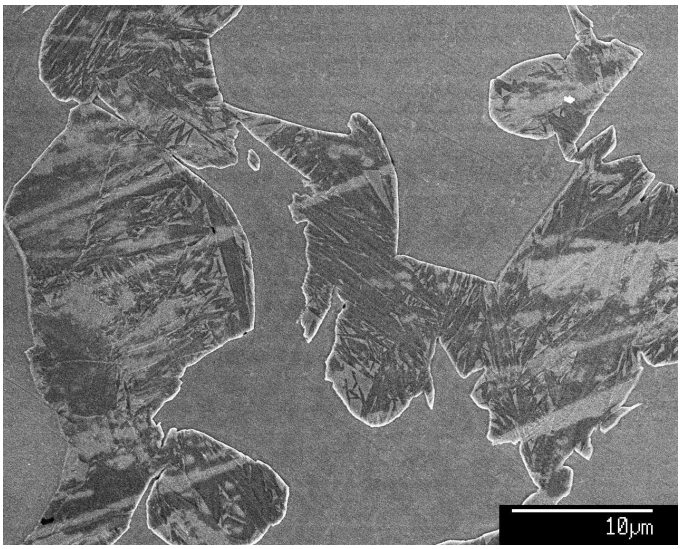

(a)

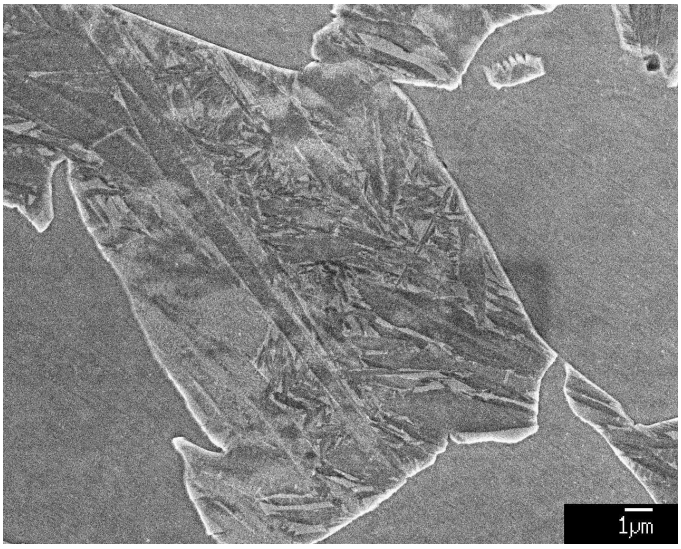

(b)

Figure 5.5: FEGSEM images revealing the martensite-like plates in the residual phase. Some of the plates contain a midrib which is consistent with high-carbon martensite.

Phase	Weight fraction	
	from hardness	from point count
δ-ferrite	0.77	0.74±0.04
Residual phase	0.23	0.26±0.01

Table 5.3: Weight fractions of the constituent phases in the as-cast microstructure.

culated, Table 5.4. It therefore appears that the alloy solidified by forming δ-ferrite upto a temperature of around 1400°C.

Phase	Amount / wt%	Composition / wt%					
		C	Mn	Si	Al	P	Cu
Ferrite	79.5	0.2	2.1	0.4	1.7	0.2	0.4
Liquid	20.5	1.2	3.7	0.7	1	0.2	0.4

Table 5.4: Calculated amounts and the chemical composition of the phases in equilibrium for the alloy A at 1400°C.

The liquid coexisting with the δ-ferrite at 1400°C is rich in carbon (Table 5.4). The austenite that will form from the liquid, and hence the martensite, can be expected to inherit the high carbon content. This supports the high hardness of the residual martensitic phase in the as-cast microstructure (Table 5.2). However, there must also be some austenite remaining untransformed, due to its high carbon content. X-ray diffraction was used to detect the presence of austenite and the analysis was carried out with the help of X'Pert Plus software which uses the Reitveld refinement method due to Wiles and Young [1981]. This gave about 7.8±0.7 wt% of retained austenite to be present in the sample.

A set of as-cast samples of the alloy was tempered at 300°C for varying time periods, mainly to confirm the high carbon content of the martensitic

residual phase. The microhardness of the phase was found to decrease drastically with increase in tempering time, as illustrated in Table 5.5. The average values of 20 readings with the error as one standard deviation are reported in Table 5.5.

Figure 5.6 shows the FEGSEM images obtained from a tempered sample. Compared to the as-cast condition (Figure 5.5), the residual phase after tempering appears with better contrast (Figure 5.6). This might be due to carbide precipitation from the martensite during tempering, increasing the interfacial area per unit volume thereby resulting in more intense etching.

Tempering time / h	**Microhardness / HV**
0	801±57
1	655±23
2	606±30
4	529±36

Table 5.5: Drop in microhardness of the residual martensitic phase with tempering time at 300°C.

The two-step heat-treatment of the as-cast samples were carried out to produce a microstructure comprised of δ-ferrite, bainite and austenite. Calculations using MTDATA with SGTE database revealed alloy A to consist of 60 wt% austenite in equilibrium with 40 wt% ferrite at 810°C (Figure 5.3). Samples of the alloy were therefore heated at 810°C for 12 h followed by a second isothermal hold at 300°C for 6 h. The MAP_STEEL_MUCG73 program was used to determine the time and temperature of the bainite reaction. The chemical composition of the austenite formed at 810°C was calculated using MTDATA and used as the input to the MAP_STEEL_MUCG73 program.

Figure 5.7 reveals elongated grains of δ-ferrite and a dark-etching sec-

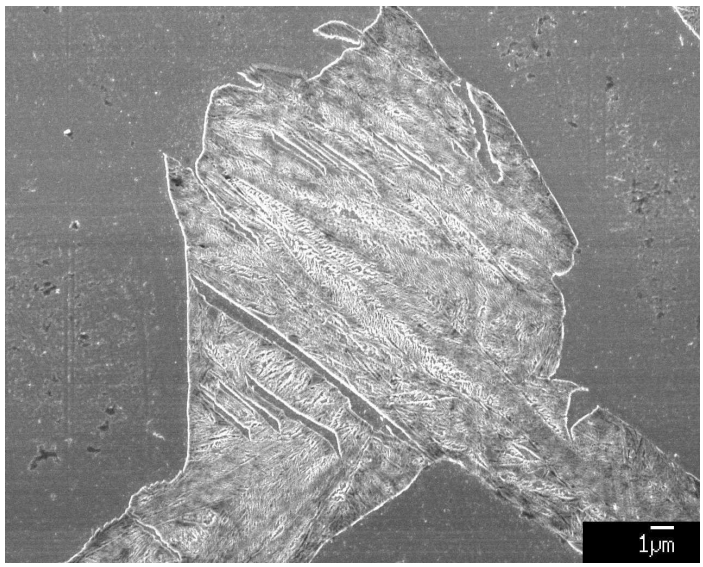

(a)

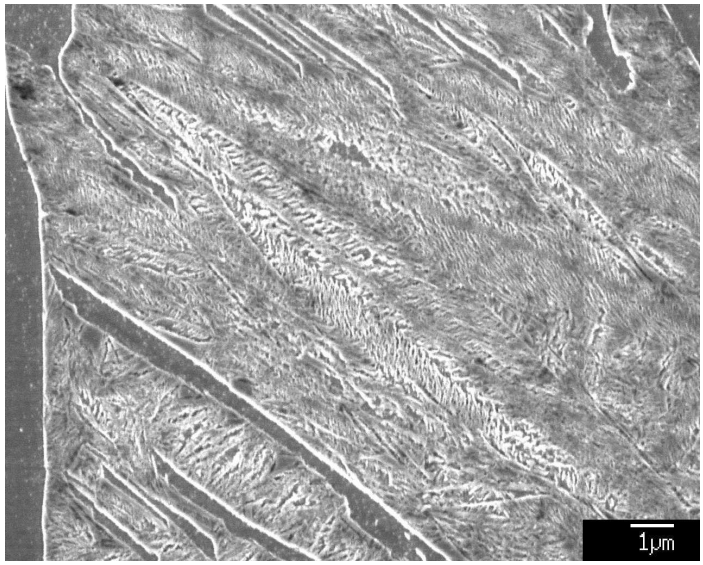

(b)

Figure 5.6: FEGSEM images of the sample tempered at 300°C for 4 h.

ond phase, the nature of which is not clear. The FEGSEM images of the sample are presented in Figure 5.8. It appears that the second phase is made up of bainite and retained austenite. The presence of about 14.3±0.7 wt% retained austenite is revealed by X-ray diffraction analysis. This is, however, seen to be less than both the amount of retained austenite predicted by the genetic algorithm and that calculated using the bainite transformation theory. The carbon content of the retained austenite was estimated to be 1.35±0.02 wt% from the lattice parameter of austenite, using the equation proposed by Dyson and Holmes [1979].

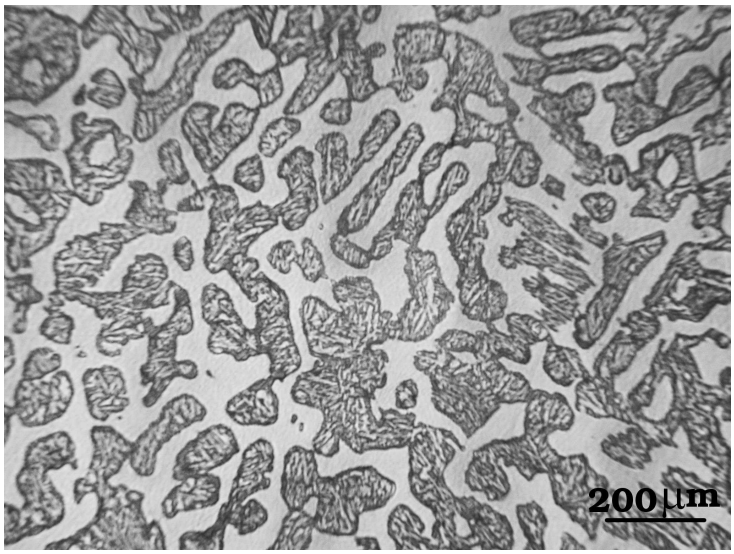

(a)

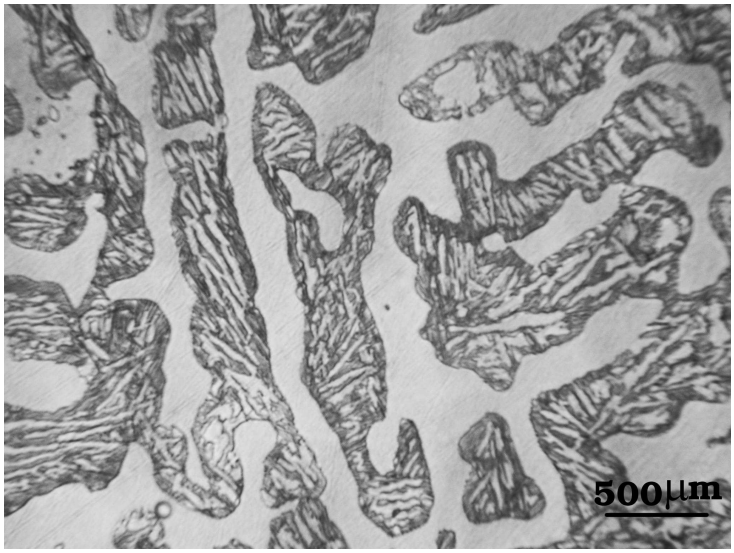

(b)

Figure 5.7: Optical micrographs of alloy A heat-treated to form bainite.

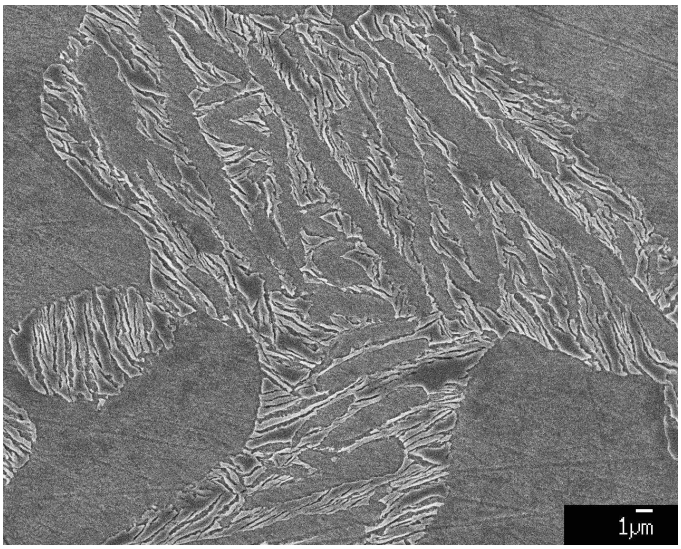

(a)

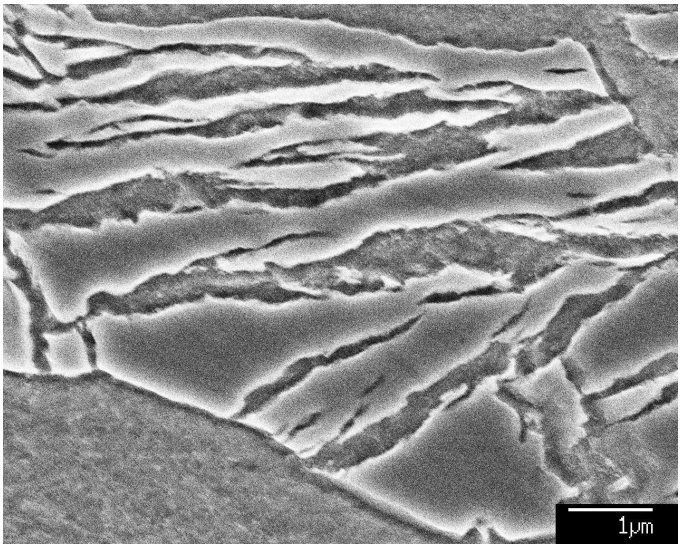

(b)

Figure 5.8: FEGSEM images of the heat-treated sample of alloy A revealing bainite.

Alloy B

As expected from Figure 5.9, the microstructure of the alloy in the as-cast condition reveals the presence of δ-ferrite, embedded in a dark-etching residual phase (Figure 5.10(a)). The microhardness of the residual phase in this alloy was recorded as 382±22 HV and that of the δ-ferrite as 214±8 HV. Unlike alloy A, the residual phase of this material does not therefore appear to be martensitic. Figure 5.10(b) reveals the residual phase to be pearlite.

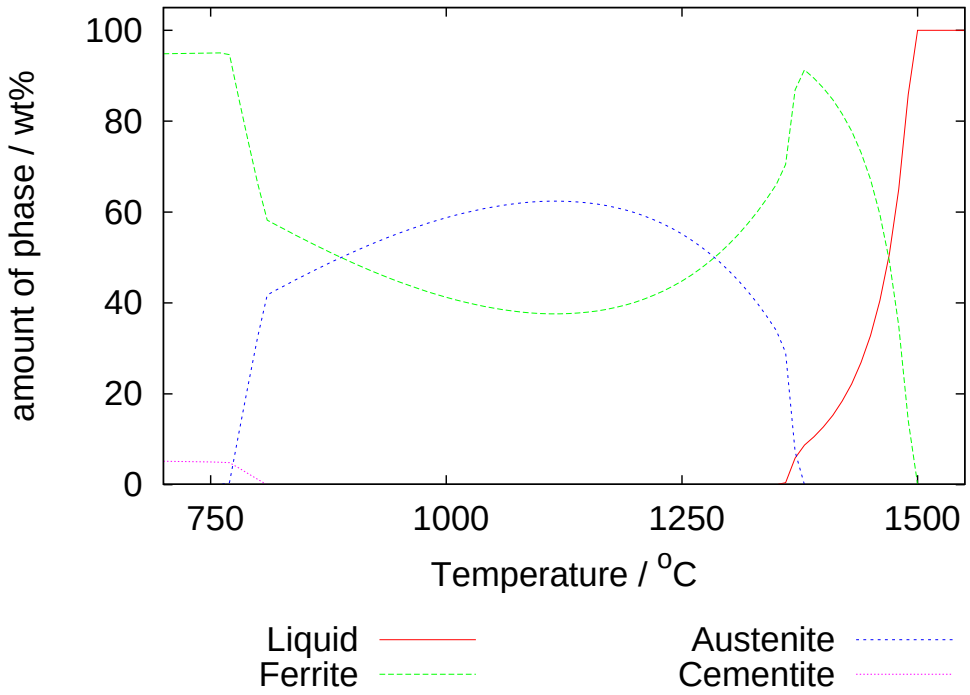

Figure 5.9: Amounts of phases in equilibrium at different temperatures for the alloy B, calculated using MTDATA with SGTE database.

Samples of alloy B were subjected to the two-step heat-treatment. Figure 5.9 reveals the alloy to exist as a mixture of 45 wt% ferrite and 55 wt% austenite in equilibrium at 940°C. Samples were therefore initially heated at

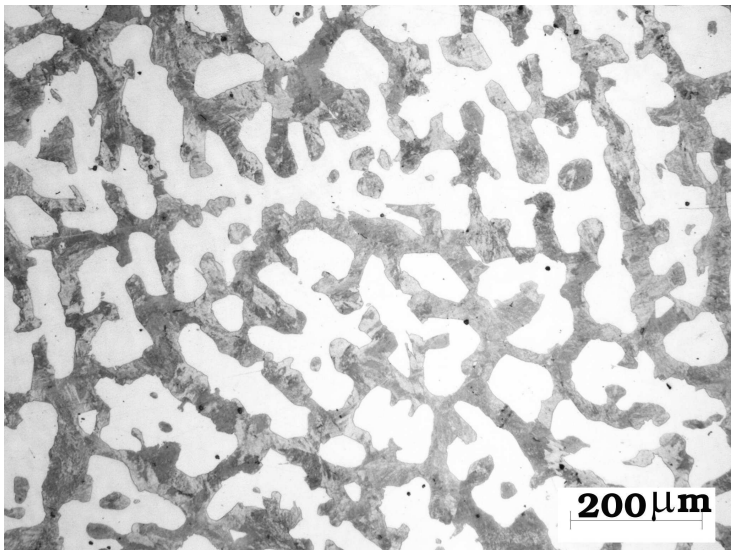

(a)

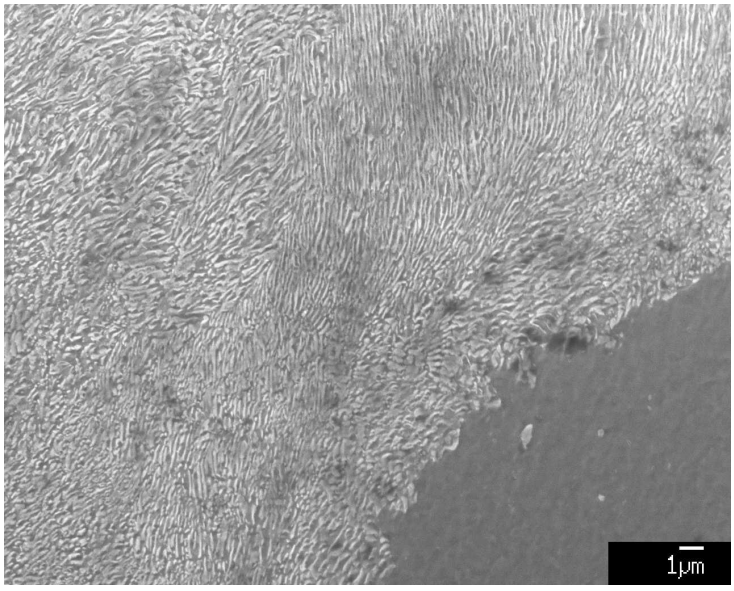

(b)

Figure 5.10: Microstructures of the as-cast sample of alloy B, (a) optical micrograph and (b) FEGSEM image.

940°C for 12 h and were subsequently allowed to transform into bainite at 300°C for 3 h.

Figure 5.11 depicts the microstructures of the heat-treated sample. The distinct morphology of the δ-ferrite is seen to have been retained after the heat-treatment, along with the formation of bainite. The presence of retained austenite in the heat-treated sample was confirmed with X-ray diffraction analysis, which revealed 13.5±0.9 wt% of retained austenite containing about 1.17±0.03 wt% carbon.

The microhardnesses of δ-ferrite and bainite along with the bulk hardness of the heat-treated sample are presented in Table 5.6. Hardness data and point counts were used to estimate the fractions of δ-ferrite and bainite, as described previously. Assuming that the densities of δ-ferrite and the bainitic phase are approximately equal, the measurements effectively represent the weight fraction of each phase, as presented in Table 5.7. The fraction of bainite is seen to be in reasonable agreement with that of the austenite present at the intercritical annealing temperature, calculated using MTDATA (Figure 5.9).

Phase	**Hardness / HV**
δ-ferrite	267±9
Bainite	519±13
Bulk	385±40

Table 5.6: Microhardnesses of the constituent phases and the bulk hardness of the heat-treated sample of alloy B.

Heat-treated samples of the alloy B were mechanically tested using uniaxial loading. The properties observed at room temperature are impressive with 23% total elongation and an ultimate tensile strength of 1000 MPa (Fig-

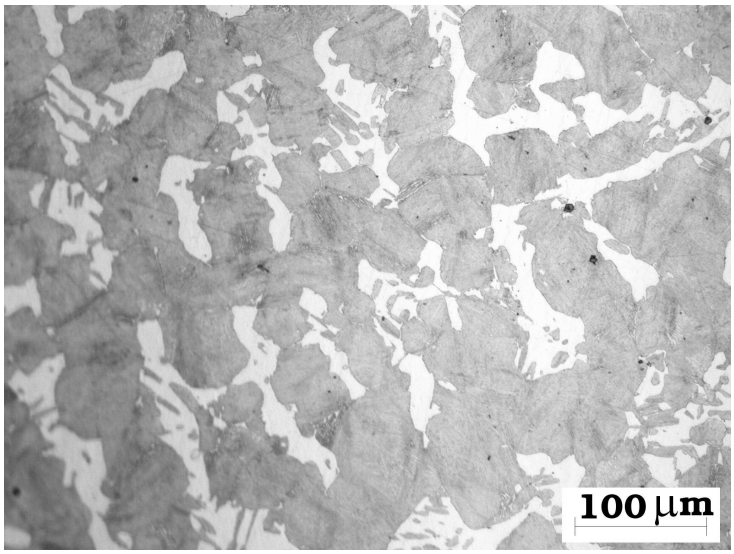

(a)

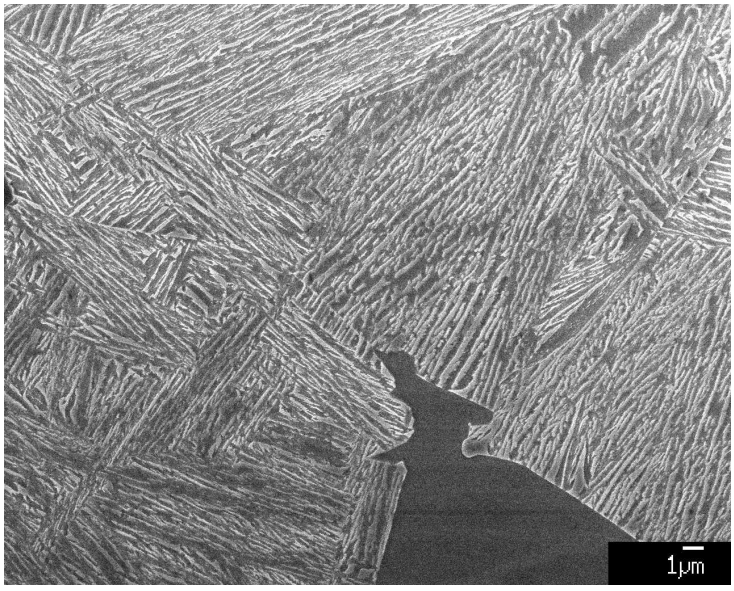

(b)

Figure 5.11: Microstructures of the heat-treated sample of alloy B, (a) optical micrograph and (b) FEGSEM image.

Phase	**Weight fraction**	
	from hardness	**from point count**
δ-ferrite	0.53	0.43±0.02
Bainite	0.47	0.57±0.03

Table 5.7: Weight fractions of δ-ferrite and bainite phases in the heat-treated sample of alloy B.

ure 5.12). The 0.2% proof stress was recorded as 700 MPa. There has been no significant necking of the sample at fracture suggesting that the elongation has mostly been uniform (Figure 5.13).

The true stress-strain plot in Figure 5.12 shows steady strain-hardening continuing until fracture. This could be due to the transformation of retained austenite into martensite during straining. The X-ray analysis of the sample cut from near the fracture surface of the tensile specimen indicated 7.0±0.8 wt% of austenite to exist. During straining, the austenite content was therefore reduced to half of that in the undeformed condition. The transformation of austenite into martensite during straining might have played a key role influencing the properties.

Figure 5.14 depicts the stress-strain curve recorded for the sample tested at 100°C. The more gradual slope of the elastic part of the curve as compared to the room-temperature tested sample is simply due to the absence of any extensometer. Compared to the properties at room temperature, the strength of the material remained unaltered but total elongation was reduced significantly when tested at 100°C. The true stress-strain plot in Figure 5.14 indicates that the strain-hardening has not been very effective unlike the specimen tested at room temperature. This might be due to the enhanced stability of austenite at the higher test temperature. The X-ray

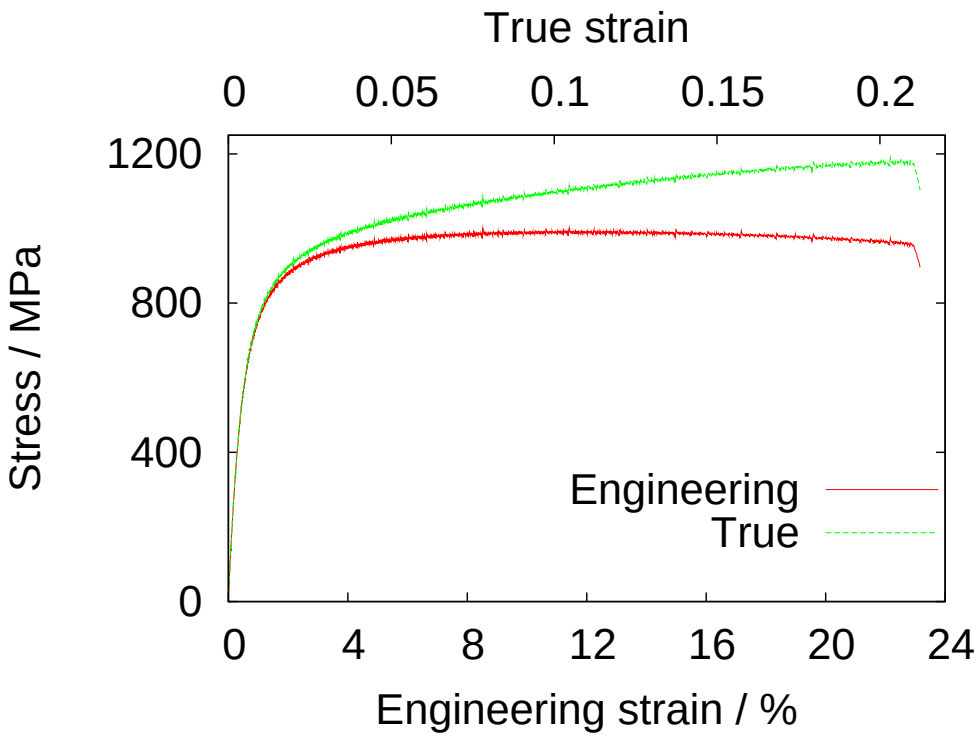

Figure 5.12: Stress-strain curve of the heat-treated material at room temperature.

Figure 5.13: No necking is observed implying the elongation is mostly uniform.

analysis confirmed about 13.0±0.7 wt% retained austenite to be present in the specimen after fracture. This is about the same as that of the heat-treated state, suggesting that there has been no transformation of austenite during straining.

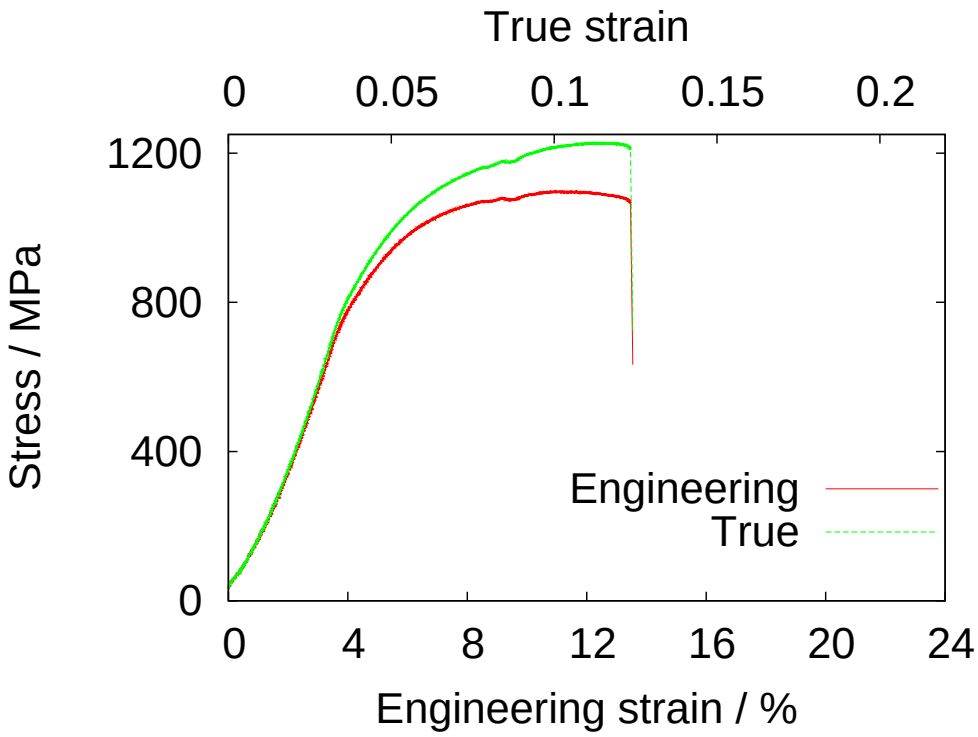

Figure 5.14: Stress-strain curve of the heat-treated material at 100°C.

Alloys C and D

Figure 5.15 indicates both the alloys C and D can be expected to have a similar phase transformation behaviour as that of the alloys A and B. However, it is surprising to observe that none of these materials revealed the presence of δ-ferrite in the as-cast condition. Figure 5.16 depicts the light-etching allotriomorphic ferrite formed along the prior austenite grain boundaries in alloys C and D. The morphology of the ferrite grains in these materials is in sharp contrast to that of the elongated δ-ferrite grains, as observed in alloys A and B.

The absence of δ-ferrite in as-cast microstructures of alloys C and D could be due to the cooling pattern during solidification. Figure 5.15 suggests that δ-ferrite forms during solidification up to around 1400°C. At lower temperatures, austenite starts gaining stability over ferrite. A fast cooling rate during solidification can bring down the temperature rapidly below 1400°C, thereby avoiding the chance of forming δ-ferrite. This might have led to the solidification of the alloys C and D forming austenite, which has transformed partly to allotriomorphic ferrite during subsequent cooling.

5.6 Summary

TRIP-assisted steels are made with silicon, which helps retaining austenite. However, silicon leads to many difficulties during processing and deteriorates the surface quality of the steel. A genetic algorithm coupled with a neural network model yielded an optimised chemical composition which is low in silicon content but rich in aluminium, manganese and copper.

Experiments to confirm the calculations gave surprising results. Some of the alloys demonstrated an enhanced tendency of δ-ferrite formation during solidification, as expected from phase diagram calculations. However, there was no evidence of the presence of δ-ferrite in the as-cast microstructures of some other alloys, which could be due to the difference in cooling pattern.

The as-cast samples of the alloys containing δ-ferrite were heat-treated to form microstructures containing δ-ferrite, bainite and retained austenite. The heat-treated samples were found to possess impressive mechanical properties at room temperature. However, increased stability of the retained austenite at higher temperature might have been responsible for impairing the ductility of the specimen tested at 100°C.

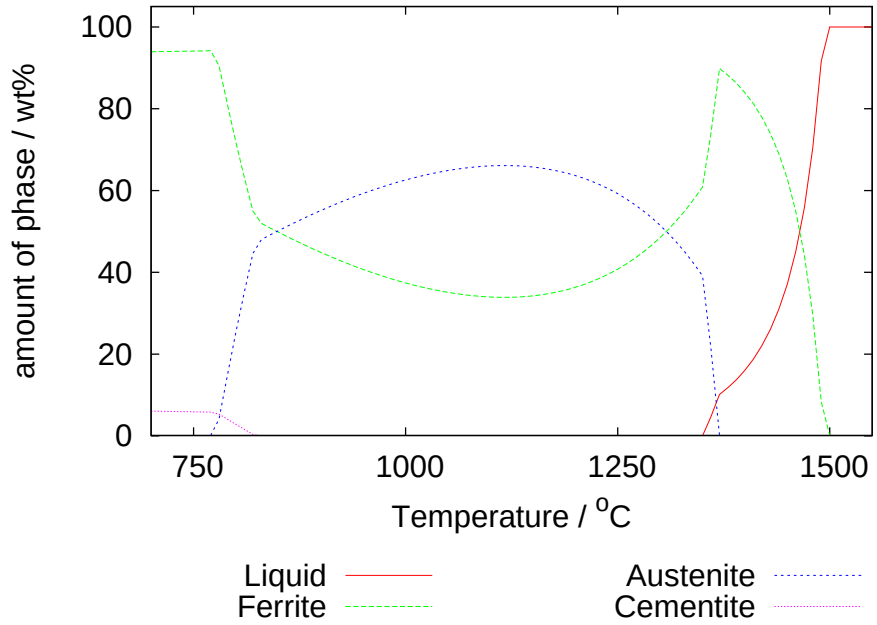

(a)

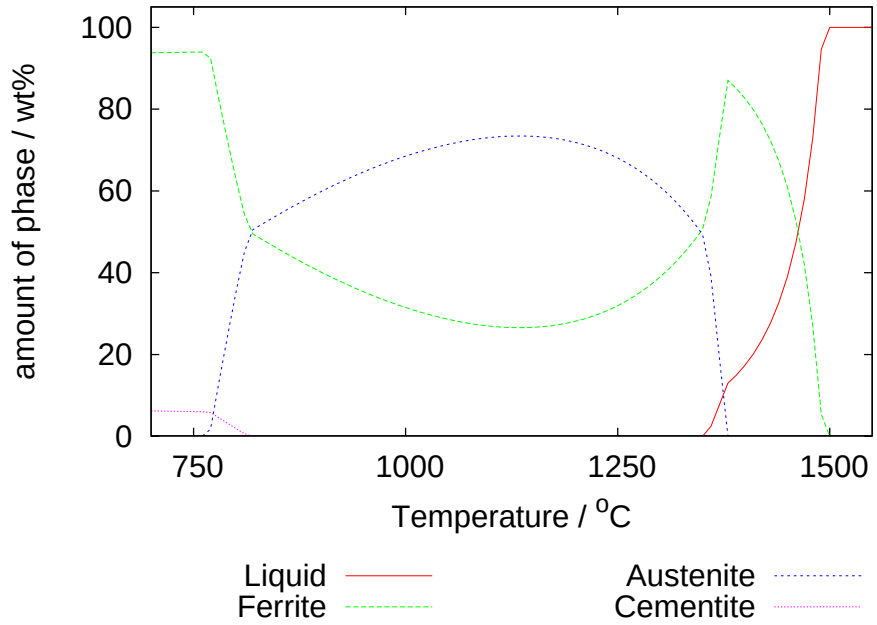

(b)

Figure 5.15: Amounts of phases in equilibrium at different temperatures for the (a) alloy C and (b) alloy D, calculated using MTDATA with SGTE database.

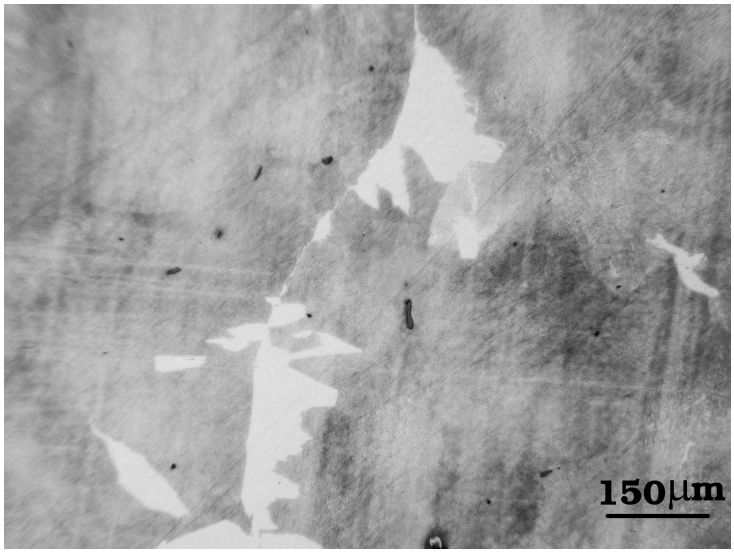

(a)

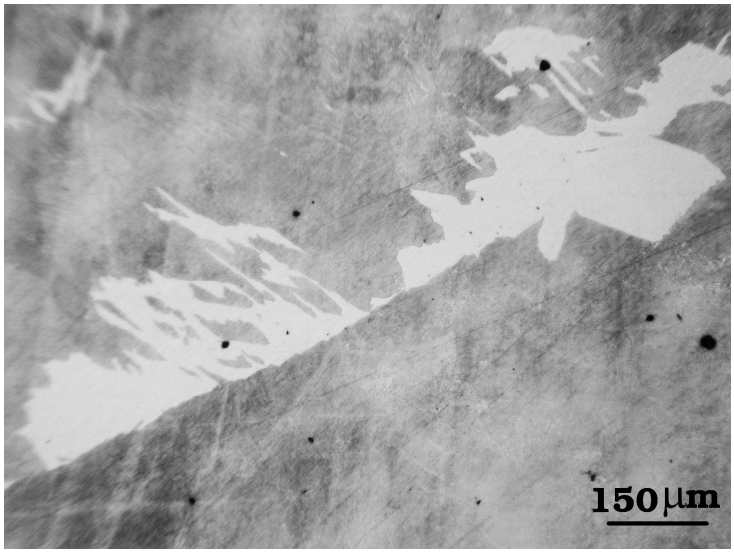

(b)

Figure 5.16: Optical micrographs from the as-cast alloys C and D showing allotriomorphic ferrite along the prior austenite grain boundary.

Chapter 6

Mechanical Stabilisation

Austenite can be induced to transform to martensite above the M_S temperature by stress or strain. This induced transition is widely believed to be the cause of the excellent mechanical properties, especially the formability, of TRIP-assisted steels. Stress adds to the thermodynamic driving force whereas plastic strain affects the kinetics of the process. Defects created in austenite due to strain provide additional nucleation sites. However, growth of martensite plates can be hindered by defects in austenite and excessive deformation can even halt the transformation, in a phenomenon known as mechanical stabilisation. The purpose of the present chapter is to study the role of stress and strain on martensitic transformations.

6.1 Mechanical driving force

Martensitic transformation during deformation of austenite was first discovered by Scheil [1932], the thermodynamics of which was explained by Patel and Cohen [1953]. Stress makes transformation possible above the M_S tem-

perature by supplying the shortfall of the necessary thermodynamic driving force. This is illustrated schematically in Figure 6.1. The free energy change, ΔG_1, available at the M_S temperature is the critical driving force necessary for transformation. At a temperature T_1 above M_S, the magnitude of the free energy change due to transformation, ΔG_2, is less than the critical driving force, ΔG_1. Martensite can only be formed at this temperature by supplying additional energy of a magnitude U, so that $U + \Delta G_2 = \Delta G_1$. This can be done by applying stress. The work done by external stress adds to the available chemical free energy change as a mechanical driving force for transformation at any temperature.

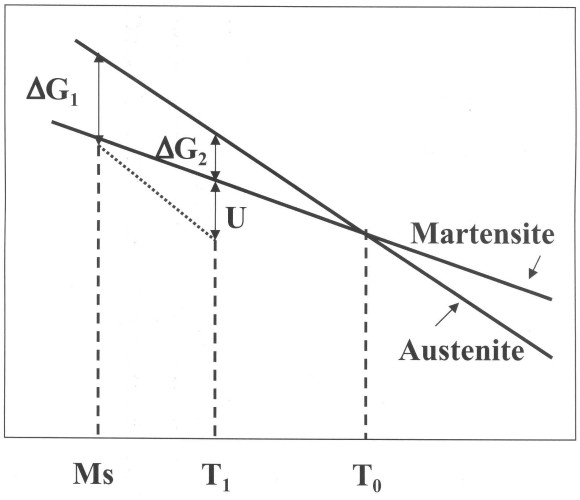

Figure 6.1: A shortfall in driving force for martensitic transformation above the M_S temperature can be compensated for by the application of stress.

Transformation of austenite to martensite is accomplished by a permanent shape deformation. This is characterised by an invariant-plane strain deformation with ζ and s as the dilatational and shear components of the shape deformation respectively. The mechanical driving force due to an ex-

ternal stress, σ, can then be expressed as:

$$\Delta G_{mechanical} = \sigma_N \zeta + \tau s \tag{6.1}$$

where σ_N is the normal component and τ is the shear component of the applied stress resolved along the direction of the shear displacement of the shape deformation. Both σ_N and τ act on the crystallographic plane of austenite on which the plate of martensite forms (Figure 6.2).

Work done by the shear component of the applied stress is always expected to be positive whereas that due to the normal component may be positive (in tension) or negative (compression). In steels, the shear component of the shape deformation is much higher in magnitude than the dilatational component. Thus the observed effect of stress arises mainly from the work done by the shear component. However, hydrostatic stress interacts only with the dilatational component and therefore is not very effective for inducing transformation in steels. Hydrostatic compression, in fact, suppresses transformation since in steels, there is a volume expansion on martensitic transformation.

6.2 Role of strain

As is apparent from Figure 6.1, the higher the temperature above M_S, the greater the stress required to initiate transformation. It is possible therefore that above a critical temperature austenite will be plastically deformed before transformation, which is often referred as strain-induced transformation.

Plastic strain in austenite creates defects that can act as additional

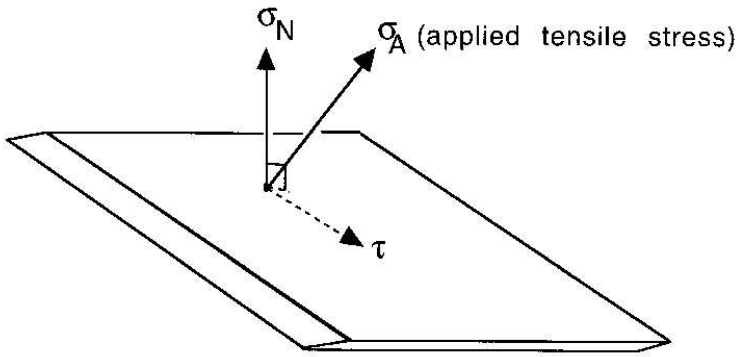

Figure 6.2: Resolved normal and shear components of the external stress [Bhadeshia, 2001].

nucleation sites for transformation. This is in contrast to the stress-assisted transformation that starts from the same nucleation sites as athermal transformation but with the thermodynamic assistance of external stress. Plastic strain thus renders a kinetic advantage over the thermodynamic contribution of the accompanying stress [Lecroisey and Pineau, 1972; Manganon and Thomas, 1970; Olson and Cohen, 1972; Venables, 1964].

Transformation from plastically strained austenite has been generally observed to occur at a stress level lower than that expected from the contribution of stress alone. There is a difference in opinion regarding the cause of such an observation:

- Olson and Cohen [1979] ascribed this behaviour to the higher potency of the nucleation sites created by plastic strain.

- Onodera and Tamura [1979] explained the same behaviour in terms of the stress concentration at defects, which may reach the critical stress required for transformation, even when the magnitude of the applied stress is less.

In spite of the nucleation advantage, plastic strain in austenite may actually act to retard transformation. Defects generated due to strain can hinder the growth of martensite plates. This is generally explained in terms of the martensite-austenite interface structure, which is made up of a set of screw dislocations, as depicted schematically in Figure 6.3 [Christian, 2002].

Growth of a martensite plate involves translation of the glissile interface, which can be made sessile by obstacles like grain boundaries. Plates of martensite are therefore never observed to traverse austenite grain boundaries. Smaller defects like isolated dislocations resist the motion of the interface but can often be incorporated into the lattice of martensite. However, heavy dislocation debris in austenite generated by severe plastic deformation can halt the transformation. This is known as mechanical stabilisation [Bhadeshia, 1999b; Breedis and Robertson, 1963; Leslie and Miller, 1964; Machlin and Cohen, 1951; Raghavan, 1992].

6.3 Mathematical formulation

The purpose here is to developed a theory to predict the critical strain necessary for causing mechanical stabilisation of austenite. The problem is one of balancing the force required to sustain the motion of the transformation interface against the resistance due to the dislocation debris in austenite.

Dislocation theory

At low homologous temperatures, plastic deformation is caused by the translation of dislocations. The resultant plastic strain ϵ is given by [Honeycombe,

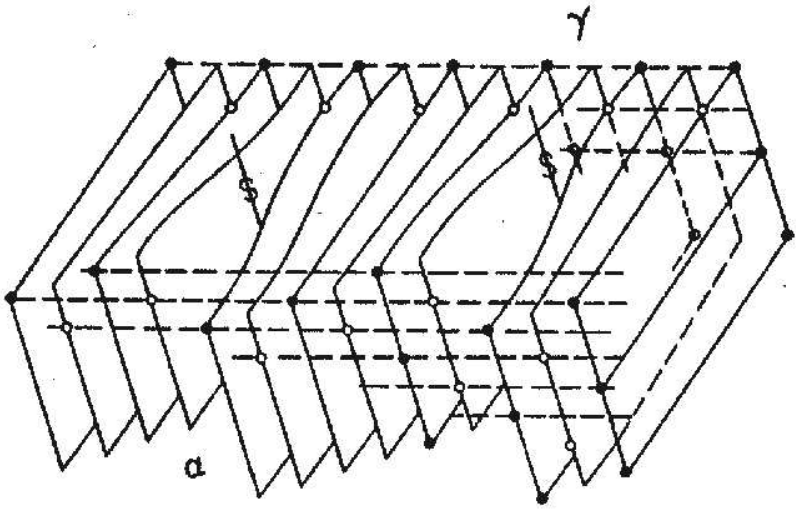

Figure 6.3: Model of austenite-martensite interface (after Frank [1953]), a screw dislocation with a lattice Burgers vector is necessary at every sixth atomic closed-packed plane to match the atomic rearrangements [Christian, 2002].

1984]:

$$\epsilon = \rho b L \tag{6.2}$$

where ρ is the dislocation density, b is the Burgers vector and L is the average distance moved by the dislocations.

For a given dislocation density, the spacing between the dislocations is given by $l = \rho^{-\frac{1}{2}}$. Under these circumstances, the mean shear stress τ required to move dislocations past each other is given as [Honeycombe, 1984]:

$$\tau = \frac{Gb}{8\pi(1-\nu)l} = \frac{Gb\rho^{\frac{1}{2}}}{8\pi(1-\nu)} \tag{6.3}$$

where G is the shear modulus and ν the Poisson's ratio. On combining with equation 6.2 and noting that the force per unit length is τb,

$$\tau b = \frac{G b^{\frac{3}{2}}}{8\pi(1-\nu)}\sqrt{\frac{\epsilon}{L}} \tag{6.4}$$

The mean free distance L must decrease as the plastic strain increases [Barlat *et al.*, 2002]:

$$L = \frac{\delta D}{\delta + D\epsilon} \tag{6.5}$$

where D is the original grain size of austenite prior to straining and δ is a coefficient about equal to $1\,\mu$m [Barlat *et al.*, 2002].

Besides dislocation strengthening, solid-solution hardening adds to the total resistance to interface motion [Olson and Cohen, 1976a-c; Ghosh and Olson, 2001]. Solid solution hardening coefficients for various solutes in austenite have been reported for tensile strength by Irvine *et al.* [1969]. These values can be converted into shear stress equivalents τ_S using the Tresca criterion.

Chemical driving force

The stress τ_T driving the motion of the interface originates from the chemical free energy change ΔG of transformation [Olson and Cohen, 1976a-c]:

$$\tau_T = \phi \Delta G \tag{6.6}$$

where ϕ is a constant assumed to be equal to unity and $\Delta G = G_\gamma - G_\alpha$ *i.e.,* the magnitude of the driving force which is a function of temperature and the chemical composition of the alloy.

Lattice distortions due to the accommodation of the shape deformation accompanying transformation must be accounted for in terms of stored energy. The magnitude of this is given by Christian [1979] to be about 600 $\mathrm{J\,mol^{-1}}$. This has to be subtracted from the free energy change of transformation (obtained using MTDATA), in order to determine the stress driving the interface motion. The magnitude of force per unit length available for driving the austenite-martensite interface can be obtained by multiplying τ_T with the Burgers vector b.

Model

Mechanical stabilisation occurs when the force driving the interface equals that opposing its motion:

$$\tau_T = \tau + \tau_S \tag{6.7}$$

$$b\Delta G = \frac{1}{8\pi(1-\nu)} G b^{\frac{3}{2}} \sqrt{\frac{\epsilon}{L}} + \tau_S b \tag{6.8}$$

This equation can now be used to calculate the critical strain for mechanical stabilisation.

6.4 Results and discussion

The key input to the model for calculating the critical strain necessary for mechanical stabilisation is the free energy change accompanying the transformation of austenite to martensite, ΔG. The free energy change is a function of temperature and the composition of the steel and can be calculated using the software MTDATA. The software accesses the thermodynamic database SGTE to calculate phase stabilities and free energies. The free energy values

obtained from MTDATA were reduced by 600 J mol^{-1} to account for the stored energy of martensite. The magnitudes of different constants used in calculations are listed in Table 6.1.

Property	Value
Shear modulus of austenite	8×10^{10} Pa
Poissons ratio	0.27
Burgers vector	2.52×10^{-10} m

Table 6.1: Values of constants used in the model.

6.4.1 Austenitic stainless steels

A range of chemical compositions of austenitic stainless steels are listed in Table 6.2. The reason for varying the nickel concentration was to study the effect of the chemical driving force for transformation on the stabilisation to martensitic transformation. All the calculations were carried out allowing for solid-solution strengthening and for a variety of temperatures.

Alloy	C	Mn	Si	Cr	Ni	Mo	N
Alloy 1	0.05	1.5	0.75	18.0	6.0	0.0	0.03
Alloy 2	0.05	1.5	0.75	18.0	8.0	0.0	0.03
Alloy 3	0.05	1.5	0.75	18.0	10.0	0.0	0.03
Alloy 4	0.05	1.5	0.75	18.0	12.0	0.0	0.03
316L	0.01	0.53	0.75	17.1	11.9	2.0	

Table 6.2: Chemical compositions (wt%) of different austenitic stainless steels.

Figure 6.4 shows the chemical driving force (before the subtraction of the 600 J mol^{-1} stored energy) as calculated using MTDATA. It is seen that these are very large driving forces, especially for 300 K which is normally the

ambient deformation temperature. The original grain size was taken to be 40 μm.

The critical strain calculated using the model for each alloy at different temperatures is presented in Figure 6.5. It can be seen that the strain values are very large, ranging from ϵ =2.9–4.5. The strain values increase with decreasing nickel concentration *i.e.*, increasing the free energy change, ΔG, of transformation.

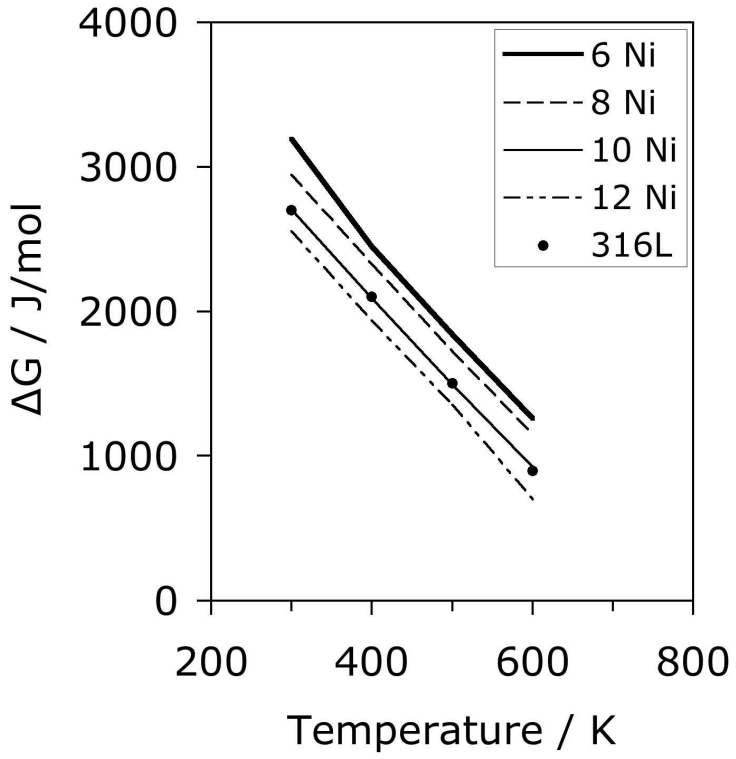

Figure 6.4: Free energy change in different alloys as listed in Table 6.2 at different temperatures.

In physical terms, this means that the mean free path L has to be very small, less than 1 μm, as illustrated in Figure 6.6. Huge plastic strains are required to achieve the necessary defect density, so such a result may at first

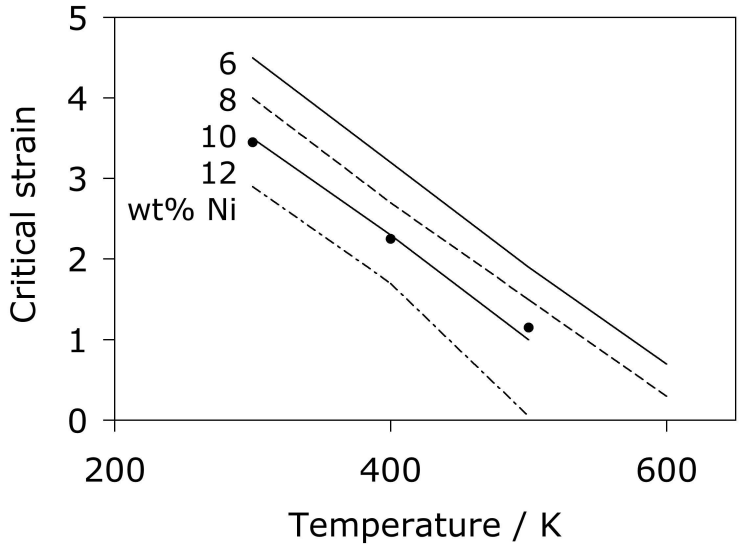

Figure 6.5: Calculated strain to initiate mechanical stabilisation at different temperatures for various alloys.

sight seem unlikely. However, experiments carried out with 316L austenitic stainless steel deformed to a true strain of $\epsilon = 6.3$ confirms that severe deformation is indeed necessary to mechanically stabilise the austenite [Wang *et al.*, 2005].

Figure 6.7 shows the curve obtained by fitting to experimental data from the 316L experiments [Wang *et al.*, 2005]. It was demonstrated that thermodynamically the alloy should be able to transform completely into martensite, were it not for the fact that the deformed austenite becomes mechanically stabilised. In fact, the amount of strain-induced martensite is limited to 57%, with much of this formed at low strains before the onset of stabilisation. On the basis of the fitted curve (Figure 6.7), the onset of mechanical stabilisation, *i.e.* the strain at which strain-induced martensite ceases to significantly increase with strain, is about $\epsilon = 2 - 3$.

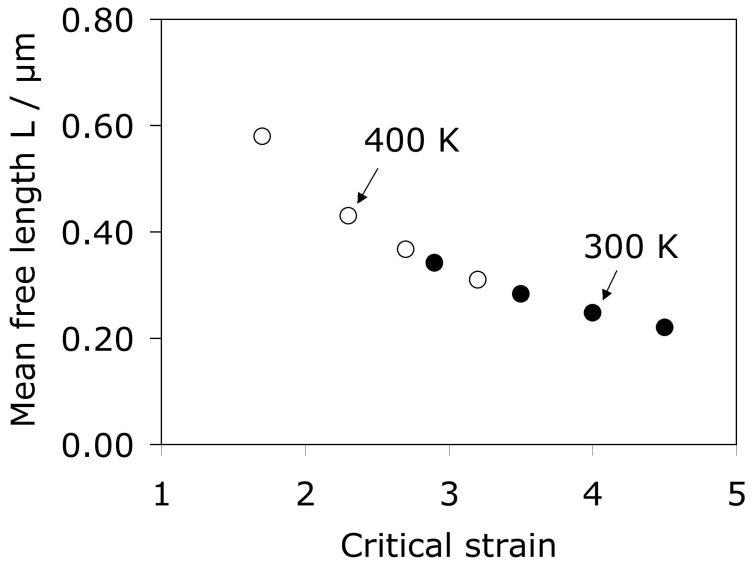

Figure 6.6: Variation of the mean free path with strain for mechanical stabilisation, open circles for 400 K and filled circles for 300 K.

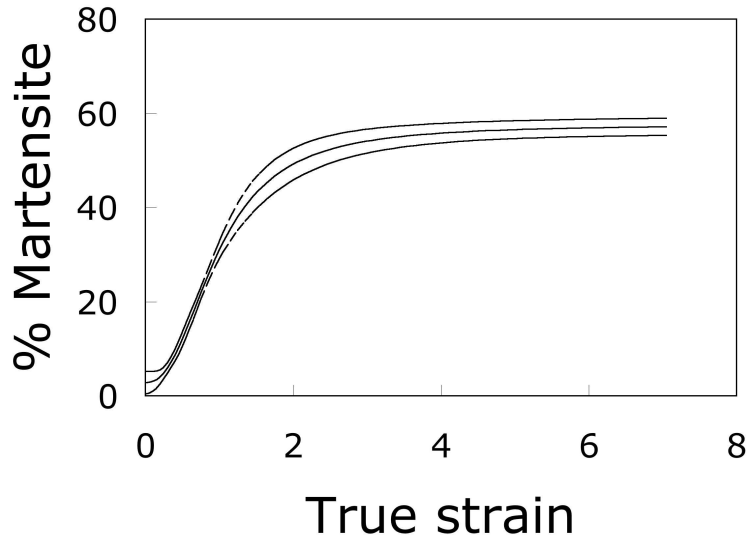

Figure 6.7: Experimental fitted curve for strain-induced martensite formation in 316L stainless steel [Wang *et al.*, 2005].

The calculated data for 316L are presented as points in Figure 6.5; they show that the critical strain for mechanical stabilisation is 3.45, 2.25 and 1.45 for the temperatures 300, 400 and 500 K respectively. The large strain data of the experiments are based on wire drawing and it is conceivable that the temperature rises by around 200 K during the deformation [Wang *et al.*, 2005]. The calculations are therefore consistent with the experimental data. Furthermore, the analysis shows that large strains needed to achieve stabilisation is due to the large values of ΔG for transformation in such stainless steels at the deformation temperature.

6.4.2 TRIP-assisted steels

In TRIP-assisted steels, high-carbon retained austenite transforms to martensite during deformation. In order to calculate the strain required to cause mechanical stabilisation in these steels, the chemical composition of the retained austenite grains must be known precisely.

These steels are intercritically annealed in the $(\alpha+\gamma)$ two phase region prior to the bainite reaction. Retained austenite gets enriched with carbon subsequent to the bainite reaction. The carbon content of retained austenite is generally reported for these steels [Itami *et al.*, 1995; Jacques *et al.*, 2001c; Sugimoto *et al.*, 1992b; Tomita and Morioka, 1997]. However, substitutional solutes do not partition during bainitic transformation. Therefore, the concentrations of these elements in the final retained austenite remain the same as that before the bainite reaction. The dwell time during intercritical annealing is very short and so equilibrium partitioning of the substitutional solutes is very unlikely. By contrast, the carbon concentration can be expected to

attain equilibrium in austenite within the short intercritical annealing period. The substitutional solute content of the retained austenite can be calculated using MTDATA, assuming the existence of equilibrium and paraequilibrium during intercritical annealing separately.

The thermodynamic driving force for transformation of austenite to martensite was calculated using MTDATA at the temperature of deformation. Retained austenite grains in these steels are generally reported to be very fine (about 1 μm) [Jacques, 2003]. These values were used as inputs to the model to determine the critical strain necessary for mechanical stabilisation (Figure 6.8).

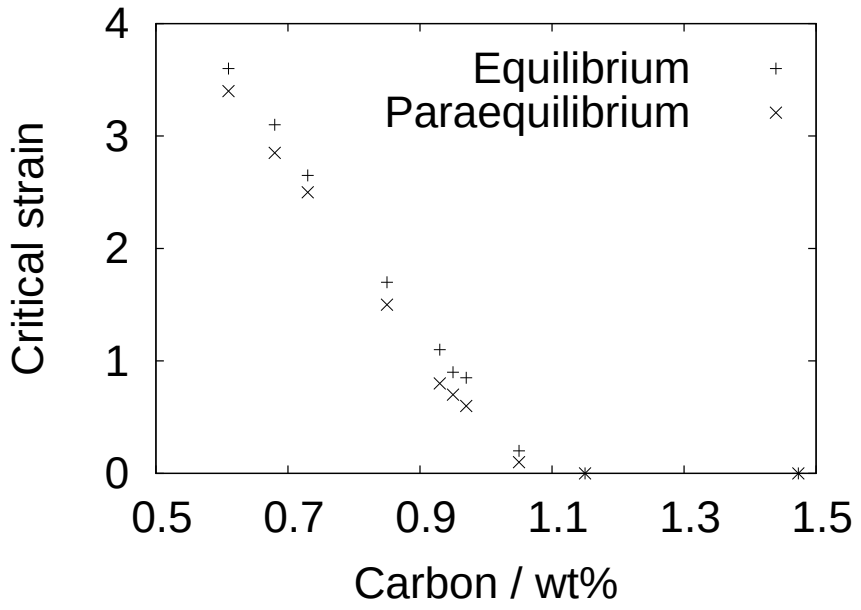

Figure 6.8: Critical strain necessary for onset of mechanical stabilisation in high-carbon austenite of TRIP-assisted steels.

As seen from Figure 6.8, the critical strain for onset of mechanical stabilisation in these steels decreases with increasing carbon content of retained

austenite. This is due to the lower chemical driving force for martensitic transformation for higher carbon containing austenite. A range of critical strain values are predicted for each carbon level: the upper and lower limits arise from the existence of the equilibrium or paraequilibrium partitioning of the substitututional solutes during intercritical annealing. However, the range of predicted strain values is small in magnitude, possibly due to the subtle difference between the equilibrium and the paraequilibrium concentrations of the substitutional solutes in the austenite.

Figure 6.8 further demonstrates the occurrence of mechanical stabilisation at small plastic strain in austenite with carbon content higher than about 1.1 wt%. It appears therefore that transformation of austenite with such a carbon level can never be strain-induced. Interestingly, high-carbon austenite is known to be the hardest phase in the microstructures of these steels [Furnemont *et al.*, 2002]. Austenite might thus be thought to remain unstrained till the late stage of the deformation. It might be possible therefore that high-carbon austenite in these steels transforms to martensite due to the effect of elastic stress rather plastic strain.

Stress-assisted transformation

Stress provides the shortfall in the chemical driving force for transformation to occur. However, the magnitude of the assistance rendered by stress depends on the nature of the stress state. For a simple uniaxial loading, the stress coefficient is reported by Olson [1982] to be 0.86 J mol^{-1} MPa^{-1}. With this value, the total driving force (chemical + mechanical) can be calculated as a function of temperature using MTDATA.

Figure 6.9 illustrates the total thermodynamic driving force for transformation at different stress levels for a hypothetical composition of austenite as Fe-1C-2Mn-2Si, all in wt%. The figure reveals the remarkable increase in the total driving force of transformation due to stress. The diagram also helps to understand the effect of a given stress level in terms of an equivalent thermal undercooling necessary to achieve the same additional thermodynamic driving force. For example, application of a stress of 400 MPa may be considered as an equivalent undercooling of 55 K, resulting in additional transformation.

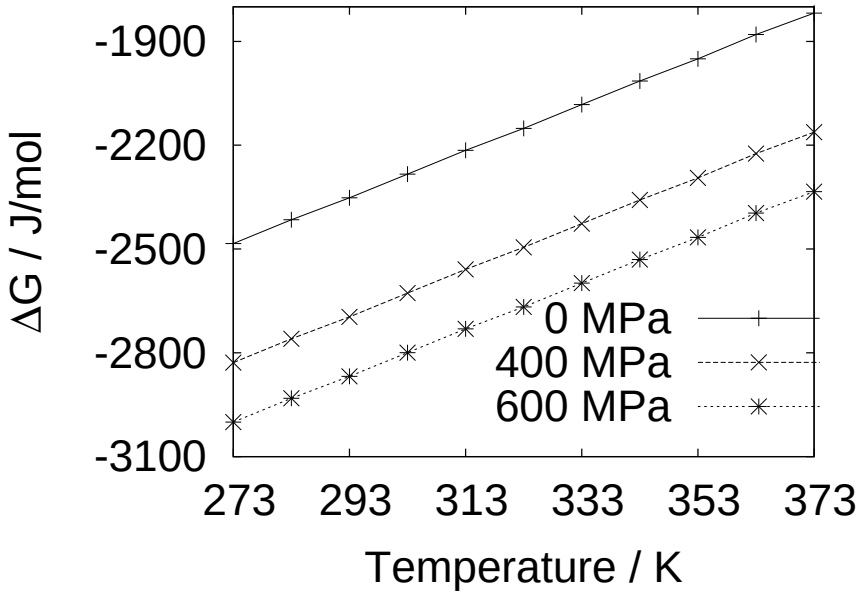

Figure 6.9: Total driving force for austenite to martensite transformation for Fe-1C-2Mn-2Si (wt%) austenite at different stress levels.

It can therefore be argued that the influence of stress on the extent of transformation can be computed in a similar way to athermal transformation,

using the empirical equation given by Koistinen and Marburger [1959]:

$$1 - \xi = \exp\{-C(M_S - T_Q)\} \tag{6.9}$$

where ξ is the martensite volume fraction at temperature T_Q and C is a constant equal to 0.011 K^{-1}. Knowing the M_S temperature of austenite and the equivalent thermal undercooling produced by a given stress level, the fraction of austenite transforming to martensite can be calculated using this equation.

Table 6.3 presents data, reported by Jacques *et al.* [2001d], that have been used to calculate the influence of stress on transformation of austenite, using the principle described above.

Sample	Athermal α' (vol.%)	γ_R (vol.%)	C in γ_R (wt%)	M_S (K)
L30s	7	8.8	0.61	351 (calculated)
L60s	5	8.1	0.68	341 (calculated)
H360	∼0	7.9	0.85	298 (stated)

Table 6.3: Data for decomposition of residual austenite to martensite during cooling to room temperature, γ_R is retained austenite [Jacques *et al.*, 2001d].

The M_S temperature for sample H360 has been indicated by Jacques *et al.* [2001d] to be close to room temperature *i.e.* 298 K, as only a small amount of martensite was detected in this sample. On the other hand, the M_S temperatures for samples L30s and L60s were calculated using Koistinen-Marburger equation, based on the reported amount of transformation at 298 K.

Stress levels corresponding to different strain values, at which the retained austenite volume fractions were reported, were worked out from the

relevant true stress-strain curve. These values are presented in Table 6.4. The table also shows the expected retained austenite fractions, as calculated considering the thermodynamic effect of stress alone.

Sample	Stress / MPa	Calculated γ_R vol.%	Reported γ_R vol.%
L30s	375	5.4	6.5
	463	4.9	4.8
	593	4.1	3.6
	659	3.8	2.7
	794	3.2	1.9
L60s	379	5.0	7.9
	466	4.5	5.3
	572	3.9	5.3
	639	3.6	3.2
	698	3.3	2.2
	769	3.0	1.6
H360	500	4.0	6.0
	710	3.0	4.8
	830	2.6	3.6
	914	2.3	3.4

Table 6.4: Calculated amounts of retained austenite (γ_R) and the corresponding amounts as reported by Jacques *et al.* [2001d] at each stress level.

Table 6.4 reveals the reported extent of transformation is higher than that calculated for samples L30s and L60s. There is no contention of mechanical stabilisation at the carbon levels of these samples (Figure 6.8). Plastic strain in austenite creates defects that act as additional nucleation sites. This can be considered to drive the transformation to a greater extent than that expected from the effect of stress alone.

By contrast, transformation has been reported to a lower extent than the computed ones for sample H360. Austenite in this sample contains about 0.85 wt% carbon. The high carbon level of austenite in H360 sample implies

a high hardness level [Furnemont *et al.*, 2002]. Thus austenite in this sample might not have strained plastically. It is possible therefore that transformation has been due to the effect of stress alone.

6.4.3 Bainitic steels

One of the fascinating aspects of the bainite reaction in steels is the *sub-unit* mechanism of its growth. A platelet of ferrite grows to a limited size even though there is no impingement with obstacles such as austenite grain boundaries. The transformation then propagates by the nucleation and growth of another sub-unit, the collection of sub-units being known as a *sheaf* [Hehemann, 1970]. The reason why each platelet only grows to a limited size is that the shape deformation accompanying transformation is plastically accommodated in the austenite adjacent to the plate [Bhadeshia and Edmonds, 1979]. This results in the creation of an intense dislocation debris which renders the interface immobile, as illustrated in Figure 6.10.

Calculations were carried out for a Fe-0.4C-3Mn-2Si (wt%) steel, which is also the material from which the micrograph in Figure 6.10 originates with a transformation temperature of 623 K. As pointed out previously, the stored energy has to be subtracted from the free energy change of transformation. For bainite, the magnitude of this is given by Bhadeshia [1981] as 400 J mol^{-1}. The results of calculations are presented in Table 6.5.

The shear strain associated with the growth of bainite is estimated to be about 0.26 [Swallow and Bhadeshia, 1996]. This, in comparison with the calculated data, can be expected to be sufficient for onset of *local* mechanical stabilisation, and hence a sub-unit mechanism of growth. Furthermore, the

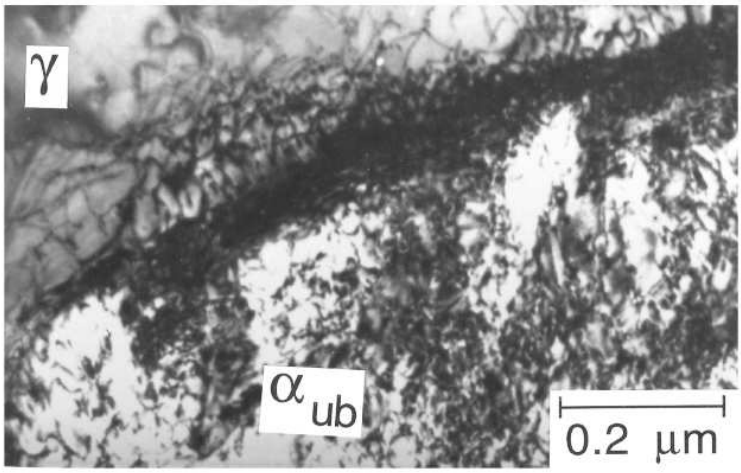

Figure 6.10: Intense dislocation debris at, and in the vicinity of the bainite (α_{ub})-austenite (γ) interface, the steel has a chemical composition Fe-0.43C-3Mn-2.12Si wt% and is transformed at 623 K [Bhadeshia and Edmonds, 1979].

Temperature / K	Critical Strain
500	2.1
600	0.6
650	0.06

Table 6.5: Strain necessary for mechanical stabilisation in the bainitic steel.

length of the sub-unit is expected to become larger and this is qualitatively consistent with experimental data on bainite, the plates become more slender as the transformation temperature is reduced (ΔG increased) [Garcia-Mateo *et al.*, 2003]. It may be further noted that martensite forms in this steel below about 500 K [Bhadeshia and Edmonds, 1979].

6.4.4 Athermal martensite

Austenite on cooling starts transforming to martensite only below a critical temperature, M_S. This temperature varies with chemical composition of the steel. Most of the common alloying elements, except aluminium and cobalt, are known to depress M_S. Finer austenite grain sizes also lead to a lower M_S temperature [Raghavan, 1992]. This is generally believed to be due to the hardening of austenite due to finer grain sizes, hindering the growth of martensite. Transformation from plastically deformed austenite in a similar way can be expected to start at lower temperature, as reported in a steel of composition Fe-0.75C-1.02Mn-0.28Si-0.11Cr-0.05Ni-0.015S-0.009P-0.08Cu (all in wt%) [Maalekian *et al.*, 2006]. This is becasue of the strengthening of austenite due to a higher dislocation density than that in the undeformed condition. A methodology is described in this section to calculate the depression of the M_S temperature caused by prior plastic strain in austenite.

The theory for mechanical stabilisation relies on balancing the force required to move the austenite-martensite interface through a forest of dislocations against the force due to the chemical free energy change (ΔG) driving the interface:

$$\frac{Gb\rho^{\frac{1}{2}}}{8\pi(1-\nu)} = |\Delta G| \tag{6.10}$$

where $b = 0.252$ nm is the magnitude of the Burgers vector, $G = 8 \times 10^{10}$ Pa is the shear modulus of the austenite, $\nu = 0.27$ is its Poisson's ratio and ρ is the dislocation density. The extra driving force, $\Delta(\Delta G)$, necessary for transformation in a plastically deformed sample can be expressed as:

$$\frac{Gb}{8\pi(1-\nu)}[\rho^{\frac{1}{2}} - \rho_0^{\frac{1}{2}}] = \Delta(\Delta G) \tag{6.11}$$

where the dislocation density ρ has a value ρ_0 at zero plastic strain.

ΔG for transformation of austenite to ferrite without a composition change was calculated using MTDATA for the Fe-0.75C-1.02Mn-0.28Si-0.11Cr-0.05Ni-0.015S-0.009P-0.08Cu (wt%) steel as a function of temperature:

$$\Delta G = 7.0337T - 5218 \text{ J mol}^{-1} \qquad \text{or} \qquad \Delta(\Delta G) \equiv 7.0337\Delta T \tag{6.12}$$

where T is the absolute temperature. The equation applies over the temperature range 450-510 K. The above expression therefore relates the magnitude of the change in available driving force due to the presence of dislocations in the austenite, $\Delta(\Delta G)$, with the corresponding reduction in the M_S temperature, ΔT.

It follows that the depression of the transformation temperature can be calculated as a function of the change in the dislocation density of the austenite. However, it would be useful to be able to estimate the change in M_S as a function of plastic strain rather than dislocation density. It is necessary therefore to derive a relationship between plastic strain (ϵ) and dislocation density, which will necessarily be approximate. So two alternative methods were attempted as follows:

Data from Vodopivec *et al.* [1999] are used to obtain an empirical relationship as:

$$\rho = \underbrace{2 \times 10^{13}}_{\rho_0} + 2 \times 10^{14}\epsilon \qquad \text{m}^{-2} \tag{6.13}$$

In the alternative approach, it is assumed that only 5% of the plastic work is stored in the material, both due to changes in the austenite grain

surface per unit volume, ΔS_V, and due to the expected change in dislocation density. By balancing the plastic work stored against the energy of defects created, we obtain:

$$0.05\sigma_y\epsilon \simeq \sigma_{\gamma\gamma}\Delta S_V + \phi\Delta\rho \tag{6.14}$$

where σ_y is the yield stress of austenite (measured to be 30 MPa at 1000°C [Maalekian *et al.*, 2006]), $\phi \simeq 0.5\mu b^2$ is the dislocation energy per unit length and $\sigma_{\gamma\gamma}$ is the austenite grain boundary energy per unit area. The magnitude of grain boundary energy must vary with the chemical composition of alloy and temperature. In absence of the actual data, this has been taken to be $0.6\,\mathrm{J\,m^{-2}}$ [Murr *et al.*, 1982].

For axisymmetric compression [Zhu *et al.*, 2006],

$$\frac{S_V}{S_{V_0}} = \frac{[8e^{\epsilon} + 4e^{-2\epsilon}]^{\frac{1}{2}} + \frac{1}{3}[e^{-\epsilon} + 2\sqrt{e^{\epsilon}}]}{1 + 2\sqrt{3}} \tag{6.15}$$

The value of S_V at zero deformation is given by $S_{V_0} = 2/d_\gamma$ where $d_\gamma = 26 \pm 3\,\mu$m is the mean lineal intercept defining the austenite grain size [Maalekian *et al.*, 2006].

The stored energy due to deformation is simply calculated using the term on the left-hand side of equation 6.14. Removing the component due to the change in S_V (equation 6.15) from equation 6.14 gives the change in dislocation density.

The predicted depression in the martensite-start temperature with increasing prior plastic strain in austenite is shown in Figure 6.11. The calculated trends compare well with the measured value.

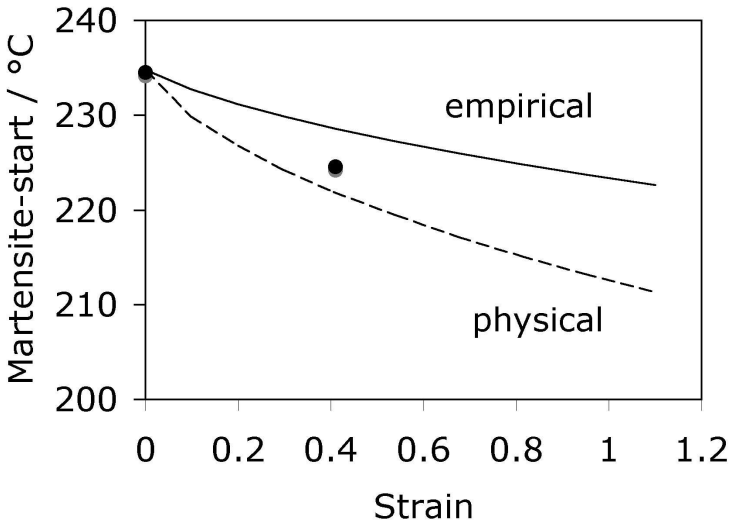

Figure 6.11: Calculated change in M_S as a function of plastic strain in austenite prior to its transformation, the points represent experimental data.

6.5 Summary

The role of stress and strain on martensitic transformation has been studied. A theory has been developed to calculate the critical strain necessary for the onset of mechanical stabilisation in steels. The chemical composition of the alloys along with the transformation temperature are used as key inputs to the model.

The theory has been used to demonstrate why large strain values are necessary to stabilise certain stainless steels at ambient temperature. The theory also helps to interpret the sub-unit mechanism of bainite growth and the depression of M_S temperature with prior plastic strain in austenite. The theory indicates the possibility that high-carbon austenite in TRIP-assisted steels might actually transform to martensite due to stress, rather strain, during deformation.

Chapter 7

Formability

TRIP-assisted steels are expected to possess enhanced formability. This is the ability of a material to be shaped, an ability related to plasticity. Formability is characterised by different test methods. The purpose of the present chapter is to study the influence of simple mechanical properties such as the strength and elongation on formability.

7.1 Stretch-flangeability

Several methods have been designed to characterise the forming ability, one of which is the hole expansion test. During this test, a hole is first made in the steel blank. The hole is then allowed to expand under a punch until cracks appear on the surface. The ratio of the increase in diameter to the initial diameter is called the hole expansion ratio. The higher the ratio, the better is the stretch-flangeability of the steel.

There are examples of strong steels tested for stretch-flangeability [Matsumura *et al.*, 1992; Sudo *et al.*, 1982]. Each of these materials possesses a

similar ferrite-rich microstructure with a dispersion of a hard phase which could be martensite or bainite or both. The steels may also contain retained austenite.

There has been much research in understanding the effect of microstructure on the stretch-flangeability of these steels. For example, delayed strain-induced transformation of the retained austenite into martensite is known to improve the properties [Sugimoto *et al.*, 1999]. Volume fraction, hardness and distribution of the hard phase may also influence the performance [Hasegawa *et al.*, 2004]. It has even been possible to achieve superior hole-expansion ratio over the multiphase steels by using either fully bainitic or martensitic steels [Sugimoto *et al.*, 2002a,b, 2000].

However, there is no proper understanding on the influence of the simple mechanical properties, such as strength and elongation, on the stretch-flangeability. During a tensile test, the specimen first undergoes uniform deformation. But plastic instability sets in when the work-hardening can no longer compensate for the increased stress due to the reduction of cross section. The resulting non-uniform strain is generally not considered to be useful during forming, as this might degrade the aesthetic of the formed component. To study the relationship between the tensile properties and the hole expansion ratio forms the aim of the present work.

7.2 Neural networks

Neural network analysis was adopted in this study. This represents a general method of regression that fits a non-linear function to experimental data. Details of the method can be found in Chapter 4.

Analysis

The data presented in Table 7.1 are due to Fang *et al.* [2003a,b]; Hasegawa *et al.* [2004]; Sudo *et al.* [1982]; Sugimoto *et al.* [1999]. They originate from steels with microstructures of ferrite-martensite or ferrite-bainite, with or without retained austenite. The data were used to create models for predicting the hole expansion ratio (λ) against various combinations of the tensile properties *viz.* yield strength (YS), ultimate tensile strength (UTS), uniform elongation (UEL), total elongation (TEL), yield ratio (YR) and the strength-elongation product (UTS-UEL and UTS-TEL).

Each variable in the database was normalised as

$$x_n = \frac{x - x_{min}}{x_{max} - x_{min}} - 0.5 \tag{7.1}$$

where x_n is the normalised value of the variable x, with x_{min} and x_{max} as the minimum and the maximum values respectively. The database was divided randomly into two halves. Each model was trained using one half of the dataset. The other half was used to test the performance of the model with unseen data.

7.3 Results and discussion

The first model was created with the YS, UTS, UEL, YR and UTS-UEL as the input parameters. Figure 7.1(a) illustrates the reduction in the noise level with increasing number of hidden units. The final model is formed as a committee of models based on the minimum combined test error on increasing the number of networks (Figure 7.1(b)). The final committee in

Inputs	Minimum	Maximum	Average	S.D.
YS / MPa	335	783	444	92
UTS / MPa	484	1028	675	155
UEL / %	8	39	18	7
TEL / %	10	43	27	8
YR	0.49	0.82	0.67	0.09
UTS-UEL / MPa-%	6992	29715	12192	6113
UTS-TEL / MPa-%	9016	32379	18069	6894
Output	Minimum	Maximum	Average	S.D.
λ / %	9	151	65	45

Table 7.1: Data used in the analysis, S.D. represents standard deviation.

this case was made of only one sub-model.

Figure 7.2 compares the measured hole expansion ratios with the corresponding model predictions made over the entire dataset. In general, the predicted hole expansion ratios compare well with the corresponding measured values, but there are a few outliers. However, the uncertainty is seen to be large. The model-perceived significances of the input variables influencing the hole expansion ratio are presented in Figure 7.3. As can be seen, UTS gained the maximum importance followed by the YS and the YR. Contrary to general belief, UEL and UTS-UEL were perceived to be insignificant.

The apparent irrelevance of the UEL and the UTS-UEL might be real. This is because, the attainment of UTS in the flow curve implies the end of UEL. Therefore, UTS and UEL are actually not independent variables. To test this hypothesis, two separate models were created. One of these had the UTS with the UEL as the input variables while the other had the YS with the UEL. Both these models were found to consist of only one sub-model in the final committee.

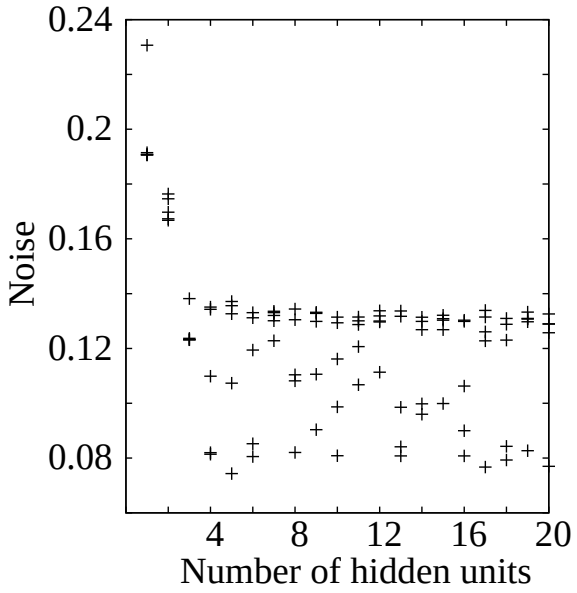

(a)

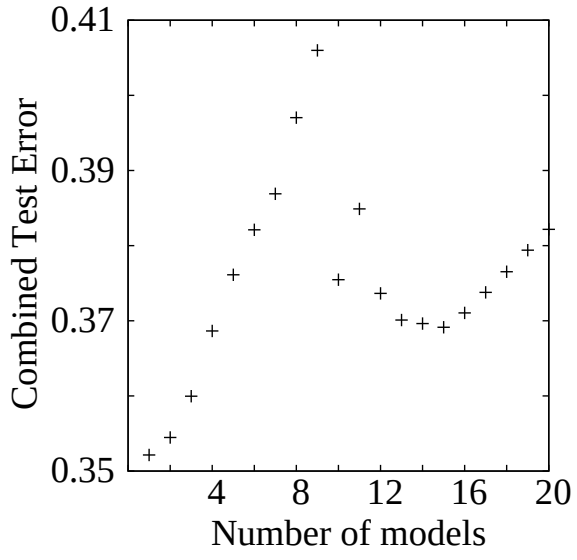

(b)

Figure 7.1: Variation of (a) noise level, σ, with increasing number of hidden units and (b) combined test error with number of models in committee.

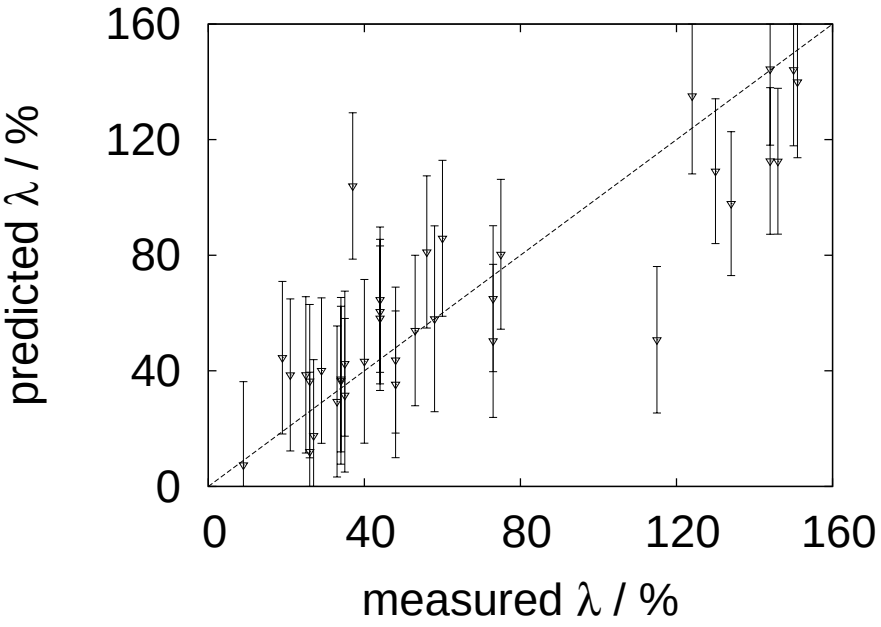

Figure 7.2: Predicted hole expansion ratios compared with the measured values using the model with YS, UTS, UEL, YR and UTS-UEL as the input parameters.

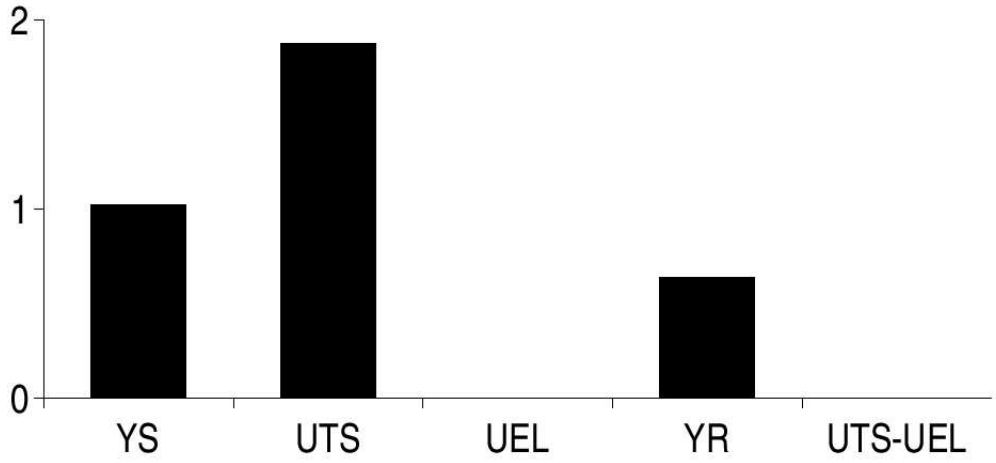

Figure 7.3: Significances of YS, UTS, UEL, YR and UTS-UEL as the input variables.

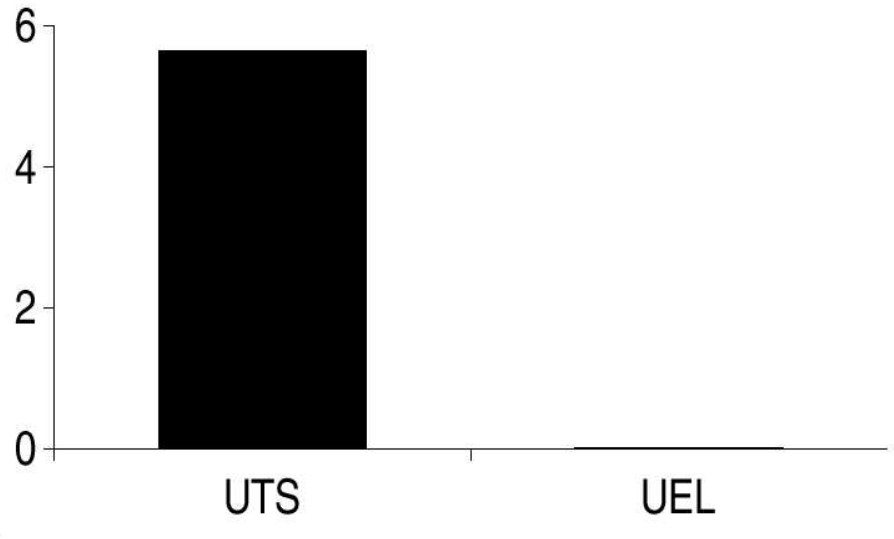

(a)

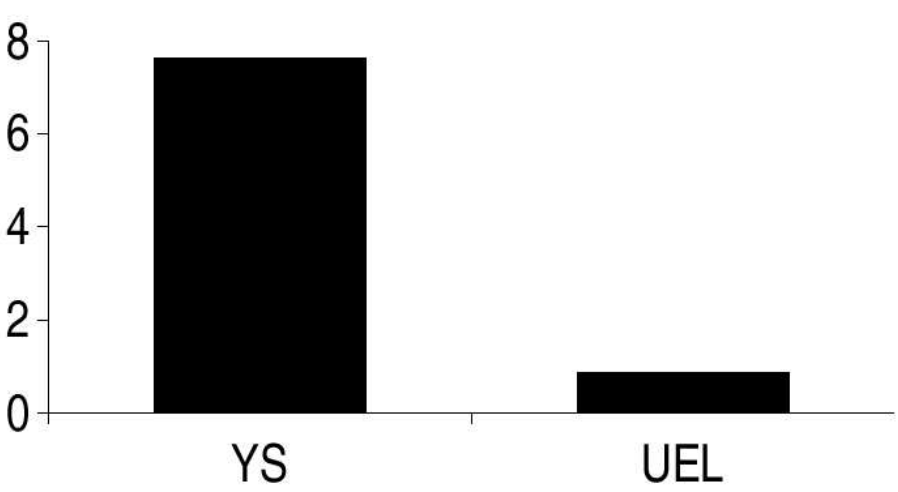

(b)

Figure 7.4: Significances of (a) UTS and UEL and (b) YS and UEL as the input variables.

Figure 7.4 shows the significances of the variables as perceived by the model. The significance of UEL was indeed boosted in the presence of the YS, as compared to that with the UTS. However, its magnitude remained small (Figure 7.4(b)). This indicates a possibility that the TEL could be a better parameter than the UEL in describing the hole expansion ratio. A model was therefore created with YS, UTS, TEL, YR and UTS-TEL as the input variables. The final committee of the model was found to have eight sub-models.

Figure 7.5 presents the significances of the input variables as perceived by each sub-model in the final committee. UTS, UTS-TEL and TEL were found to exert considerable influence on the hole expansion ratio, while YS and YR did not gain any importance. However, the significances for each input parameters vary in different sub-models.

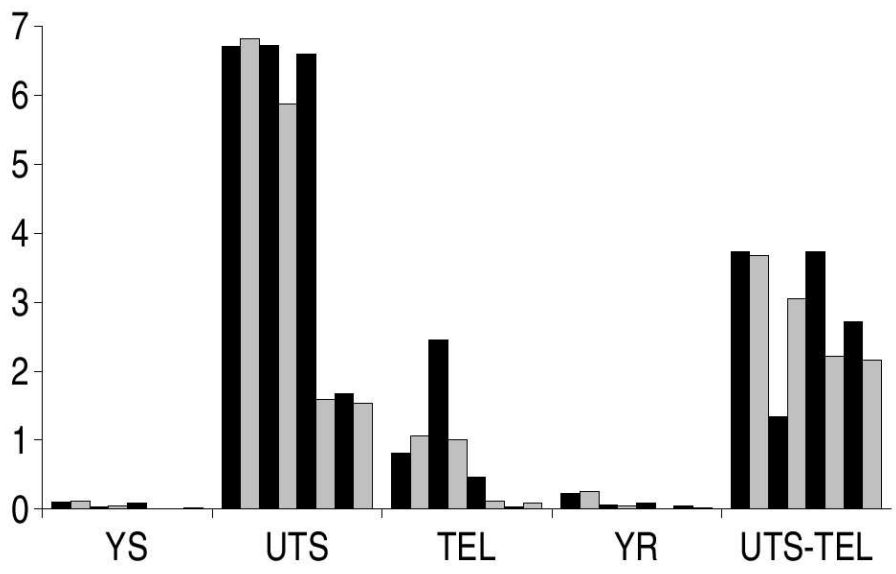

Figure 7.5: Significances of YS, UTS, TEL, YR and UTS-TEL as the input variables.

Figure 7.6 depicts the predictions made using this model over the entire dataset. The predicted values compare well with the measured values. Furthermore, the magnitudes of the error bars associated with the predictions using this model are much reduced as compared to the first model (Figure 7.2). There are no significant outliers in the predictions. All these suggest, the model with the TEL as an input performs appreciably better than the one with the UEL as an input.

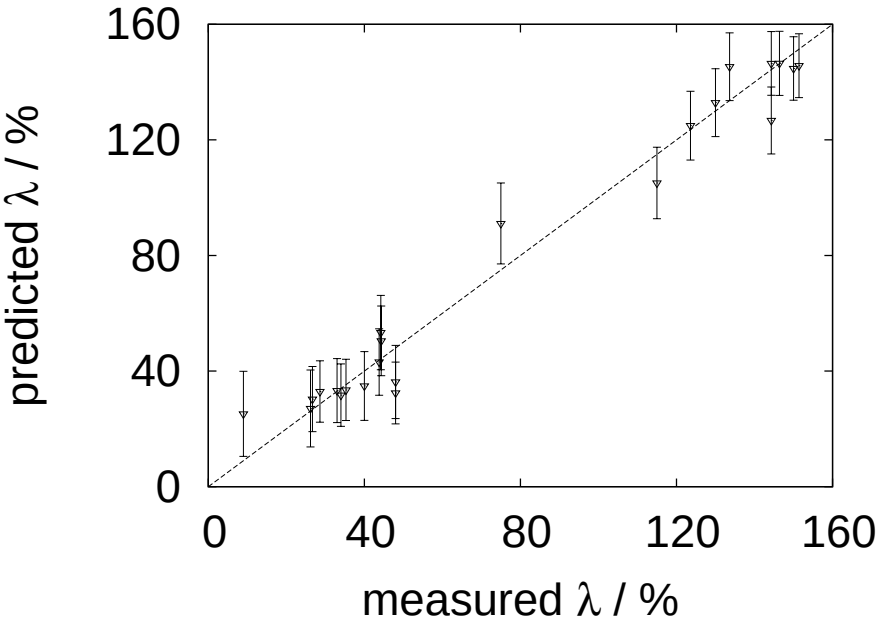

Figure 7.6: Predicted hole expansion ratios compared with the measured values using the model with YS, UTS, TEL, YR and UTS-TEL as the input parameters.

The above results indicate the importance of UTS, TEL and UTS-TEL in controlling the hole expansion ratio. This appears to be physically reasonable, given that the hole is allowed to expand until cracks appear on the surface. This therefore tests the ability of the material to deform plastically

until fracture, albeit locally. Two different models were therefore created with the input parameters as UTS and UTS-TEL in one case while UTS and TEL in the other.

From Figure 7.7, the significances of both UTS-TEL and TEL can be seen to be appreciable, although quantitatively these are less than that of the UTS. In each case, the model consisted of only one sub-model. Figure 7.8 shows that the predictions made over the entire dataset compare well with the corresponding measured values.

These models were used further to predict the variation in the hole expansion ratio as function of UTS, TEL and UTS-TEL. Figure 7.9 and Figure 7.10 present the results as surface plots with the corresponding uncertainties which were between 10-25. At constant UTS-TEL, the hole expansion ratio seems to be higher at lower UTS (Figure 7.9(a)). This might be due to the higher TEL (keeping UTS-TEL the same). However, at the same UTS, the ratio is seen to be decreasing with increasing UTS-TEL, ultimately becoming constant with UTS-TEL exceeding 20000 MPa-%. This is therefore not consistent with the beneficial effect of the total elongation.

Figure 7.10(a) illustrates a more drastic reduction in the hole expansion ratio with increasing UTS as compared to Figure 7.9(a). At constant UTS, the ratio is however seen to remain almost constant with increasing total elongation, although a positive correlation between the stretch-flangeability and TEL could be imagined ideally.

7.4 Summary

The present work identifies the ultimate tensile strength to be the most important tensile property influencing the hole expansion ratio. The uniform elongation loses its significance as an input to the model, which also includes the ultimate tensile strength as a variable. This is because both the properties appear to be identical with respect to the flow curve.

The stretch-flangeability deteriorates with increasing ultimate tensile strength. Total elongation might be thought to be important, as hole expansion tests rely on the cracking of the surface while expanding the hole. However, the present work suggests that increasing total elongation, keeping the ultimate tensile strength same, might not be beneficial.

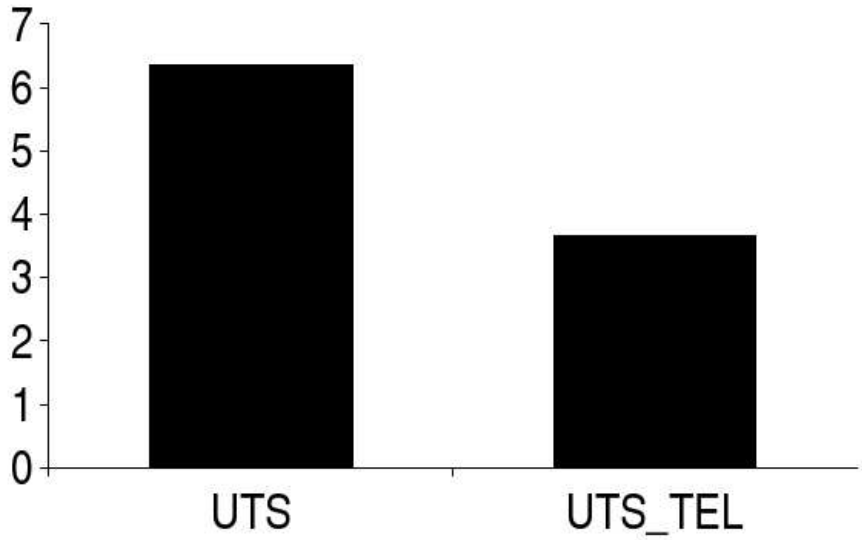

(a)

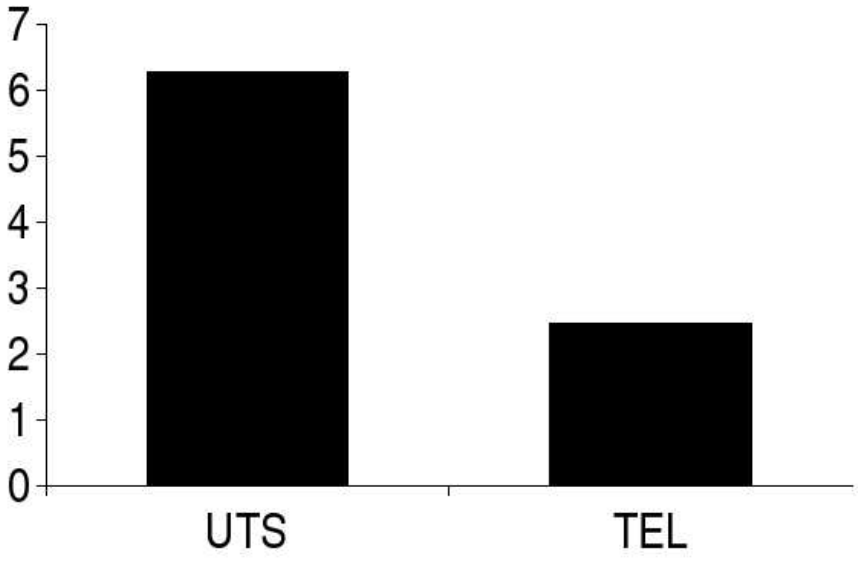

(b)

Figure 7.7: Significances of (a) UTS and UTS-TEL and (b) UTS and TEL as the input variables.

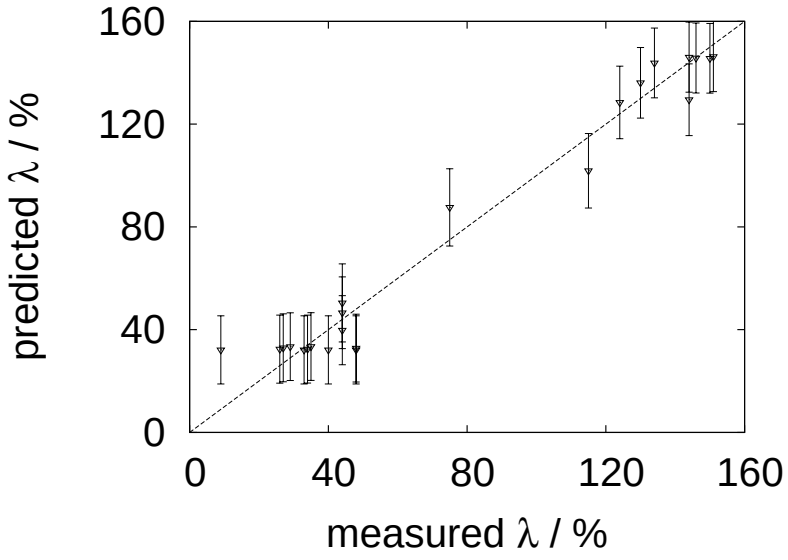

(a)

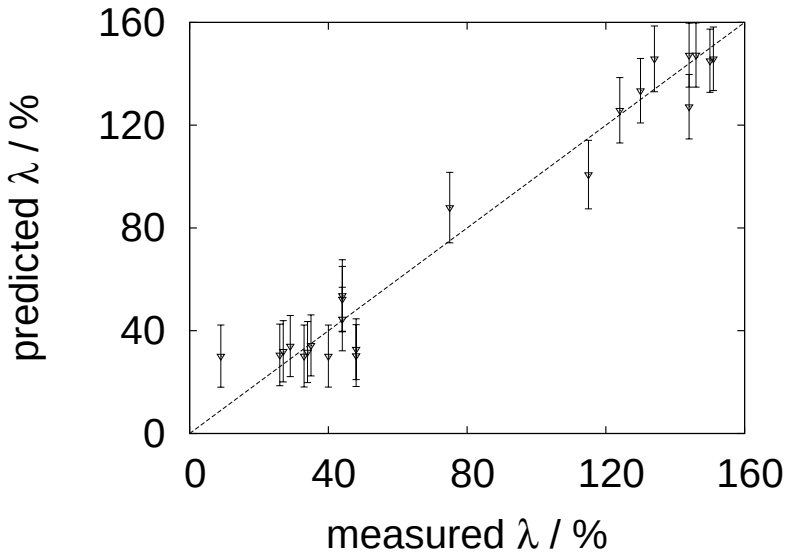

(b)

Figure 7.8: Predicted hole expansion ratios compared with the measured values using the models with (a) UTS and UTS-TEL and (b) UTS and TEL as the input parameters.

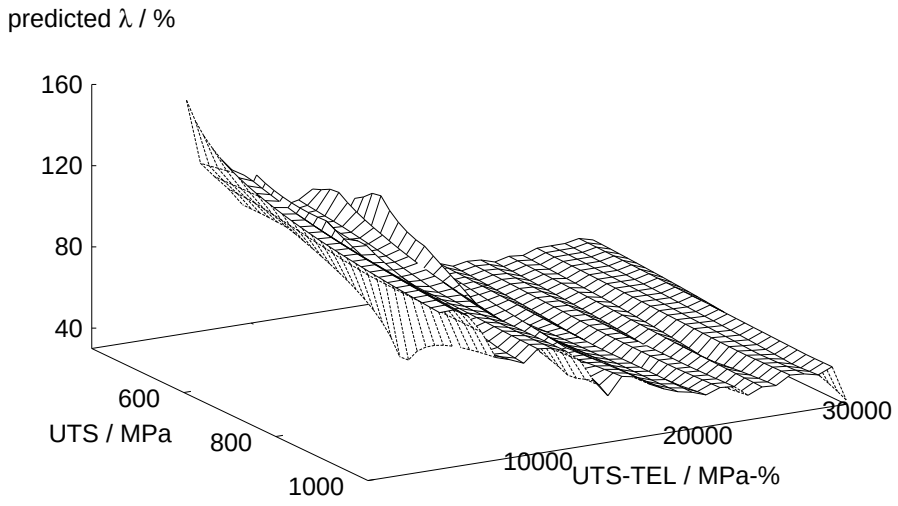

(a)

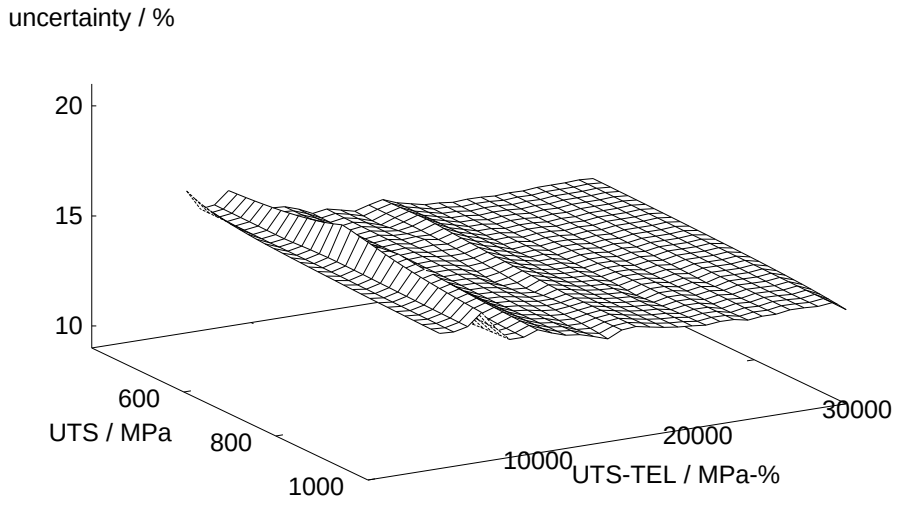

(b)

Figure 7.9: Predicted variation in (a) the hole expansion ratio with UTS and UTS-TEL and (b) the corresponding uncertainties.

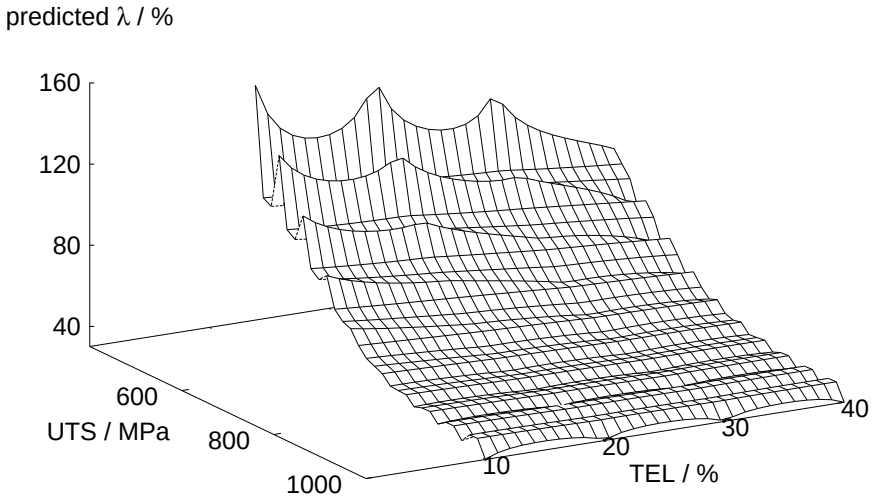

(a)

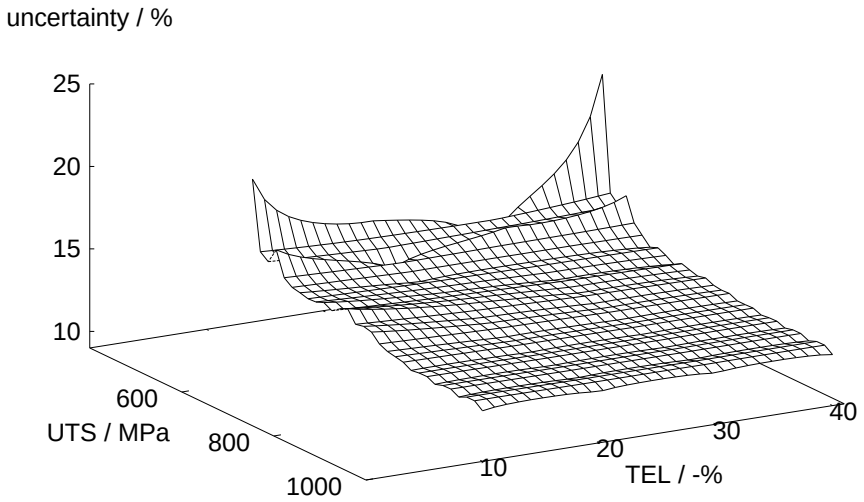

(b)

Figure 7.10: Predicted variation in (a) the hole expansion ratio with UTS and TEL and (b) the corresponding uncertainties.

Chapter 8

Conclusions

TRIP-assisted steels have the advantage of large uniform elongation in spite of the high strength. This makes them suitable for making cars with lighter body weight but adequate safety. The steels contain some 10-30 vol.% high-carbon retained austenite in ferrite-rich microstructures. The transformation of austenite into martensite during deformation is generally believed to be responsible for the properties of these steels. This is despite the fact that the martensite that forms in these steels must inherit the carbon of austenite and hence should be brittle.

It has been demonstrated here that the finer martensite plates are better able to resist cracking. In TRIP-assisted steels, retained austenite exists in a finely divided state with the grain size of around 1 μm. The martensite that forms from this austenite therefore remains with a fine plate size and hence is not a liability for these steels, in spite of its high carbon content.

To maximise the properties, the stability of the retained austenite should be such that it transforms progressively during deformation. Carbon content of the austenite influences its stability. Retained austenite vol-

ume fraction and its carbon content are therefore important microstructural parameters influencing the properties of these steels. Using published data, neural network models were created relating these parameters with the chemical composition and the heat treatment conditions of these materials. These models were found to be capable of illustrating the effects of various factors on the retained austenite fraction and its carbon content, as expected from the metallurgical principles.

The retained austenite content in steels transformed to bainite increases with the addition of silicon. However, silicon leads to complications during processing and deteriorates the surface condition of the steel. The neural network model, along with a genetic algorithm, was used to formulate an alloy, lean in silicon concentration yet capable of retaining austenite in copious amounts. The computational methods gave rise to a new type of material, here designated δ-TRIP steel. The alloy shows an enhanced tendency for δ-ferrite formation during solidification and cannot be made fully austenitic. Usually the ferrite, that constitutes the microstructure of TRIP-assisted steel, is generated out of the allotriomorphic transformation of austenite. By contrast, the present alloy gives an opportunity to substitute some of the allotriomorphic ferrite in these materials by δ-ferrite.

Experiments using alloys based on the optimisation calculation demonstrated the formation of δ-ferrite during solidification. These alloys were further heat-treated producing radically different microstructures containing δ-ferrite, bainite and retained austenite. Specimens in heat-treated conditions recorded impressive mechanical properties at room temperature. However, the ductility deteriorates when the tests are done at 100°C. This could

be due to the enhanced stability of the retained austenite against transformation into martensite at the high temperature.

The transformation of the retained austenite into martensite during deformation could be either due to stress or strain. Stress generally adds to the driving force while plastic strain retards the growth of martensite plates, eventually causing the mechanical stabilisation of the austenite. A theory capable of predicting the critical strain necessary for the onset of stabilisation has been developed. Using the theory, it has been possible to explain the requirement of the large strain for stabilising certain austenitic steels and the sub-unit mechanism of bainite growth. Calculations involving the theory indicate that the high-carbon retained austenite in TRIP-assisted steels may actually transform due to stress rather strain. Further experimental work is necessary to clarify the role of stress and strain on the transformation of retained austenite in these steels.

There are various complex tests to assess the formability of these materials. However, there has been no proper attempt in understanding these results in terms of the tensile properties. Published data on stretch-flangeability of these steels were analysed using neural networks. It has been shown that the ultimate tensile strength of the steel is the most important criterion influencing the stretch-flangeability.

Bibliography

Andrews, K. W. *Journal of The Iron and Steel Institute* **203** (1965) 721

Angel, T. *Journal of The Iron and Steel Institute* **177** (1954) 165

Barlat, F., Glazov, M. V., Brem, J. C. and Lege, D. J. *International Journal of Plasticity* **18** (2002) 919

Basuki, A. and Aernoudt, E. *Journal of Materials Processing Technology* **89-90** (1999) 37

Bhadeshia, H. K. D. H. and Honeycombe, R. W. K. *Steels: Microstructure and Properties*, Elsevier, UK, (2006)

Bhadeshia, H. K. D. H. *ISIJ International* **42** (2002) 1059

Bhadeshia, H. K. D. H. *Bainite in Steels*, IOM Communications Ltd, UK (2001)

Bhadeshia, H. K. D. H. *ISIJ International* **39** (1999) 966

Bhadeshia, H. K. D. H. *Materials Science and Engineering A* **273-275** (1999) 58

Bhadeshia, H. K. D. H. *Acta Metallurgica* **29** (1981) 1117

Bhadeshia, H. K. D. H. and Edmonds, E. V. *Metallurgical and Materials Transactions A* **10** (1979) 895

Bouet, M., Fillipone, R., Essadiqi, E., Root, J. and Yue, S. *42nd Mechanical Working and Steel Processing Conference Proceedings*, Iron and Steel Society/AIME, USA, **38** (2000) 55

Bouet, M., Root, J., Es-Sadiqui, E. and Yue, S. *40th Mechanical Working and Steel Processing Conference Proceedings*, Iron and Steel Society/AIME, USA, **36** (1998) 675

Bouet, M., Root, J., Es-Sadiqi, E. and Yue, S. *Materials Science Forum* **284-286** (1998) 319

Breedis, J. F. and Robertson, W. D. *Acta Metallurgica* **11** (1963) 547

Capdevila, C., Caballero, F. G. and Garcia de Andres, C. *Journal de Physique IV* **112** (2003) 217

Chen, H. C., Era, H. and Shimizu, M., *Metallurgical and Materials Transactions A* **20** (1989) 437

Choi, I. D., Bruce, D. M., Kim, S. J., Lee, C. G., Park, S. H., Matlock, D. K. and Speer, J. G. *ISIJ International* **42** (2002) 1483

Choi, B. Y., Krauss, G and Matlock, D. K. *Scripta Metallurgica* **22** (1988) 1575

Christian, J. W. *The Theory of Transformations in Metals and Alloys*, Pergamon, UK (2002)

Christian, J. W. *Proceedings of ICOMAT'79*, MIT Press, USA (1979) 230

Cox, H. L. *British Journal of Applied Physics* **3** (1952) 72

Davies, R. G. and Magee, C. L. *Metallurgical and Materials Transactions A* **3** (1972) 307

De Meyer, M., Vanderschueren, D., De Cooman, B. C., *ISIJ International* **39** (1999) 813

De Meyer, M., Vanderschueren, D., De Cooman, B. C., *41st Mechanical Working and Steel Processing Conference Proceedings*, Iron and Steel Society/AIME, USA, (1999) 265

Dieter, G. E., *Mechanical Metallurgy*, McGraw-Hill, UK (1988)

Dyson, D. J. and Holmes, B *Journal of The Iron and Steel Institute* **208** (1979) 469

Epogy 2003 Users' guide, Synaps Inc

Fang, X., Fan, Z., Ralph, B., Evans, P. and Underhill, R. *Journal of Materials Processing Technology* **132** (2003) 215

Fang, X., Fan, Z., Ralph, B., Evans, P. and Underhill, R. *Journal of Materials Science* **38** (2003) 3877

Fischer, J. C. *Metals Transactions* **185** (1949) 688

Frank, F. C. *Acta Metallurgica* **1** (1953) 15

Furnemont, Q., Kempf, M., Jacques, P. J., Goken, M. and Delannay, F. *Materials Science and Engineering A* **328** (2002) 26

Garcia-Mateo, C., Caballero, F. G. and Bhadeshia, H. K. D. H. *ISIJ International* **43** (2003) 1238

Gallagher, M. F., Speer, J. G. and Matlock, D. K. *Symposium on the Thermodynamics, Kinetics, Characterization and Modeling of: Austenite Formation and Decomposition*, Minerals, Metals and Materials Society (TMS), USA, (2003) 563

Gerberich, W. W., Thomas, G., Parker, E. R. and Zackay, V. F. *Proceedings of 2nd International Conference on Strength of Metals and Alloys*, USA, **3** (1970)

Ghosh, G., and Olson, G. B. *Journal of Phase Equilibrium* **22** (2001) 199

Girault, E., Martens, A., Jacques, P., Houbaert, Y., Verlinden, B. and Van Humbeeck, J. *Scripta Materialia* **44** (2001) 885

Goel, N. C., Sangal, S. and Tangri, K. *Metallurgical and Materials Transactions A* **16** (1985) 2013

Guimaraes, J. R. C. and Saavedra, A. *Materials Science and Engineering A* **62** (1984) 11

Guimaraes, J. R. C. and Gomes, J. C. *Acta Metallurgica* **26** (1978) 1591

Guimaraes, J. R. C. *Scripta Metallurgica* **6** (1972) 795

Hanzaki, A. Z., Hodgson, P. D. and Yue, S. *ISIJ International* **35** (1995) 324

Hanzaki, A. Z., PhD Thesis, McGill University, (1994)

Hasegawa, K., Kawamura, K., Urabe, T. and Hosoya, Y. *ISIJ International* **44** (2004) 603

Hashimoto, S., Ikeda, S., Sugimoto, K-I. and Miyake, S. *ISIJ International* **44** (2004) 1590

Hassani, F. and Yue, S. *41st Mechanical Working and Steel Processing Conference Proceedings*, Iron and Steel Society/AIME, USA, **37** (1999) 493

Hehemann, R. F. *Phase Transformations*, ASM, USA (1970) 397

Hiwatashi, S., Takahashi, M., Katayama, T. and Usuda, M., *Journal of the Japan Society for Technology of Plasticity* **35** (1994) 1109

Honeycombe, R. W. K. *The Plastic Deformation of Metals*, Second Edition, Edward Arnold, London, (1984)

Im, D. B., Lee, C. G., Kim, S. J. and Park, I. M. *Journal of the Korean Institute of Metals and Materials* **40** (2002) 8

Im, D. B., Lee, C. G., Kim, S. J. and Park, I. M. *Journal of the Korean Institute of Metals and Materials* **38** (2000) 447

Im, D. B., Lee, C. G., Song, B. H., Kim, S. J. and Park, I. M. *Journal of the Korean Institute of Metals and Materials* **38** (2000) 1328

Imai, N., Komatsubara, N. and Kunishige, K. *Japan Technical Information Service* (1992) 25

Irvine, K. J., Gladman, T. and Pickering, F. B. *Journal of The Iron and Steel Institute* **207** (1969) 1017

Itami, A., Takahashi, M. and Ushioda, K. *ISIJ International* **35** (1995) 1121

Jacques, P. *Journal de Physique IV* **112** (2003) 297

Jacques, P. J., Girault, E., Martens, A., Verlinden, B., Van Humbeeck, J, and Delannay, F. *ISIJ International* **41** (2001) 1068

Jacques, P. J., Girault, E., Harlet, P. and Delannay, F. *ISIJ International* **41** (2001) 1061

Jacques, P., Furnemont, Q., Mertens, A. and Delannay, F. *Philosophical Magazine A* **81** (2001) 1789

Jacques, P., Ladriere, J. and Delannay, F. *Metallurgical and Materials Transactions A* **32** (2001) 2759

Jacques, P., Girault, E., Catlin, T., Geerlofs, N., Kop, T., Van der Zwaag, S. and Delannay, F. *Materials Science and Engineering A* **273-275** (1999) 475

Jiao, S., Hassani, F., Donaberger, R. L., Essadiqi, E. and Yue, S. *ISIJ International* **42** (2002) 299

Kim, S. J., Lee, C. G., Lee, T. H. and Oh, C. S. *ISIJ International* **42** (2002) 1452

Kim, S. J., Lee, C. G., Choi, I. and Lee, S. *Metallurgical and Materials Transactions A* **32** (2001) 505

Kim, C. *Metallurgical and Materials Transactions A* **19** (1988) 1263

Kim, S. J. and Lee, C. G. *Journal of the Korean Institute of Metals and Materials* **37** (1999) 774

Koh, H. J., Lee, S. K., Park, S. H., Choi, S. J., Kwon, S. J. and Kim, N. J. *Scripta Materialia* **38** (1998) 763

Koistinen, P. P. and Marburger, R. E. *Acta Metallurgica* **7** (1959) 59

Konieczny, A. A. *Processing and Fabrication of Advanced Materials XI*, ASM International, USA, (2003) 345

Lecroisey, F. and Pineau, A. *Metallurgical and Materials Transactions A* **3** (1972) 387

Lee, C. G., Kim, S. J., Lee, T. H. and Lee, S. *Material Science and Engineering A* **371** (2004) 16

Lee, C. G., Kim, S. J., Song, B. H. and Lee, S. *Metals and Materials* **8** (2002) 435

Lee, C. G., Kim, S. J., OH, C. S. and Lee, S. *ISIJ International* **42** (2002) 1162

Leslie, W. C. and Miller, R. L. *ASM Transactions Quaterly* **57** (1964) 972

Ludwigson, D. C. and Berger, J. A., *Journal of The Iron and Steel Institute* **207** (1969) 63

Maalekian, M., Lendinez, M. L., Kozeschnik, E., Brantner, H. P., Cerjak, H., Effect of hot plastic deformation of austenite on the transformation characteristics of eutectoid carbon steel under fast heating and cooling conditions, (2006, unpublished work)

Machlin, E. S. and Cohen, M. *Trans. AIME* **191** (1951) 746

MacKay, D. J. C., *Information Theory, Inference and Learning Algorithms*, Cambridge University Press, UK, (2003)

Mahieu, J., De Cooman, B. C., Maki, J., and Claessens, S. *Iron and Steelmaker* **29** (2002) 29

Mahieu, J., Claessens, S. and De Cooman, B. C. *Verlag Stahleisen GmbH, Galvatech '2001*, Germany, (2001) 644

Manganon, P. L. and Thomas, G. *Metallurgical and Materials Transactions A* **1** (1970) 1577

Manohar, P. A., Kunishige, K., Chandra, T. and Ferry, M. *Materials Science and Technology* **18** (2002) 856

Manohar, P. A., Kunishige, K. and Chandra, T., *Materials Science Forum* **426-432** (2003) 1127

MAP_STEEL_MUCG73 available freely in the world wide web, http://www.msm.cam.ac.uk/map/steel/programs/mucg73-b.html

Maki, J., Mahieu, J., De Cooman, B. C. and Claessens, S. *Journal of Materials Science and Technology* **19**(2003) 125

Maki, J., Mahieu, J., Claessens, S. and De Cooman, B. C. *Verlag Stahleisen GmbH, Galvatech '2001*, Germany, (2001) 623

Mark, C. *Proceedings of Cambridge Philosophical Society* **52** (1956) 216

Matas, S. J. and Hehemann, R. F. *Trans. Met. Soc. AIME* **221** (1961) 179

Matsumura, O., Sakuma, Y. and Takechi, H. *ISIJ International* **32** (1992) 1014

Matsumura, O., Sakuma, Y. and Takechi, H. *Transactions of the Iron and Steel Institute* **27** (1987) 570

Matsumura, O., Sakuma, Y. and Takechi, H., *Scripta Metallurgica* **27** (1987) 1301

Mintz, B. *Materials Science Forum* **426-432** (2003) 1219

Mintz, B. *International Materials Reviews* **46** (2001) 169

MTDATA, National Physical Laboratory, Teddington, London, 2005

Murr, L. E. *Interfacial phenomena in metals and alloys*, Addison-Wesley Publication Co., USA, (1975) 131

Murugananth, M., Babu, S. S. and David, S. A. *Welding Journal*, Supplement, October, (2004) 267

Nagasaka, A., Sugimoto, K. and Kobayashi, M. *ASM International*, USA, (1996) 557

Nakagaito, T., Shimizu, T., Furukimi, O. and Sakata, K., *Tetsu-to-Hagane* **89** (2003) 841

Nagasaka, A., Sugimoto, K-I., Kobayashi, M., Kobayashi, Y., Hashimoto, S. *Tetsu-to-Hagane* **85** (1999) 885

Nagasaka, A., Sugimoto, K-I., Kobayashi, M. and Hashimoto, S. *Tetsu-to-Hagane* **85** (1999) 552

Nagasaka, A., Sugimoto, K-I., Kobayashi, M., Shirasawa, H. *Tetsu-to-Hagane* **84** (1998) 218

Nelder J. A. and Mead R. *Computer Journal* **7** (1965) 308

Olson, G. B. *Deformation, Processing and Structure*, American Society of Metals, USA, (1982) 391

Olson, G. B. and Cohen, M. *Proceedings of US-Japan Seminar on Mechanical Behaviour of Metals and Alloys Associated with Displacive Transformation*, Troy, NY, (1979) 7

Olson, G. B. and Cohen, M., *Metallurgical and Materials Transactions A* **7** (1976) 1897

Olson, G. B. and Cohen, M. *Metallurgical and Materials Transactions A* **7** (1976) 1905

Olson, G. B. and Cohen, M., *Metallurgical and Materials Transactions A* **7** (1976) 1915

Olson, G. B. and Cohen, M. *Metallurgical and Materials Transactions A* **6** (1975) 791

Olson, G. B. and Cohen, M. *Journal of the Less-common Metals* **28** (1972) 107

Onodera, H. and Tamura, I. *Proceedings of US-Japan Seminar on Mechanical Behaviour of Metals and Alloys Associated with Displacive Transformation*, Troy, NY (1979) 24

Patel, J. R. and Cohen, M. *Acta Metallurgica* **1** (1953) 531

Pereloma, E. V., Timokhina, I. B. and Hodgson, P. D. *Materials Science and Engineering A* **273-275** (1999) 448

Pichler, A., Traint, S., Arnolder, G., Stiaszny, P., Blaimschein, M., and Werner, E. A. *Iron and Steelmaker*, USA, **30**, (2003) 21

Pichler, A., Traint, S., Arnoldner, G., Stiaszny, P., Blaimschein, M. and Werner, E. A. *44th Mechanical Working and Steel Processing Conference Proceedings*, Iron and Steel Society/AIME, USA, **40** (2002) 121

Pichler, A., Stiaszny, P., Potzinger, R., Tikal, R. and Werner, E. *40th Mechanical Working and Steel Processing Conference Proceedings*, Iron and Steel Society/AIME, USA **36** (1998) 259

Pickering, F. B. *Physical Metallurgy and the Design of Steels*, Applied Science Publishers Ltd, England, (1978)

Pyshmintsev, I. Y., De Meyer, M., De Cooman, B. C., Savray, R. A., Shveykin, V. P.and Vermeulen, M., *Metallurgical and Materials Transactions A* **33** (2002) 1659

Raghavan, V. *Martensite, A tribute to Morris Cohen*, ASM International, USA, (1992) 197

Rao, B. V. N. and Rashid, M. S. *Metallography* **16** (1983) 19

Rashid, M. S. *Formable HSLA and Dual Phase Steels*, USA, (1979) 1

Rashid, M. S. *Dual Phase and Cold Pressing Vanadium Steels in the Automobile Industry*, Berlin, (1979) 32

Reisner, G., Warner, E. A. and Fischer, F. D. *International Journal of Solid Structures* **35** (1998) 2457

Rigsbee, J. M. *Proceedings of the ICOMAT'79* Cambridge, MA, USA (1979) 381

Sadhukhan, S., Das, K. P., Bandyopadhyay, N. R. and Banerjee, M. K. *Journal of the Institution of Engineers*, India, **82** (2001) 65

Sakuma, Y., Matlock, D. K., Krauss, G. *Materials Science and Technology* **9** (1993) 718

Sakuma, Y., Matlock, D.K., Krauss, G., *Metallurgical and Materials Transactions A* **23** (1992) 1221

Sakuma, Y., Matsumara, O. and Takechi, H., *Metallurgical and Materials Transactions A* **22** (1991) 489

Sakuma, Y., Matsumura, O. and Akisue, O. *ISIJ International* **31** (1991) 1348

Sangal, S., Goel, N. C. and Tangri, K. *Metallurgical and Materials Transactions A* **16** (1985) 2023

Scheil, E., *Zeitschrift für anorganische and allgemeine, Chemie* **207** (1932) 21

Schrader, A. and Wever, F. *Arch. Eisenhittenwesen* **23** (1952) 489

Sherif, M. Y., Garcia-Mateo, C., Sourmail, T. and Bhadeshia, H. K. D. H. *Materials Science and Technology* **40** (2004) 319

Shi, W., Li, L., Zhou, Y., Fu, R. Y. and Wei, X. C. *Heat Treatment of Metals*, China, **8** (2002) 9

Song, S. M., Sugimoto, K-I., Kandaka, S., Futamura, A., Kobayashi, M. and Masuda, S. *Materials Science Research International*, Japan, **9** (2003) 223

Song, S. M., Sugimoto, K-I., Kandaka, S., Futamura, A., Kobayashi, M. and Masuda, S. *Journal of the Society of Materials Science*, Japan, **50** (2001) 1091

Streicher, A. M., Speer, J. G. and Matlock, D. K. *Steel Research* **73** (2002) 287

Sudo, M., Tsukatani, I. and Shibata, Z. *Metallurgy of Continuous Annealed Sheet Steel*, AIME (1982) 310

Sugimoto, K-I., Tsunezawa, M., Hojo, T. and Ikeda, S. *ISIJ International* **44** (2004) 1608

Sugimoto, K-I., Nakano, K., Song, S-M. and Kashima, T. *ISIJ International* **42** (2002) 450

Sugimoto, K-I., Kanda, A., Kikuchi, R., Hashimoto, S. I., Kashima. T. and Ikeda, S. *ISIJ International* **42** (2002) 910-915

Sugimoto, K-I., Sakaguchi, J., Iida, T. and Kashima, T. *ISIJ International* **40** (2000) 920

Sugimoto, K-I., Nagasaka, A., Kobayashi, M. and Hashimoto, S. I. *ISIJ International* **39** (1999) 56

Sugimoto, K-I., Kobayashi, M. and Nagasaka, A. *Canadian Institute of Mining, Metallurgy and Petroleum (Canada)* (1996) 503

Sugimoto, K-I., Kobayashi, M. Nagasaka, A. and Hashimoto, S. I. *ISIJ International* **35** (1995) 1407

Sugimoto, K-I. and Kobayashi, M., Iron and Steel Society/AIME, USA (1994) 255

Sugimoto, K-I., Misu, M., Kobayashi, M. and Shirasawa, H. *ISIJ International* **33** (1993) 775

Sugimoto, K-I., Usui, N., Kobayashi, M. and Hashimoto, S. I. *ISIJ International* **32** (1992) 1311

Sugimoto, K-I., Kobayashi, M. and Hashimoto, S. I., *Metallurgical and Materials Transactions A* **23** (1992) 3085

Swallow, E. and Bhadeshia, H. K. D. H. *Materials Science and Technology* **12** (1996) 121

Takahashi, M. *Nippon Steel Technical Report* **88** (2003) 2-7

Takechi, H., Matsumura, O., Sakuma, Y. *Japan Kokai Tokyo Koho Japan Patent 62, 188, 729* (1987)

Tamura, I., Maki, T., Hato, H., Tomota, Y. and Okada, M. *Proceedings of 2nd International Conference on Strength of Metals and Alloys*, Asilomar, CA, **3** (1970) 894

Tomita, Y. and Morioka, K. *Materials Characterization* **38** (1997) 243

Traint, S., Pichler, A., Stiaszny, P. and Wemer, E. A. *44th Mechanical Working and Steel Processing Conference Proceedings*, Iron and Steel Society/AIME, USA **40** (2002) 139

Traint, S., Pichler, A., Tikal, R., Stiaszny, P., Wemer, E. A., *42nd Mechanical Working and Steel Processing Conference Proceedings*, Iron and Steel Society/AIME, USA **38** (2000) 549

Uenishi, A., Kuriyama, Y. and Takahashi, M. *Nippon Steel Technical Report (Japan)* **81** (2000) 17

ULSAB-AVC, http://www.worldautosteel.org/ulsab-avc

Venables, J. A. *Philosophical Magazine* **7** (1964) 35

Vodopivec, F., Reskovi, S. and Mamuzic, I. *Materials Science and Technology* **15** (1999) 1293

Wang, H. S., Yang, J. R., Bhadeshia, H. K. D. H. *Materials Science and Technology* **21** (2005) 1323

Wang, Z. C., Kim, S. J., Lee, C. G. and Lee, T. H., *Journal of Materials Processing Technology* **151** (2004) 141

Wei, X. C., Li, L., Fu, R. Y. and Shi, W. *Journal of Iron and Steel Research International*, China, **10** (2003) 49

Wei, X., Fu, R., Li, L. and Shi, W., *Shanghai Jinshu (Shanghai Metals)*, China, **24** (2002) 32

Wei, X. C., Li, L., Fu, R. Y. and Shi. W. *Acta Metallurgica Sinica (English Letters)*, China **15** (2002) 285

Wiles, D. B. and Young, R. A. *Journal of Applied Crystallography* **14** (1981) 149

Yan, B. *44th Mechanical Working and Steel Processing Conference Proceedings*, Iron and Steel Society, AIME, USA, **40** (2002) 509

Yan, B. and Xu, K. *Iron and Steelmaker* **30** (2003) 33

Yan, B. and Xu, K. *44th Mechanical Working and Steel Processing Conference Proceedings*, Iron and Steel Society, AIME, USA **40** (2002) 493

Zackay, V. F., Parker, E. R., Fahr, D. and Bush, R., *Trans. ASM* **60** (1967) 25

Zaefferer, S., Ohlert, J. and Bleck, W. *Acta Materialia* **52** (2004) 2765

Zhu, C. M. S. Q., Sellars, C. M. and Bhadesiha, H. K. D. H. *Materials Science and Technology* (2006) submitted